

Renate Høvik Berge
Fredrik Rudfoss Haugland
Ida Erika Witt Langseth

Optimization of Microgrids

*Feasibility Study and Economic Analysis
of Rye Microgrid*

Bachelor's project in Renewable Energy
Supervisor: Håvard Karoliussen and Robert Bock
May 2019

Renate Høvik Berge
Fredrik Rudfoss Haugland
Ida Erika Witt Langseth

Optimization of Microgrids

*Feasibility Study and Economic Analysis
of Rye Microgrid*

Bachelor's project in Renewable Energy
Supervisor: Håvard Karoliussen and Robert Bock
May 2019

Norwegian University of Science and Technology
Faculty of Engineering
Department of Energy and Process Engineering



Department of Energy and Process Engineering
Faculty of Engineering Science

Bachelor Thesis

Project Title Optimization of Microgrids <i>Feasibility Study and Economic Analysis of Rye Microgrid</i>	Given Date 08.11.2018
Norwegian Project Title Optimalisering av mikronett <i>Mulighetsvurdering og økonomisk analyse av Rye Mikronett</i>	Deadline 24.05.2019
	Pages/Appendix 89/26
	Project Number FEN1902
Study Program Engineering Renewable Energy	
Group Members Renate Høvik Berge, email: renatehvikberge@gmail.com Ida Erika Witt Langseth, email: idaerikawl@gmail.com Fredrik Rudfoss Haugland, email: fredrikhaugland@gmail.com	
Supervisors Associate Professor Håvard Karoliussen, email: havard.karoliussen@ntnu.no Postdoctoral Research Fellow Robert Bock, email: robert.bock@ntnu.no	
Industry Partner TrønderEnergi AS	
Contact Anniken Auke Borgen, email: anniken.borgen@tronderenergi.no	

Available



Available by agreement with employer

The report is released after

<input checked="" type="checkbox"/>
<input type="checkbox"/>
<input type="checkbox"/>

Abstract

Microgrids have the potential to be the future solution for remote area energy supply. TrønderEnergi is exploring this business possibility as a part of the REMOTE project at Froan, a group of islands by the coast of Trøndelag in Norway. The microgrid intended at Froan is tested in a pilot project at Rye, 12 km west of the city of Trondheim. The main goal of the pilot project is to gain experience and later expand the project to guarantee energy deliverance to remote areas.

Rye Microgrid consist of energy production from a wind turbine and a PV system as well as energy storage in the form of a battery and a hydrogen unit. The goal of the microgrid is to supply enough energy to cover 95% of the energy consumed at the site, while the remaining 5% is supplied by the utility grid. The microgrid at Rye is evaluated by five cases consisting of different components. This done is to highlight the consumer- and grid company perspective on the feasibility of the microgrid. The cases were simulated in a Simulink model of Rye Microgrid, based on a combination of measured- and simulated data. The calculations were done in MATLAB and Microsoft Excel.

The results concerning the security of supply, the economic aspect and the environmental aspect of the case are presented and discussed, and tied together from a consumer- and grid company perspective. As the consumer owns the wind turbine, the options are to either invest in the PV system or the battery. The combination of the wind turbine and PV system has a high yearly profitability and an investment in the PV system leads to a profit of 663.4 kNOK at the end of the PV system lifetime. The positive attributes from the battery is outweighed by the high investment costs. Therefore the optimal investment for the consumer is the PV system.

From a grid company perspective, it can be observed that Rye Microgrid cover 94.3% of the energy consumption. In order to achieve the goal of 95%, adjustments were made separately to the wind- and solar energy production as well as the battery and hydrogen storage capacities. It can be concluded that increasing the solar energy production leads to a higher self supply percentage than increasing the wind energy production with the same amount. The hydrogen energy storage system supplies 10.9% of the energy demand, leading to the microgrid operating 94.3% self supplied. The battery capacity would have to be increased by 5.3 times in order to provide an equal self supply percentage.

All the cases are profitable during a year in a varying degree, when excluding operation and maintenance costs. Therefore, the greatest economic differences were visible in the NPV evaluation. The two main observations were that solar energy production contribute to an increasing NPV on a yearly basis, and the cases including energy storage were significantly lower, and decreased on yearly basis. The microgrid solution reduces the carbon emissions compared to the European energy market. In addition, the renewable energy share at Rye Microgrid is equivalent to renewable energy share of the Norwegian grid.

Preface

This thesis is submitted as a part of the degree of Bachelor of Science in Renewable Energy Engineering at the Norwegian University of Science and Technology. The bachelor thesis is graded from A to F, and accounts for 20 credits. The thesis is written in collaboration between three students, Renate Høvik Berge, Fredrik Rudfoss Haugland and Ida Erika Witt Langseth.

The industry partner for this thesis is TrønderEnergi AS and together with Anniken Auke Borgen, a problem statement was developed. Our motivation for this thesis is to increase the understanding and insight in the future of microgrids, considering the feasibility in regards to security of supply, economic factors and environmental impact.

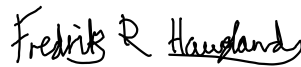
We would like to thank Eirik Lockertsen, Solbes AS, for assistance with the simulation in PVsyst, and theoretical knowledge of PV systems. In addition, we also got the chance to help install the PV system at Rye. This is an experience we really appreciate, and we would therefore like to thank Eirik Lockertsen for this opportunity.

Anniken Auke Borgen deserves a sincere thanks for contributing to the thesis with inputs, data and experience. We would also like to express great gratitude to our supervisors Håvard Karoliussen and Robert Bock for guidance and support throughout the semester.

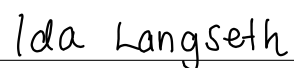
Trondheim, 24. May 2019



Renate Høvik Berge
260124



Fredrik Rudfoss Haugland
476017



Ida Erika Witt Langseth
476031

Contents

Abstract	v
Preface	vii
Lists	xi
1 Introduction	1
1.1 Project Background	2
1.2 Presentation of Rye Microgrid	3
1.3 Problem Statement	5
1.4 Problem Approach	5
1.5 Limitations	5
1.6 Thesis Outline	6
2 Power Systems	7
2.1 Power Market	8
2.2 Carbon Intensity	8
2.3 Microgrid	9
2.4 Transformers and Transmission Lines	10
3 Renewable Energy Sources	13
3.1 Wind Power	14
3.2 Solar Power and Photovoltaic Systems	14
3.2.1 Solar Radiation	15
3.2.2 Global Horizontal Irradiance	16
3.2.3 Planning and Installing a Photovoltaic System	18
3.3 Renewable Energy Sources in Norway	20
3.4 Renewable Energy Generation Costs	22
3.4.1 Economic Analysis of Renewable Energy Projects	22
3.4.2 Cost Trends of Renewable Energy Sources	23
4 Energy Storage Technologies	25
4.1 Lithium-ion Battery	26
4.1.1 Battery Market	27
4.2 Hydrogen Energy Storage System	27
4.2.1 PEM Fuel Cell and Electrolysis Cell	28
4.2.2 Hydrogen Market	29
5 Components and Case Descriptions	31
5.1 The Components of Rye Microgrid	32
5.2 Case Descriptions	34
6 Methods	39
6.1 Data Acquisition	40
6.1.1 Measured Data	40
6.1.2 Simulated Solar Energy Production	42
6.1.3 Calculated Losses	44
6.2 Simulation of Rye Microgrid in Simulink	45
6.3 Calculations and Approaches	47
6.3.1 Security of Supply	47

6.3.2	Economic Analysis	49
6.4	Environmental Impact Rye Microgrid	52
7	Security of Supply	53
7.1	Annual Energy Consumption	54
7.2	Annual Energy Production	54
7.3	Energy Storage	57
7.4	Self supply	58
7.5	Off Grid Potential	61
8	Economic Analysis	65
8.1	Energy Exchange with TEN	66
8.2	Profitability	68
8.3	Net Present Value	69
8.4	LCOE	71
9	Environmental Impact	73
9.1	Carbon Emissions	74
9.2	Implementation at Froan	76
10	Evaluation of Rye Microgrid	77
10.1	Consumer Perspective	78
10.2	Grid Company Perspective	79
11	Conclusion	81
	Further Work	83
	References	85
	List of Appendices	
	A REC Twinpeak 2 Mono Series Datasheet	A-1
	B REC Twinpeak 2 Series Datasheet	B-1
	C SolarEdge Power Optimizer Datasheet	C-1
	D SolarEdge Inverter Datasheet	D-1
	E Battery Energy Storage System	E-1
	F PVsyst Guide to Rye Microgrid	F-1
	G PVsyst Simulation Report	G-1
	H Simulink Model Description	H-1

List of Symbols

η	Efficiency [%]
ρ	Resistivity [Ω/km]
C	Net cash flow [NOK]
CI	Carbon intensity [$\text{gCO}_{2,\text{eq}}/\text{kWh}$]
$\cos(\phi)$	Power factor [-]
E	Energy [kWh]
ED	Energy density [kWh/kg]
F	Fuel costs [NOK]
I	Current [A]
I_C	Investment Cost [NOK]
L	Length [km]
M	Operation- and maintenance costs [NOK]
m	Mass [kg]
P	Power [W]
R	Resistance [Ω]
r	Discount rate [%]
S	Apparent power [VA]
t	Time [years]
T	Expected lifetime [years]
V	Voltage [V]

List of Terms

Albedo value	Indicates a surface's ability to reflect radiation, and varies between 0 and 1.
Array	PV modules connected together in series, parallel or a combination of both.
Azimuth angle	Indicating the position of an object e.g southward facing is 0°.
Carbon intensity	Amount of emissions in gCO _{2,eq} /kWh caused by an energy producing unit.
C-rate	The rate of which a battery can fully charge or discharge in reference to 1C equalling a full charge/discharge in 1 hour.
Depth of discharge	The percentage of the capacity to which the battery discharges.
Diffuse horizontal irradiance	The solar radiation scattered in the atmosphere by dust or molecules, that reach a horizontal surface.
Diffuse solar radiation	The solar radiation scattered in the atmosphere by dust or molecules, that reaches earth.
Direct normal irradiance	The solar radiation that passes directly through the atmosphere and perpendicular to the surface.
Direct solar radiation	The solar radiation that passes directly through the atmosphere and reaches earth.
Far shading	Shading from objects far away from the PV field, usually more than 10 times the size of the total PV system.
Geostationary satellite	Satellites orbiting the equator.
Global horizontal irradiance	The total global horizontal irradiance consisting of the direct normal irradiance and the diffuse horizontal irradiance while accounting for the incidence angle.
Incidence angle	The angle between the perpendicular of the module and the solar irradiation.
Inverter	An electrical component converting DC to AC.
Microgrid	Small scale electricity grid, including groupings of power generation and control systems that either operate on or off grid.
Near shading	Shading from objects close to the PV modules e.g chimney, wind turbine, trees etc.
NEH-S	Main fuse less or equal to 125 A at 230 V or 80 A at 400 V.
Polar satellite	Satellites orbiting the poles.

Power optimizer	DC/DC converter connected to the solar modules with the main function of increasing the power output of a PV system.
Reflected solar radiation	The solar radiation reflected from surfaces on the earth consisting of both direct- and diffuse radiation.
Soiling losses	Losses from unwanted substances on or around the PV modules blocking the sun e.g. snow, dust etc.
String	A set of PV modules connected in series.
Tilt angle	The angle between the surface of the PV module and the horizontal surface.
Transmission grid	Connects energy producers and consumers domestically and abroad.
Utility grid	The power lines reaching the consumer.

List of Abbreviations

AM	Air Mass
CHP	Combined Heat and Power
DHI	Diffuse Horizontal Irradiance
DNI	Direct Normal Irradiance
DoD	Depth of Discharge
ESD	Energy Storage Device
ESS	Energy Storage System
G2P	Gas to Power
GHI	Global Horizontal Irradiance
GO	Guarantees of Origin
HESS	Hydrogen Energy Storage System
IAM	Incidence Angle Modifier
LCOE	Levelized Cost Of Energy
NPV	Net Present Value
NTNU	Norwegian University of Science and Technology
PEMEC	Proton Exchange Membrane Electrolysis Cell
PEMFC	Proton Exchange Membrane Fuel Cell
P2G	Power to Gas
P2P	Power to Power
PV	Photovoltaic
RES	Renewable Energy Source
SRP	Standard Reduction Potential
SoC	State of Charge
TEK	TrønderEnergi Kraft
TEN	TrønderEnergi Nett
Q	Quarter

List of Figures

1.1	Map over Froan presenting the three islands Sørburøy, Nordøy and Sauøy that are intended to be supplied by the microgrid. [2]	2
1.2	REMOTE-project concept. [3]	2
1.3	Photograph from Rye presenting the wind turbine and the installed PV system.	4
1.4	Schematic sketch of Rye Microgrid. [2]	4
2.1	Illustration of a single phase transformer. [22]	10
3.1	A general power curve for a wind turbine. [29]	14
3.2	An illustration of the solar radiation components. [33]	15
3.3	An illustration of AM and its impact on the radiation intensity. [40]	16
3.4	World map illustrating the varying GHI in the world. [41]	17
3.5	Geostationary- and polar orbits for satellites. [43]	17
3.6	An illustration of a PV system. [47]	18
3.7	Important angles to determine the orientation of a PV module. [50]	19
3.8	The sun path chart illustrating the suns trajectory at different times of the year. [44]	19
3.9	Energy production balance in Norway in 2018. [55]	20
3.10	Wind speed distribution in Norway over the year. [57]	21
3.11	Map over Norway illustrating the varying GHI in Norway during January and July. [60]	21
3.12	Global LCOE from utility scale renewable energy generation technologies, 2010-2017. [67]	23
3.13	NVEs prediction for LCOE development from 2018-2040 in øre/kWh. [62]	24
4.1	Description of charge- and discharge mechanism of Li-ion batteries. [72]	26
4.2	Battery prices until 2018 and prediction of prices until 2030 for Li-ion battery packs. [77]	27
4.3	Illustration of a PEMEC and PEMFC. [80]	28
5.1	The power curve for a Vestas V27 wind turbine. [87]	32
5.2	An illustration of the installed PV system.	33
5.3	Schematic sketch of case Wi.	34
5.4	Schematic sketch of case WiSo.	35
5.5	Schematic sketch of case WiBa.	35
5.6	Schematic sketch of case WiSoBa.	36
5.7	Schematic sketch of case WiSoBaHy.	37
6.1	Energy consumption composition.	41
6.2	The composition of wind production data.	41
6.3	The simulated energy produced by the PV system including the losses.	43
6.4	Screenshot from Simulink illustrating the model used to simulate Rye Microgrid.	45
6.5	The subsystem in the model of Rye Microgrid, presenting the battery storage.	46
6.6	The simplification of the losses taken into account in the Simulink model of Rye Microgrid.	47
7.1	The energy consumption with monthly average energy consumption.	54
7.2	Wind energy production with hourly inputs and monthly averages.	54
7.3	The simulated production from the PV system with hourly inputs and monthly averages.	55
7.4	Total production including wind- simulated solar-, and the monthly average energy production.	55
7.5	Hourly energy consumption, wind- and solar energy production.	56
7.6	Battery status with hourly inputs for case WiBa.	57
7.7	Battery status with hourly inputs for case WiSoBa and WiSoBaHy.	57

7.8	Hydrogen status with hourly inputs for case WiSoBaHy.	58
7.9	The energy supply from the different energy sources in all the cases.	59
7.10	The excess and deficit energy for case WiSoBaHy, in an off grid scenario.	61
7.11	The excess and deficit energy for case WiSoBa, in an off grid scenario.	63
7.12	The energy distribution in an 94.3% off grid scenario for cases WiSoBa and WiSoBaHy.	63
8.1	Hourly net exchange with TEN for case Wi.	66
8.2	Hourly net exchange with TEN for case WiSo.	66
8.3	Hourly net exchange with TEN for case WiBa.	67
8.4	Hourly net exchange with TEN for case WiSoBa.	67
8.5	The annual profitability development for all the cases.	68
8.6	The net present value over 30 years for all cases including the base case.	70
8.7	The NPV development for the expanded case WiSo.	71
F.1	Project menu in PVsyst for a grid connected system.	F-1
F.2	The "Grid system definition" window before inputting the PV components. . . .	F-2
F.3	SolarEdge "string configuration" illustrating the finished PV system string configuration for the PVsyst simulation.	F-3
F.4	Sub-array#1 after the system parameters were filled in	F-4
F.5	The estimated monthly values for soiling losses.	F-5
H.1	The relevant blocks used in the Simulink model of Rye Microgrid.	H-1
H.2	Screenshot from Simulink illustrating the model used to simulate the microgrid. .	H-2
H.3	The subsystem of the model showing the grid exchange in case Wi. The model is the same for the grid exchange calculation in case WiSo.	H-3
H.4	The subsystem of the model showing the battery energy storage system in case WiBa. The model is the same for the battery in case WiSoBa and WiSoBaHy. .	H-3
H.5	The subsystem of the model showing the hydrogen energy storage system in case WiSoBaHy.	H-4
H.6	The subsystem of the model that includes the rate limiter for the hydrogen charge and discharge. The rising slew rate is 55 kW and the falling slew rate is -100 kW.	H-5

List of Tables

1.1	Presentation of the cases with the associated combination of components.	5
2.1	Fixed- and energy dependent grid rent prices for 2018 for a NEH-S consumer. [11]	8
2.2	Carbon intensity values for different energy sources. [12–14]	8
3.1	Surfaces and their respective albedo. [38, p.13]	15
5.1	Transformer specifications for the two transformer types on the site.	34
6.1	The composition of energy consumption data.	40
6.2	Wind energy production composition.	41
6.3	PVsyst system parameters for the simulated PV system.	42
6.4	Array soiling losses for each month from the PVsyst report for the PV system at Rye.	43
6.5	The IAM losses estimated for the PV system at Rye from the PVsyst report. . .	43
6.6	Specifications for the transformers with the calculated losses and efficiency. . . .	44
6.7	The self produced energy used to cover the energy demand in the five cases. . . .	48
6.8	Battery- and hydrogen capacity for the test points in the sensitivity test.	48
6.9	Battery- and hydrogen capacity for the test points in the sensitivity test.	48
6.10	Required investments for all of the components in the microgrid.	51
6.11	The calculated LCOE for the energy sources at Rye Microgrid.	52
7.1	Self supply percentage in the five cases.	58
7.2	The energy supply from the different energy sources in all the cases.	59
7.3	Percentage self supply in the cases with the 27 m and 29 m diameter wind turbine.	60
7.4	Percentage self supply in the cases containing solar energy production, comparing original PV system and a 1.63 times larger PV system.	60
7.5	Percentage self supply in case WiSoBaHy when expanding the capacity of the battery.	61
7.6	Percentage self supply in case WiSoBaHy when expanding the capacity of the hydrogen gas tank.	61
7.7	Percentage self supply in case WiSoBa with different storage capacities for the battery.	62
8.1	The profit from energy exchange with the grid, self supply, battery- and hydrogen usage for all of the cases in kNOK.	68
8.2	The net present value for each case after 20 and 30 years in MNOK.	69
8.3	The calculated LCOE for the energy sources at Rye Microgrid.	71
9.1	Calculated carbon emissions from Rye Microgrid both with and without GO . .	74
9.2	The total carbon intensity taken into account all energy production required to supply the microgrid in all five cases.	75
9.3	The total carbon intensity while accounting the energy production required to supply the microgrid in all five cases.	75
10.1	The energy storage capacities required to reach a self supply percentage of 95% in cases WiSoBa and WiSoBaHy.	79
E.1	Technical proposal for the battery energy storage system at Rye from PowiDian.	E-1
E.2	Main components of the battery energy storage system.	E-1

Chapter 1

Introduction

TrønderEnergi AS is an energy company based in Trøndelag County in Norway. The company focuses on environmentally friendly energy production and energy related services for the region. During the last couple of years TrønderEnergi has had a growing investment in renewable energy. The company have three main areas of focus; production of hydro- and wind power, development of forward-looking energy related services and distribution of electrical energy. [1]

TrønderEnergi include several subsidiaries, one of them is TrønderEnergi Nett (TEN), which is one of the regions biggest distributor of electrical power. The subsidiary is responsible for maintenance, operation and development of the regional grid in the southern parts of Trøndelag as well as the distribution grid in 17 municipalities. [1]

Another subsidiary is TrønderEnergi Kraft (TEK). TEK owns and is responsible for the operation, development and construction of power plants in Trøndelag. An important motive for TEK is to gain knowledge and explore business possibilities, with a focus on sustainable solutions. [2]

With the responsibility of delivering electrical energy to private- and business costumers, TEN wants to evaluate the economical benefit of having a microgrid solution for remote locations, where the current infrastructure needs to be replaced. TEK has initiated a pilot project at Rye, with the motive to gain knowledge on this business area. Moreover, the agenda is to offer this solution to grid companies, and other companies that may have interest in the solution. [1, 2]

This chapter presents the background for the thesis. Further, the problem statement is presented and the approach to the problem statement is explained. The limitations to the thesis are specified, and the thesis outline is presented.

1.1 Project Background

Froan is a group of islands located outside the island Frøya at the coast of Trøndelag, where TEN is obligated to supply energy. The submarine cable from Frøya, via Gjøsingen, to Froan needs to be replaced, which is a costly process. Therefore, TEN is considering a microgrid solution to supply the islands in Froan with electrical energy.

The microgrid at Froan is intended to consist energy production from wind turbines and a photovoltaic (PV) system, and an energy storage system (ESS) consisting of a battery and a hydrogen unit. In addition, a diesel generator is planned in order to ensure the security of supply. The islands intended to be supplied by the microgrid are Sørburøy, Nordøy and Sauøy. The islands and the submarine cable are presented on the map in figure 1.1. [2]

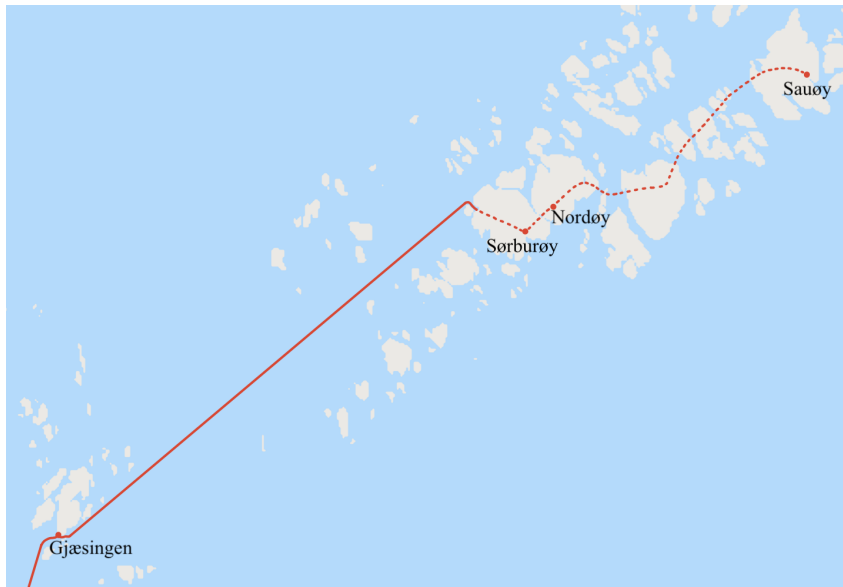


Figure 1.1: Map over Froan presenting the three islands Sørburøy, Nordøy and Sauøy that are intended to be supplied by the microgrid. The submarine cable is marked with the solid red line and the transmission line is marked with the dotted red line. Note that the map is a modified map from Google Maps and is based on information from TrønderEnergi. [2]

REMOTE-project at Froan

The project at Froan is a part of the EU-supported project REMOTE (Remote area Energy supply with Multiple Options for integrated hydrogen-based TEchnologies). The objective for the REMOTE-project is “to demonstrate the technical and economic feasibility of two fuel cells-based H_2 energy storage solutions” [3]. It is one of four DEMOs in Europe, which are all fed by renewable energy in a microgrid, either on- or off grid. Figure 1.2 presents the four DEMOs.

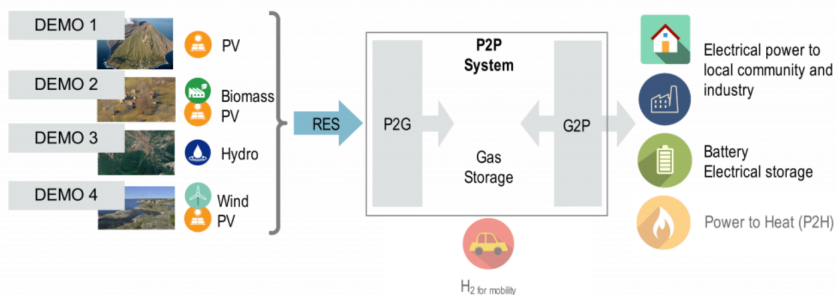


Figure 1.2: Concept for the REMOTE-project, illustrating the four DEMOs and their respective energy sources and the energy usage. [3]

Renewable Energy Sources (RESs) are used for Power to Gas (P2G), with use of hydrogen gas. Further, the stored hydrogen gas can be used for power production, Gas to Power (G2P). The DEMOs also consist of an integrated Power to Power (P2P) system. DEMO 1 is located at the island Ginostra in the south of Italy, and is supplied by solar power. DEMO 2 is located in Agkistro in Greece, and is supplied by hydro power. DEMO 3 is located in Ambornetti in the north of Italy, and is supplied by combined heat and power (CHP) fed with energy supplied by solar and biomass. DEMO 4 is the Froan project, which is supplied by wind- and solar power. All four projects receive funding through the REMOTE project for the hydrogen energy storage system (HESS). [3]

For DEMO 4 at Froan, TrønderEnergi cooperates with PowiDian, Ballard and Hydrogenics to administer- and produce the components for the microgrid. TrønderEnergi provides the site, renewable energy production and cover the expenses from the battery. PowiDian has offered a technical proposal including sizing propositions for the components and have the main responsibility when the microgrid is operating off grid. They also produce the battery, hydrogen storage tank and a master controller for the storage system. Ballard produces the fuel cell, while Hydrogenics produces the electrolysis cell. [2]

Pilot Project at Rye

It is a long process to get concession to install wind turbines at Froan as there is protected wildlife on the island. Consequently, the concept is initially tested in a pilot project at a farm at Rye, which is located 12 km west of the city of Trondheim in Trøndelag. The objective for the project is to evaluate the viability of the microgrid. The microgrid at Rye, referred to as Rye Microgrid, is intended to be scaled to supply Froan. [4, 5]

In addition to EU-support, Rye Microgrid is a Pilot-E project and has received funding from Enova. Pilot-E is a financing offer to Norwegian businesses established by Innovasjon Norge, Forskningsrådet and Enova. The goal of Pilot-E is to create new solutions and speed up the process of making these commercially available, while continuously developing new and existing industry. Enova is a Norwegian state owned enterprise. They work with implementation and development of energy- and climate solutions and technologies, working towards a low emission society. TrønderEnergi applied for Pilot-E in 2017, and has since also applied for and received funding from Enova. [2, 6, 7]

1.2 Presentation of Rye Microgrid

Rye Microgrid consists of a wind turbine, a PV system and a battery- and hydrogen energy storage system. After all the components are installed, the farm is planned to be 95% self supplied with renewable energy for two years, from 2020 to 2021. The remaining 5% is delivered by TEN. When the microgrid is operating off grid, the exchange with TEN is restricted to only purchase deficit energy. To ensure the security of supply in case of unforeseen circumstances additional energy exchange with TEN is allowed. During the installation process, until the microgrid is disconnected from the grid, the consumer acts as a small scale power producer allowing surplus energy to be sold to TEN. [4, 5]

The microgrid is planned to be fully installed by the end of 2019, however, several of the components are already operational. The wind turbine was installed in 2016. The PV system was installed in March 2019 and has been operational since April 2019. The battery and the HESS are projected to be installed during the fall of 2019. The installed wind turbine and the installed PV system at Rye are presented in figure 1.3. [4, 5]



Figure 1.3: Photograph from Rye presenting the wind turbine and the installed PV system.

Rye Microgrid includes three transformers, two substations and two advanced meters from Safebase. By the wind turbine there is a 415 V/22 kV transformer and an advanced meter with a 400 V TN-grid, which are both installed. In addition, the 22 kV/240 V transformer and an advanced meter with a 230 V IT-grid by the consumer are also installed. The third transformer, a 415 V/22 kV, will be installed by the PV system and the ESS. This is done for safety concerns, as the capacity of transformer 1 (T1) is insufficient when all components are connected to it. Further, there will also be a substation with a meter by the PV system and ESS. There is also a substation at the connection point to TEN, which includes a meter. [2]

A master controller from PowiDian will be installed, which will control how the energy is used e.g. storage or consumption. Figure 1.4 illustrates a schematic sketch of Rye Microgrid with all the components, meters and transformers. [2]

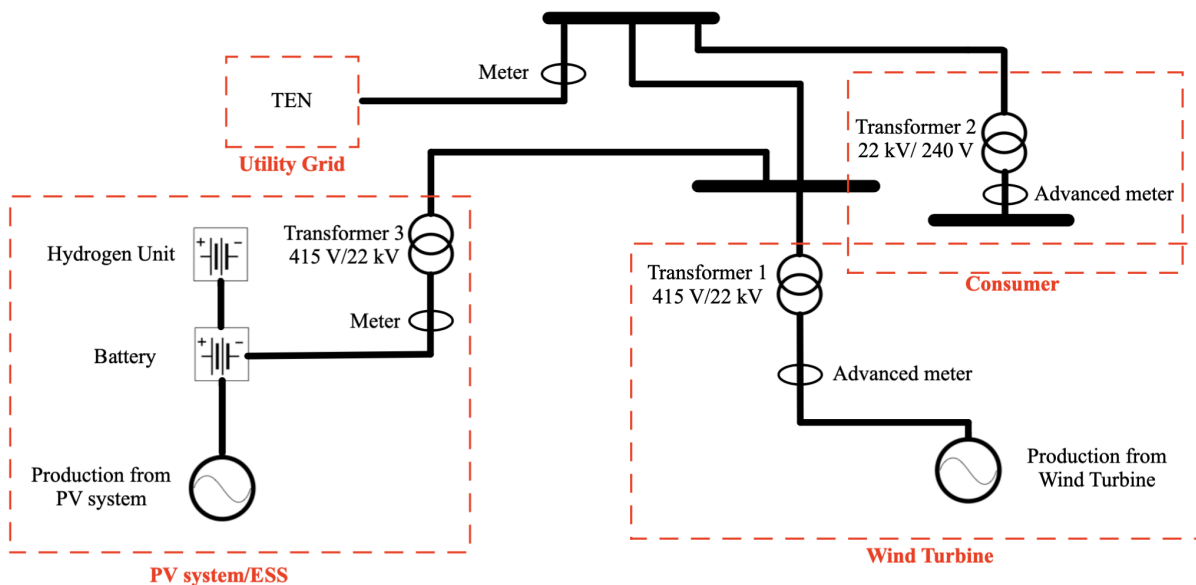


Figure 1.4: Schematic sketch of Rye Microgrid with all the components, meters and transformers. Note that the figure is simplified from the original sketch and is based on information from Tr nderEnergi. [2]

1.3 Problem Statement

The pilot project at Rye has an objective of gaining knowledge and explore business possibilities. Rye Microgrid is a significant opportunity to acquire knowledge on different aspects of the microgrid. On this basis, the problem statement for this thesis has been developed in cooperation between TrønderEnergi and NTNU. The following formulation is stated: *Optimizing Rye Microgrid considering off grid potential, economic value and environmental impact*. The main questions that are addressed are:

- What is the optimal composition of the microgrid for the consumer?
- How much does the hydrogen unit add to the microgrid, concerning security of supply?
- Which modifications are necessary for the microgrid to operate off grid?
- What is the environmental impact of the implementation of Rye Microgrid?

There is value in addressing different perspectives of microgrid establishments, both from the consumer- and the grid owner perspective. Accordingly, the problem statement has been further divided into three main focus areas, security of supply, economic value and environmental impact from the two perspectives.

1.4 Problem Approach

In cooperation with Anniken Auke Borge, TrønderEnergi Kraft, it is decided that the problem statement is approached by evaluating five test cases. Each case evaluates a different combination of components, highlighting different aspects of Rye Microgrid. Rye Microgrid refers to the actual system at Rye, while the cases are theoretical assumptions based on Rye Microgrid. The cases provide the opportunity to evaluate which combination is the most optimal for the consumer and grid company.

The cases contain an abbreviation to pinpoint which components are used. These abbreviation are Wi for wind, So for the PV system, Ba for the battery and Hy for the HESS. All the cases with the associated combination of components are presented in table 1.1.

Table 1.1: Presentation of the cases with the associated combination of components.

Case	Wind Turbine	PV System	Battery	Hydrogen Unit
Wi	✓			
WiSo	✓	✓		
WiBa	✓		✓	
WiSoBa	✓	✓	✓	
WiSoBaHy	✓	✓	✓	✓

1.5 Limitations

The limitations from the problem statement approach are specified in this section. The thesis does not include an evaluation of the type of energy producing- or energy storage components, as all the components in Rye Microgrid are specified by TrønderEnergi. The evaluation of Rye Microgrid considers the energy production of the components, the energy consumption and the ESS. There is not an evaluation of how load management impacts the energy consumption.

The energy consumption data and the wind energy production data are a combination of measured data from 2016, 2017 and 2018 at Rye. Therefore, a base year is compiled, mainly consisting of data from 2018. As the PV system was not operational before April 2019, there is no available energy production data. The energy production from the PV system is therefore simulated in PVsyst. There are limitations in PVsyst as some system parameters as the near shading profile and soiling losses are estimated in cooperation with Eirik Lockertsen, Solbes AS. The energy flow in the battery and HESS is simulated using Simulink.

A model of Rye Microgrid is made in Simulink to simulate the whole system using data from the base year. When a time perspective longer than a year is considered, the deterioration of the components and the following reduction of performance, are not taken into account. The model includes several estimations in regards to losses and how these are approximated is presented in chapter 6. The economic analysis is limited to an evaluation of the annual profitability, net present value (NPV) and levelized cost of energy (LCOE). Because there is only one year of data available, the future cash flows from energy exchange with TEN are based on the consumption- and production data from the base year.

The environmental impact is evaluated by a carbon emissions analysis, which does not include the emissions related to the energy storage devices (ESDs). The ESDs are assumed to have zero carbon emissions during their life cycle, as there are no reliable data for the material used to produce the units at Rye. Any evaluation of the microgrid at Froan is done by assuming that the results from Rye Microgrid is applied to Froan. The evaluation is done by comparing the results from Rye Microgrid with TrønderEnergi's requirements for the microgrid at Froan.

1.6 Thesis Outline

The thesis consists of a theoretical section and a practical section. Chapter 1 introduces the motive for the thesis and the problem statement. Chapter 2 presents the concept for power systems, chapter 3 describes RESs and chapter 4 explains various energy storage solutions. Chapter 5 presents all the specific components that the completed Rye Microgrid consists of and a description of the case study.

Chapter 6 presents the data acquisition, the programs used and a description of how the results were obtained. Chapters 7, 8, 9 and 10 are the core of the thesis and presents the results related to the problem statement. The results are divided into three main focus areas, security of supply, economic analysis and environmental impact. The results are eventually tied together and evaluated from the consumer and grid company perspective. Chapter 11 concludes the thesis.

Chapter 2

Power Systems

A provident power system is central in the development of a low emission society. The European power system is in a transition, due to continuous increase of renewable energy share, decrease of fossil fuel installations and electrification of the transport sector. The core of the power system is the transmission grid. The transmission grid connects producers and consumers both domestically and abroad. However, there is an increasing interest in local energy production and storage, which leads to opportunities as well as challenges. [8, 9]

This chapter presents theory related to the power market and explains how carbon emissions are considered in the power system. It gives an overview of the general configuration and status of microgrid technology. The chapter also explains transformers and transmission lines, and how they are integrated in the power system.

2.1 Power Market

Norway is a part of a shared power market with Sweden, Denmark and Finland, which is integrated in the European power market. This allows power exchange, and the power is transferred from areas with low prices to areas with higher prices. [10]

The spot price is determined at Nord Pool Spot every hour for the day ahead, and depends on the supply and demand. The price varies with precipitation and temperature, and this causes the price to vary with the time of the day and seasonally. Renewable energy sources (RES) such as hydro-, solar- and wind power have low variable costs, because the energy source is free. In contrast, thermal power from coal and gas have higher variable costs due to fuel expenses and emission quotas. When it is cold and dry in Norway, for example during the winter, the spot price increases. This is because the hydro power share is low and there is a demand for other sources with higher cost such as coal or gas. [10]

In addition to the spot price, the consumer must pay consumption tax for electric energy, value-added tax, electricity certificates and grid rent. The electricity bill also includes a surcharge for Enova. These expenses are combined into a total energy cost that is offered to the consumer. They change over time and are dependent on which provider is available in the area, and the type of consumer. The main fuse, as e.g. NEH-S, determines the prices for the consumer. NEH-S means that the main fuse is less than or equal to 125 A at 230 V or 80 A at 400 V. The total grid rent is a combination of a fixed- and an energy dependent price, and the costs for 2018 are listed in table 2.1. [10, 11]

Table 2.1: Fixed- and energy dependent grid rent prices for 2018 for a NEH-S consumer. Note that the prices are rounded from the original source. [11]

Year	Fixed Price	Energy Dependent
2018	5 000 NOK/year	0.426 NOK/kWh

2.2 Carbon Intensity

Carbon intensity is the amount of CO₂ equivalents emitted per kWh. It is dependent on the energy source and the emissions during its lifetime. Lifetime emissions include all the emissions from gathering initial material to eventual decommissioning of the system. However, the calculation of carbon intensity differs depending on the reference. Various producers will determine the emission differently resulting in various carbon intensities depending on the reference. Norway is in an unique position internationally with the high amount of renewable energy production from hydro power. Hydro power has the lowest carbon intensity of all energy producing sources at 6 gCO_{2,eq}/kWh. This can be observed from table 2.2, which presents various energy sources and their respective carbon intensity. [12]

Table 2.2: Carbon intensity values for different energy sources.

Energy Source	Carbon Intensity	Reference
Hydro	6 gCO _{2,eq} /kWh	NVE 2017 [12]
Solar	18 gCO _{2,eq} /kWh	REC [13]
Wind	20 gCO _{2,eq} /kWh	NVE 2017 [12]
Biogas	176 gCO _{2,eq} /kWh	NVE 2017 [12]
Gas	566 gCO _{2,eq} /kWh	NVE 2017 [12]
Coal	1 119 gCO _{2,eq} /kWh	NVE 2016 [14]

Guarantees of Origin

An important consideration for carbon emissions in Norway is whether the guarantees of origin (GO) are accounted for when determining carbon intensities. A producer of renewable energy can sell GO in addition to the produced energy. The goal of GO is to incentivize increased investments in renewable energy production. GO makes renewable energy production more attractive, as it leads to an additional income for the producer. Any consumer can buy GO, and state that the energy consumed originates from RESs. The price of GO varies from supplier to supplier and can be as low as 0.002 NOK/kWh to about 0.03 NOK/kWh. The price is in addition to the total energy costs. [15]

This affects the carbon emissions in Norway by increasing the apparent emissions from 16.4 gCO_{2,eq}/kWh to 531 gCO_{2,eq}/kWh in 2017, where the latter takes GO into account. The reason for the discrepancy is that most of the GO from Norwegian energy generation is sold to Europe, hence the intensity is calculated using a number based on an European mix containing mostly fossil fuels. [12]

The exchange of GO does not impact the physical flow of energy. Even though the GO are sold out of Norway, the reality is that Norwegian consumers consume the energy produced in Norway, because the energy always flows to the closest consumer. European consumers who have purchased GO from e.g. a Norwegian hydro power plant can claim that they utilize clean energy from the power plant, even if that is not physically the case. However, the market share will not reflect this. The energy production in Norway is mainly renewable, as described in section 3.3, however, the apparent carbon emissions related to the energy usage is impacted by the GO market. [12]

2.3 Microgrid

A microgrid is a small scale power grid. They are groupings of energy generation and control systems that either operate on- or off grid. This could be a competitive alternative to a reinvestment in the existing energy infrastructure, considering environmental- and economical concerns. It facilitates local production of renewable energy, and contributes to consumer participation in energy use. It also reduces losses from transmission grids by shifting the production closer to the consumer. [16–18]

Microgrid is an opportunity to optimize the energy production and distribution within a geographic area. Any excess production can go to storage or to the utility grid. The excess production distribution depends on whether the grid is completely off grid, or connected to the utility grid. [17] As the prices for investment in local energy production decrease, it is presumed that a decreasing amount of consumers will be grid connected. Simultaneously, the existing power grid needs to be updated, which leads to an increased grid rent cost for consumers. This results in a higher grid rent distributed over fewer consumers. [16]

Remote Microgrid Establishment in Norway

The first project on a worldwide basis to demonstrate a remote microgrid with hydrogen and a RES, was conducted in the municipality of Utsira in 2004. [19] Information of the operation of Utsira was obtained from 2004–2008. The project was conducted by Norsk Hydro and Statoil ASA concerning a HESS supplied by wind power. [20]

The microgrid system consisted of a wind turbine, and the HESS main components were a fuel cell, a hydrogen tank and an electrolysis cell. In addition, there was a flywheel, a Li-ion battery and a synchronous machine. The key findings from the project were that it is possible to develop stand-alone systems with wind power generation and hydrogen as a storage medium, even though the project was not viable. [21]

2.4 Transformers and Transmission Lines

Transformers and transmission lines (TL) are used to transfer power over large distances. The main reason is to mitigate losses caused by heat produced in the cable. This is done by increasing the voltage, thus reducing the current in the circuit. The two sides of the transformer are often referred to as the high voltage (HV) side and low voltage (LV) side. The power is further transmitted through the TL. Before it reaches the consumer another transformer steps down the voltage to the voltage used in household appliances. [22] Figure 2.1 presents a schematic for a single phase transformer.

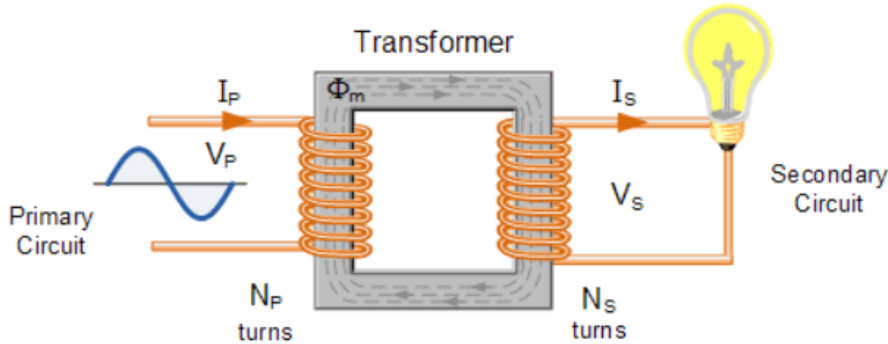


Figure 2.1: Illustration of a single phase transformer illustrating the primary and secondary circuit with associated current, voltage and turns. [22]

In order to transform the power from the primary winding to the secondary winding, Faraday's law of induction is applied. The law states that a change in the magnetic field induces an electromotive force, and on the other hand a changing electric field will induce a magnetic force. The basic principle of a transformer is that an electric force is applied in the primary circuit which leads to a magnetic flux being induced by the primary winding. The magnetic flux is led to the secondary winding by an iron core. This induces an electromotive force resulting in induced voltage in the secondary circuit. The increased or decreased voltage depends on the ratio of the number of turns between the primary- and secondary winding. [22]

When using the transformer there are several losses, depending on whether the transformer is running at load or no-load. These losses include iron-, copper-, stray- and dielectric losses. Iron losses occur in the iron core and are further divided into hysteresis and eddy current losses. Hysteresis is caused by the alternate current rapidly changing direction leading to heat production. Eddy current losses are caused by the circulating currents in the iron core. These losses can be reduced by splitting up the core with lamination, resulting in smaller currents. Copper losses are caused by heat production, because of the internal resistance in the wire. Stray losses are caused by leakage flux in the iron core, while dielectric losses are caused by the damages or deterioration in the insulation resulting in losses. In total the losses for the transformer are calculated by using equation 2.1. [22–24]

$$P_{\text{loss}} = P_0 + P_k \cdot \left(\frac{S_{\text{in}}}{S_n} \right)^2 \quad (2.1)$$

P_0 indicates no-load and P_k indicates load losses, both in W. S_{in} and S_n is respectively input- and nominal apparent power, both in VA. The relation between apparent- and active power is described by the power factor $\cos(\phi)$, as presented in equation 2.2. [22–24]

$$\cos(\phi) = \frac{P}{S} \quad (2.2)$$

This in turn leads to the calculation of the efficiency by equation 2.3.

$$\eta_T = \frac{P_{out}}{P_{in}} = \frac{P_{in} - P_{loss}}{P_{in}} \quad (2.3)$$

After stepping up the voltage in the transformer, the power is transferred in the TL to the consumer. There are two major losses in this stage, copper- and corona losses. Corona losses are caused by ionization of air molecules, and depend on line to line voltage and temperature. [25] The copper losses can be calculated from equation 2.4.

$$P_{Cu} = I^2 \cdot R \quad (2.4)$$

In order to calculate P_{Cu} the resistance in the TL has to be known. The resistance in the TL can be calculated using equation 2.5. L_{TL} is the length in km, and ρ is the resistivity in the cable in Ω/km . [25]

$$R_{TL} = \rho \cdot L_{TL} \quad (2.5)$$

Chapter 3

Renewable Energy Sources

Since the beginning of the industrial revolution, fossil fuels have been the main input in industrial production, transportation and electricity generation. With an increasing energy demand and a high percentage of fossil fuels in the energy mix, the world faces a challenge. In response, renewable energy installations, especially wind and solar, are increasing fast. [26]

This chapter begins with a brief introduction to theory on wind turbines and power control. Further, a more in depth introduction to solar radiation and utilization in solar energy production are presented, followed by an explanation of the composition of a PV system and relevant considerations.

The chapter then describes the renewable energy sources in Norway with a focus on the status and potential of wind- and solar energy production. Lastly, the chapter includes a description of economic factors important in order to evaluate an investment in a renewable energy project, and costs trends for renewable energy sources.

3.1 Wind Power

Global wind is caused by pressure differences as a result of uneven heating from solar radiation. This causes the air to shift, resulting in wind of various speeds depending on the pressure difference. The kinetic energy of the wind is utilized through wind turbines, by converting the kinetic energy to rotational energy, which is then converted to electricity. [27]

The most common wind turbine is the three bladed horizontal axis wind turbine. The size of a wind turbine is defined by the diameter of the rotor, the tower height, and the installed power capacity. The capacity of the turbine is usually given in kW or MW, and is a measure of how much power the turbine can produce at optimal wind conditions. [28]

Power Control of Wind Turbines

The wind is varying in speed and direction. To optimize the utilization of wind of varying conditions, the wind turbine can include power control. A general power curve of a wind turbine is illustrated in figure 3.1.

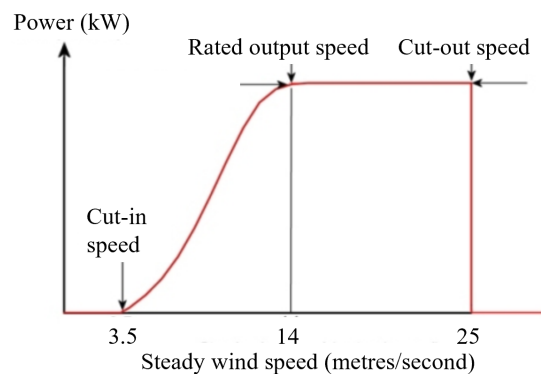


Figure 3.1: A general power curve for a wind turbine, including cut-in speed, rated speed and cut-out speed. Note that the figure is modified from the original. [29]

Wind turbines are generally designed to have optimum production at a rated wind speed. This equals the lowest wind speed where the production is maximum. The cut-in speed is the lowest wind speed where the wind turbine produces energy. At high wind speeds, the wind turbine is generally designed to stop production at a certain wind speed, often referred to as the cut-out speed. The rotor is equipped with a braking mechanism to bring the rotor to a standstill at the cut-out speed. This is to avoid damage to the rotor because of the significant load on the mechanism during high wind speeds. [29]

A wind turbine can include a pitch control. This is a power control mechanism designed to turn the rotor in the direction of the wind as well as pitching the blades. This is done to optimize the power production. Blade pitch control is achieved by rotating the blades around their longitudinal axis, generally a fraction of a degree at a time. [30]

3.2 Solar Power and Photovoltaic Systems

Solar power has the potential to be the most important energy source in the world as earth receives 15 000 times more energy than the worldwide energy demand. [31] To be able use the energy emitted from the sun, photovoltaic cells have been developed. The energy in the photons are converted into usable electric energy by a process know as the photovoltaic effect, which is utilized in PV cells. [32]

3.2.1 Solar Radiation

Solar radiation, the energy emitted from the sun, can be divided into three components; direct radiation, diffuse radiation and reflected radiation from other surfaces, as illustrated in figure 3.2. [33]

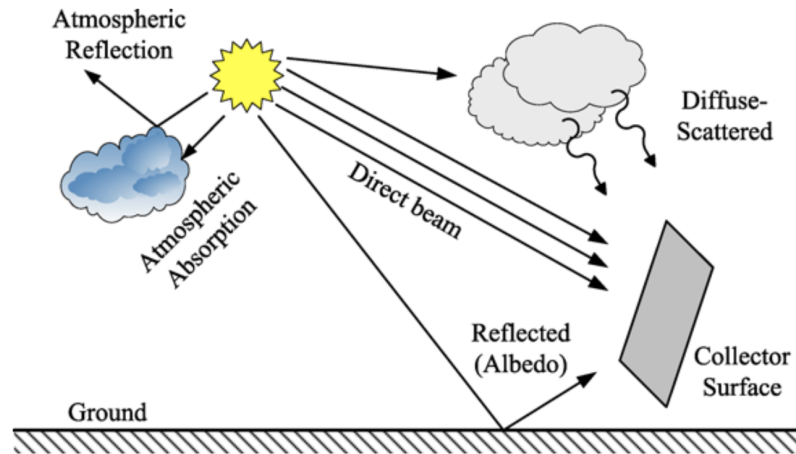


Figure 3.2: The three solar radiation components; direct radiation, diffuse radiation and reflected radiation. [33, p.198]

Solar radiation has to pass through the atmosphere to reach the earth. Direct radiation will pass unhindered through the atmosphere, without being scattered by dust or molecules. Direct normal irradiance (DNI) is the radiation perpendicular to the surface. [34, 35]

On the other hand, diffuse radiation is a result of radiation being scattered and sent in all directions. A portion of the scattered radiation will reach the earth as diffuse radiation. Diffuse horizontal irradiance (DHI) is radiation reaching a horizontal plane. Further, a portion of the radiation will be scattered back into space, be absorbed or reflected by atoms and molecules in the atmosphere. In addition, the degree of cloudiness is relevant as a light cloud cover will scatter radiation and a heavy cover will absorb radiation. [34–37]

The third component is solar radiation reflected from other surfaces. The reflection, consisting of both direct- and diffuse radiation, depends on the specific surface and its applied albedo value. The albedo value varies between 0 and 1, and accounts for a surface’s ability to reflect radiation, where a higher value indicates a higher ability to reflect sunlight. A selection of surfaces and their respective albedo value are presented in table 3.1. [38, 39]

Table 3.1: Surfaces and their respective albedo. [38, p.13]

Surface	Albedo
Fresh snow cover	0.80 - 0.90
Old snow cover	0.45 - 0.70
Plain earth	0.17
Asphalt	0.15
Wood	0.05 - 0.18

Radiation Intensity

Various atmospheric conditions such as weather, pressure and pollution will affect solar radiation as it passes through the atmosphere. As the earth rotates throughout the day, the distance through the atmosphere will change and is therefore of importance. [33] At midday, when the sun is directly overhead a specific point, the distance through the atmosphere to that point is the shortest possible. The sun is then positioned in zenith and the radiation intensity at the specific point is AM1. AM, or air mass, is a factor accounting for the impact that the atmosphere has on the radiation intensity. [37]

With an increased distance through the atmosphere, the portion of the radiation that gets absorbed or scattered increases, therefore decreasing the radiation intensity. Figure 3.3 illustrates how the distance through the atmosphere, to the same point on earth, increases as the earth rotates. [37, 38]

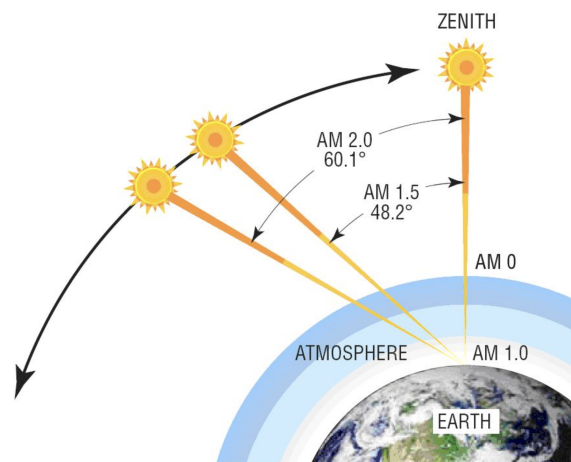


Figure 3.3: An illustration of how the distance through the atmosphere increases as the distance between the sun and zenith increases. [40]

Earth's rotation around its axis will affect the radiation intensity during the day. However, the earth's orbit around the sun will affect the intensity during the year. For instance the Northern hemisphere will tilt towards the sun during the summer and away from the sun during the winter. In addition, the earth's orbit is elliptical, hence the distance between the sun and the earth varies throughout the year. As a result, a specific area experiences varying radiation intensity and duration of sunlight during a year. [33]

3.2.2 Global Horizontal Irradiance

The total global horizontal irradiance (GHI) is the total irradiance on a horizontal surface. GHI consist of both DHI and the perpendicular component of DNI that reaches the horizontal plane. [35]

The GHI for a tilted plane also has to account for the reflected radiation from the ground. In addition, DHI will change as not all the diffuse radiation will reach the plane. [35] Figure 3.4 presents a world map illustrating the varying GHI in the world. It can be observed from the figure that the GHI is higher closer to equator. [41]

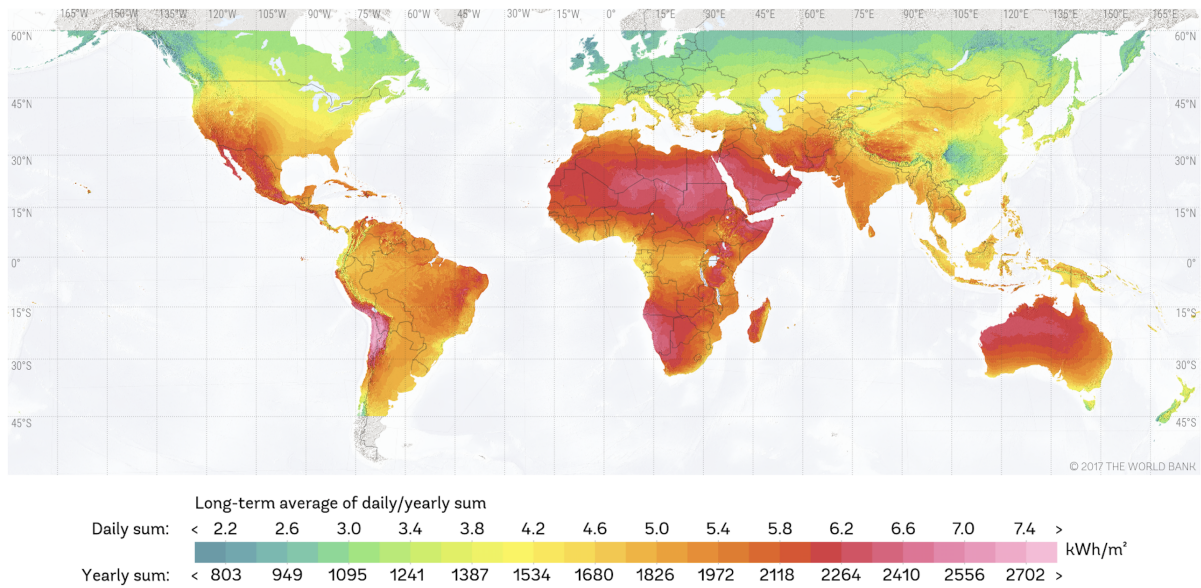


Figure 3.4: World map illustrating the varying GHI in the world. [41]

Measuring Solar Irradiance

Solar irradiance can either be measured by ground based measurement stations or satellites. There are several ground based measurement stations around the world owned by both governments and private institutions. The sensors available and the topography impacts whether the measurement stations could be utilized for solar irradiance measurements. This is because the irradiance is significantly dependent on the topography, and may vary over short distances. In addition, it is important that the station undergoes regular maintenance. If this is not the case, it is difficult to evaluate the accuracy of the measurements. [42]

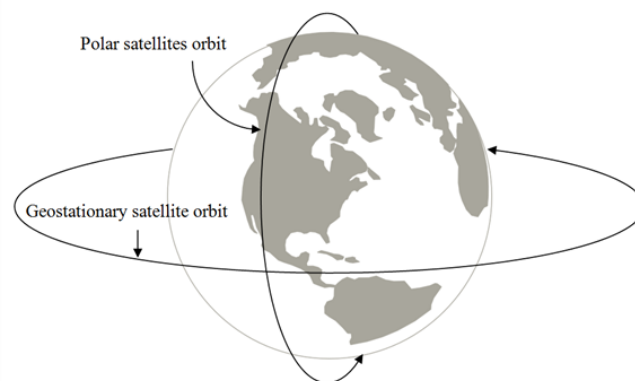


Figure 3.5: Geostationary- and polar orbits for satellites. [43]

Figure 3.5 illustrates the orbits for geostationary- and polar satellites, which are also used to measure solar irradiance worldwide. Geostationary satellites orbit around equator and will have a higher inaccuracy at northern altitudes due to the curvature of the earth. Geostationary satellites have a steep angle when measuring at these altitudes. With geostationary measurements, Norway has a large gap in measured solar irradiance at 640-900 kWh/m² due to uncertainty related to these measurements. Polar satellites orbit around the poles and is therefore better suited for higher altitudes. [42]

3.2.3 Planning and Installing a Photovoltaic System

A photovoltaic system is either grouped as a stand-alone system or a grid-connected system. A stand-alone system can be realized with or without energy storage. Solar energy is usually combined with energy storage or used as a part of a hybrid system, due to unpredictable energy production. A grid-connected system has a connection to the utility grid, either directly or via a house grid. [38]

Components of a PV System

The main component of the PV system is the PV module. PV modules consist of many PV cells connected in series to. Therefore, increasing the module voltage to the number of cells times the cell voltage. The module current is the same as the cell current and the module power output is limited by the cell with the lowest output. [44] A PV cell utilizes the potential between two layers of semiconductor material which forces the excited electrons to flow in an external circuit. [32]

There are various semiconductor materials usable in PV cells. Silicon is the most common, and crystalline silicon PV cells are in high production. There are two major types of the silicon cells, monocrystalline and multicrystalline. The two types share the same theoretical background, but there are some variations. Monocrystalline cells are cut from a single silicon crystal and are the most efficient type in common use. The manufacturing process is expensive, as a large crystal is required. By contrast, the production of multicrystalline silicon cells, also known as polycrystalline cells, have a lower cost as fragments of silicon crystals instead are melted together in the manufacturing process. However, the efficiency for the modules are lower than for monocrystalline modules. [45, 46]

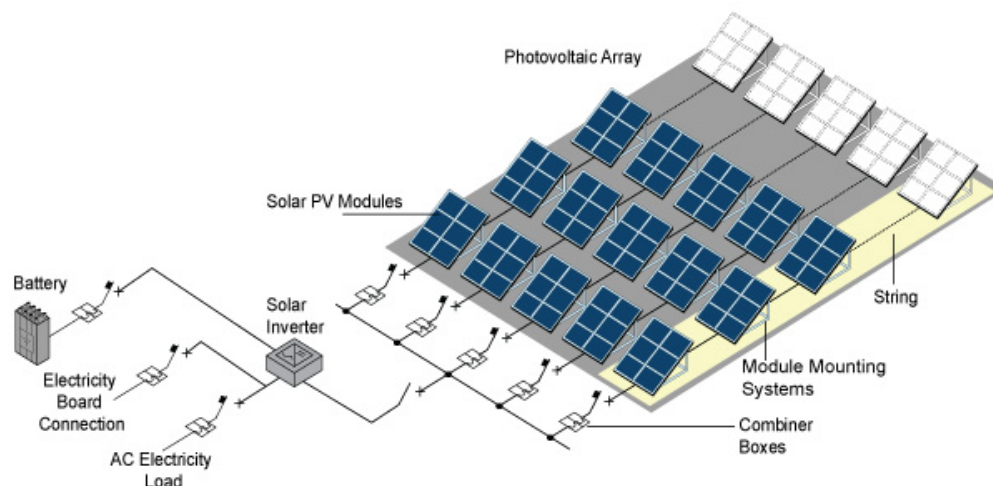


Figure 3.6: An illustration of a PV system with the most relevant components named. This includes string, array, inverter and modules. [47]

In addition to the module itself, there are other components in the system. Figure 3.6 illustrates a PV system and its components, and the most relevant components are further described below.

String: A string is a set off modules connected in series. [48]

Array: The PV modules are connected either in series, parallel or in a combination of both, to create an array. [44]

Inverter: An inverter is used to convert DC to AC. This is required as the PV arrays produce DC, and it needs to be converted into AC with the correct frequency and voltage to be suitable for the utility grid or household appliances. [48]

Power optimizer: The main function of the power optimizer is to increase power output by always tracking the maximum power point of the connected modules. It also monitors the performance data of the modules and communicates this back to the monitoring platform. Usage of a power optimizer will increase the production if a shadow is blocking the module during the day. [49]

Considerations

A consideration to be made is the orientation of the PV modules. In the Northern hemisphere the PV system should point south towards the midday sun. [44] Two important angles that can be used to describe the orientation of the PV modules are the tilt angle and the azimuth angle. The tilt angle is the angle between the surface of the PV module and the horizontal surface. [37] The azimuth angle is the angle between south and the direction of the PV module as presented in figure 3.7. If the angle is 0° the module is pointed south. [33]

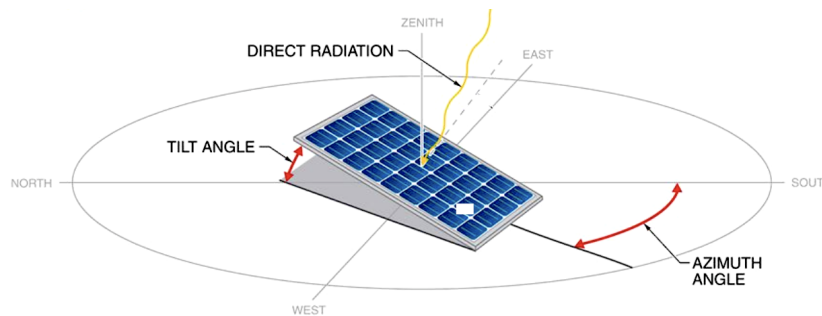


Figure 3.7: Important angles to determine the orientation of a PV module. Note that changes have been made from the original figure. [50]

Further, the suns trajectory over the PV site should be considered as the trajectory varies with both the of the time of the day and year. As the solar noon varies during the year, the PV modules should be tilted from the horizontal so that the sun beams are normal to the module surface. This is in order to capture the solar irradiance at noon. [44] The suns trajectory can be graphically represented in a sun path chart as presented in figure 3.8.

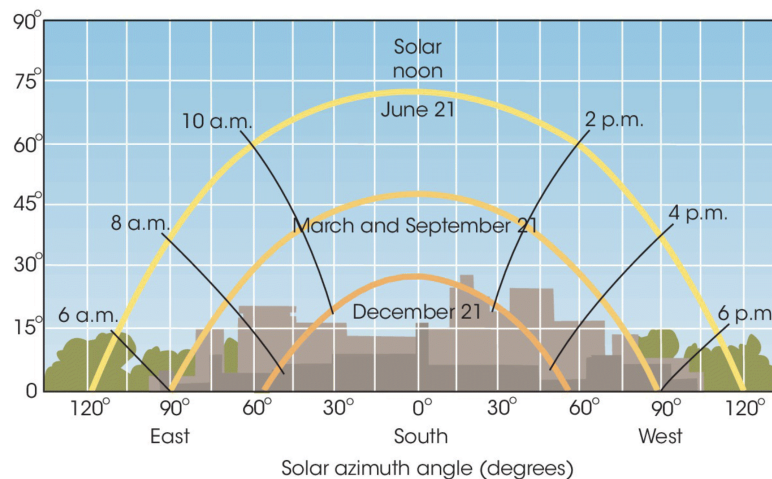


Figure 3.8: The sun path chart illustrating the suns trajectory at different times of the year. [44]

The sun path chart can also be used to study the shading at a PV site. The degree of shading depends on the sun's trajectory. Knowing the shading at a PV site is important as it can reduce the output from the modules. [44] There are two types of shading to consider, far shading and near shading. Far shading is shading from objects far away from the PV field, usually more than 10 times the size of the total PV system. This is e.g. a mountain obscuring the horizon. Near shading is shading from nearby objects e.g. a chimney or a tree. [51]

There should also be solar irradiance measurements at/nearby the site or a simulation of the irradiance. As it is important to determine the PV systems potential production and thus correctly determining the system size. The protective glass on the PV module will decrease the actual amount of radiation reaching the module. This is array incidence losses and the designated term is incidence angle modifier (IAM). The incidence angle is the angle between the perpendicular of the module and the solar irradiation. [52]

Further, the weather at the PV site should also be taken into account. The weather impacts the solar irradiance and an increase in temperature will create losses in the PV module. Soiling losses may occur due to accumulation of unwanted substances that stay on or around the modules and therefore block the sun from reaching the module e.g dust, dirt and snow. [53] The albedo value from nearby surfaces will also change during the year e.g snow has a higher albedo value than plain earth. [38]

3.3 Renewable Energy Sources in Norway

Approximately 98% of the Norwegian power production is from RESs. The total power production in 2018 was 146.84 TWh. This included 139.5 TWh from hydro power, 3.9 from wind power and 3.7 TWh from thermal power. The balance is presented in figure 3.9 [54, 55] Norway is in a good position to contribute to supply the future energy demand with RES. [26]

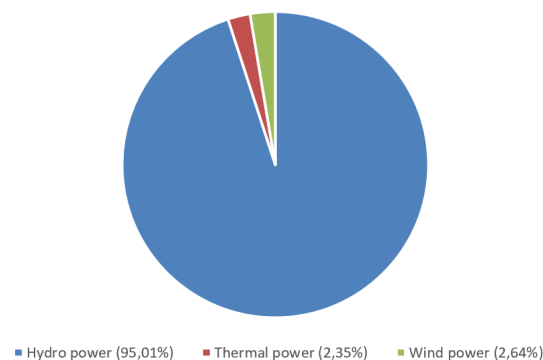


Figure 3.9: Energy production balance in Norway in 2018. Hydro power is the most dominant source with 95% of the electricity production. The resulting electricity production is thermal and wind power. [55]

Wind Power Status and Potential

By the end of 2018, the total installed wind power capacity was 1695 MW. There is additional capacity under development, and as of February 2019, there is 2315 MW under development. Assuming 3500 full load hours, this will increase the annual Norwegian wind power production from 3.9 TWh to 12 TWh. [56]

The overall wind speed in Norway is generally higher in the winter months than in the summer months. This is illustrated in figure 3.10. The figure illustrates the wind speed distribution over the days of the year. The data is based on 30 years of hourly weather model simulations. [57]

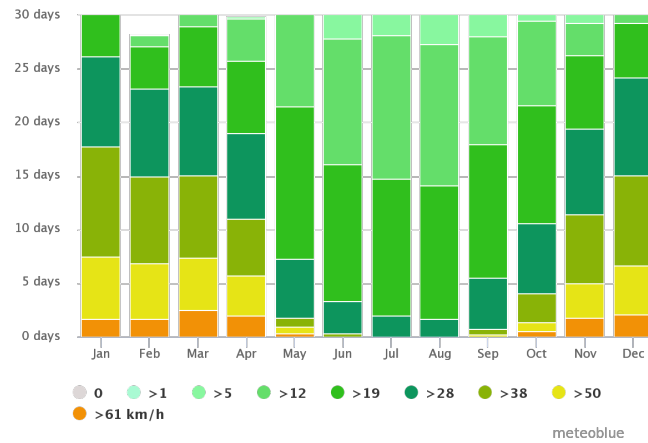


Figure 3.10: Wind speed distribution in Norway over the year stated in amount of days with a certain wind speed. [57]

In Norway, the lowest average wind speed is in July and August, with a speed of about 12 km/h, which equals 3.33 m/s. The highest average wind speed is in January, measured at about 30 km/h, or 8.33 m/s. [57]

Knowledge of the wind conditions in the area of a wind turbine or wind park is essential to optimize the production. The turbine is designed to utilize the wind of the given conditions. Wind data is acquired from measurements and simulations, as well as approximations from statistical distributions. [58]

Solar Power Status and Potential

Installed solar power in Norway has had a significant growth, especially in grid connected systems. The installed power capacity increased by 52% from 2017 to 2018, resulting in 68 MWp installed capacity. [59]

The solar irradiance in Norway varies between 700-1 000 kWh/m² with the highest solar irradiance in the southern and eastern parts of the country. Even though the solar irradiance is in the lower scale of earths solar irradiance, Norway receives 1 500 times more energy than the energy demand. However, the solar irradiance vary during the year. The highest irradiance is during the summer months May to July and lowest during the winter months January and December. [31] Figure 3.11 presents the variation in GHI during January and July in Norway.

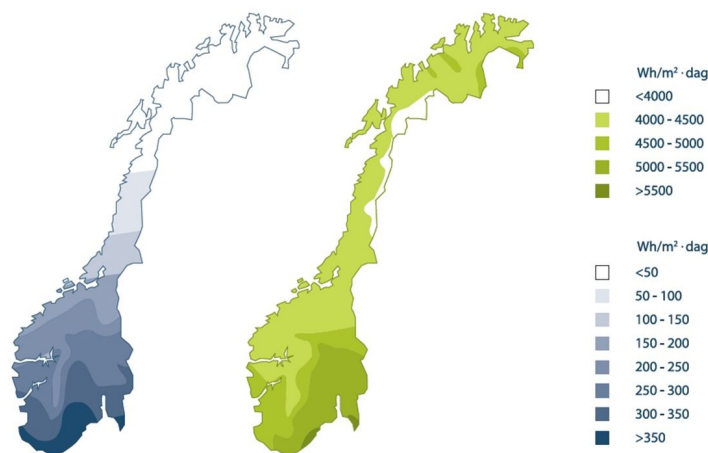


Figure 3.11: Map over Norway illustrating the varying GHI in Norway during January and July. [60]

Combination of Solar- and Wind Power

Wind- and solar power have uniquely compatible energy production curves in Norway. This can be observed from the characteristics of average wind speeds and GHI during a year, respectively in figure 3.10 and figure 3.11. The wind production normally peaks during the winter months, while the solar production peaks during the summer months. [57, 60]

This results in wind- and solar power being highly compatible when designing a microgrid where power is required consistently. This can help offset the inconsistency problem related to renewable energy generation. Essentially the combination should provide a smoother energy production curve. [57, 60]

3.4 Renewable Energy Generation Costs

The economy and the costs related to renewable energy are central for the development of green energy, and reduced costs of renewable energy generation is an important driving force to increase investments in renewable energy projects.

3.4.1 Economic Analysis of Renewable Energy Projects

To evaluate an investment in a renewable energy project there are some important parameters that need to be defined. These include net present value (NPV) and levelized cost of energy (LCOE).

Net Present Value

NPV indicates whether a project is economically viable. It is the sum of all the cash flows in the project lifetime, discounted to the year of the investment. There are different factors that need to be mapped out to find the NPV of a project. The investments and the future cash flows must be identified. The cash flow includes the difference between the costs associated with operation and maintenance and the possible income. The next step is to identify an appropriate discount rate, and discount the future cash flow to a present value. The NPV for a year n after the investment with a lifetime of T and a discount rate r is calculated as in equation 3.1.

$$NPV = \sum_{t=1}^T \frac{C_t}{(1+r)^t} - C_0 \quad (3.1)$$

C_t is the net cash flow in the year t , and C_0 is the investment cost for the project. [61] The discount rate is used to estimate how much the future cash flows are worth in the present (present value), and can be used to check if a project is profitable. The rate is risk-adjusted return requirement, and a high discount rate equals a high risk. Norges vassdrags- og energidirektorat (NVE) uses a discount rate of 4% for renewable energy projects. [62] The feasibility of a project must be evaluated when the investment cost as well as future cash flows has been discounted to a present value. [63]

Levelized Cost of Energy

LCOE is a useful metric to compare different components in an energy system in a cost perspective. LCOE incorporates initial costs as well as ongoing operating and maintenance costs. The unit for LCOE is NOK/kWh, and is calculated as in equation 3.2. [64, 65]

$$LCOE = \frac{\text{Total annual cost}}{\text{Annual power output}} = \sum_{t=1}^T \frac{\frac{I_{C,t} + M_t + F_t}{(1+r)^t}}{\frac{E_t}{(1+r)^t}} \quad (3.2)$$

The total annual costs in the year t include the investment and expenditures, $I_{C,t}$, the operation and maintenance costs, M_t , and the fuel costs, F_t . The annual energy output in the year t is E_t . r is the discount rate, and T is the expected lifetime of the energy source. The total annual costs are costs directly associated with the energy system, and do not apply to external costs, for example due to pollution from the energy system. [64, 66]

3.4.2 Cost Trends of Renewable Energy Sources

The International Renewable Energy Agency (IRENA) states that there has been a global average cost reduction of 73% between 2010-2017 of utility scale PV-projects. The significant cost reduction is illustrated in figure 3.12, where the LCOE has been reduced from 0.36 USD/kWh in 2010 to 0.10 USD/kWh in 2017 (approximately 2.99 to 0.83 NOK/kWh).

When it comes to onshore wind, the LCOE has been reduced from 0.08 USD/kWh in 2010 to 0.06 USD/kWh in 2017 (approximately 0.67 to 0.50 NOK/kWh), which equals a cost reduction of 25%. [67] The Norwegian currency values are based on the monthly average of December 2017, where 1 USD was worth 8.3147 NOK. [68]

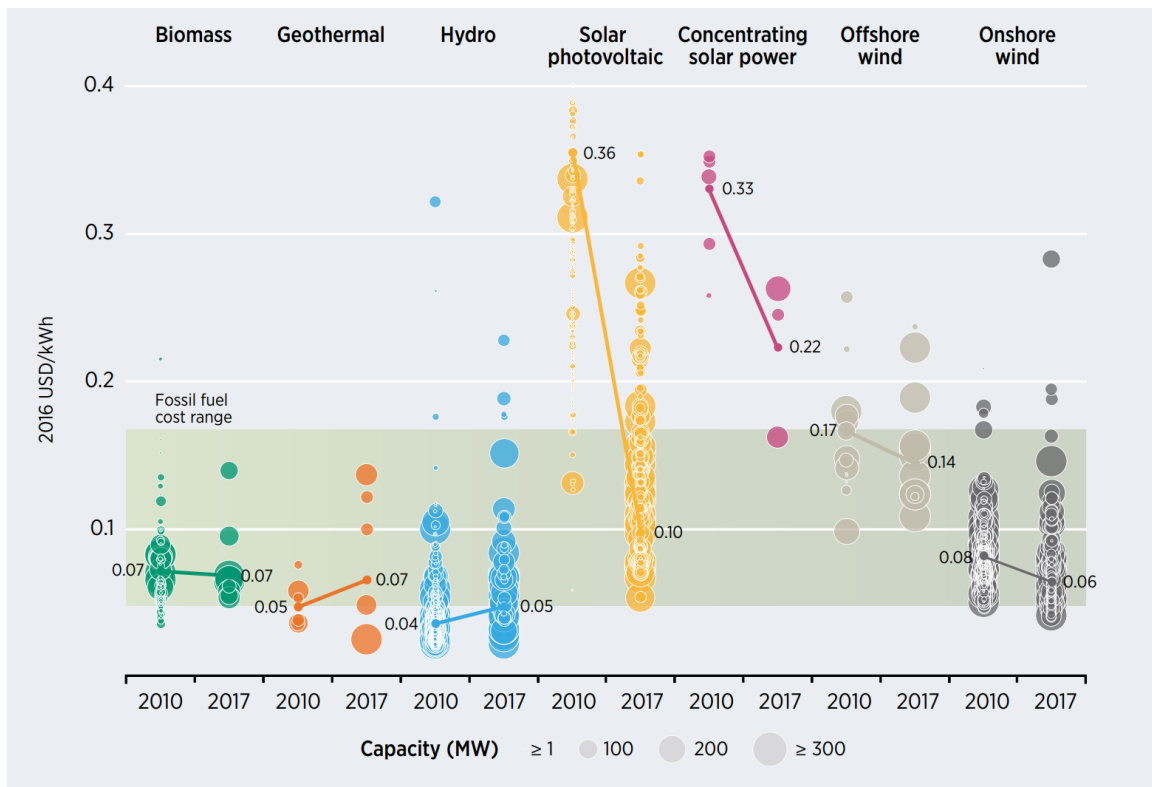


Figure 3.12: Global LCOE from utility scale renewable energy generation technologies, 2010-2017. [67]

The cost reduction driving forces for RES are primarily technology improvements, competitive procurement and a large base of experienced, internationally active project developers. [67] The energy generation prices for renewable energy sources are expected to continue decreasing through 2020 and onward. As illustrated in figure 3.12, the development of the prices of both solar PV and onshore wind will continue to decrease, reaching a LCOE which is lower than the fossil fuel cost range. [67]

According to NVE, the LCOE for solar- and land based wind power will be reduced significantly in Norway from 2018 to 2040. [62] Figure 3.13 presents the projected development of LCOE from 2018 to 2040 from NVE.

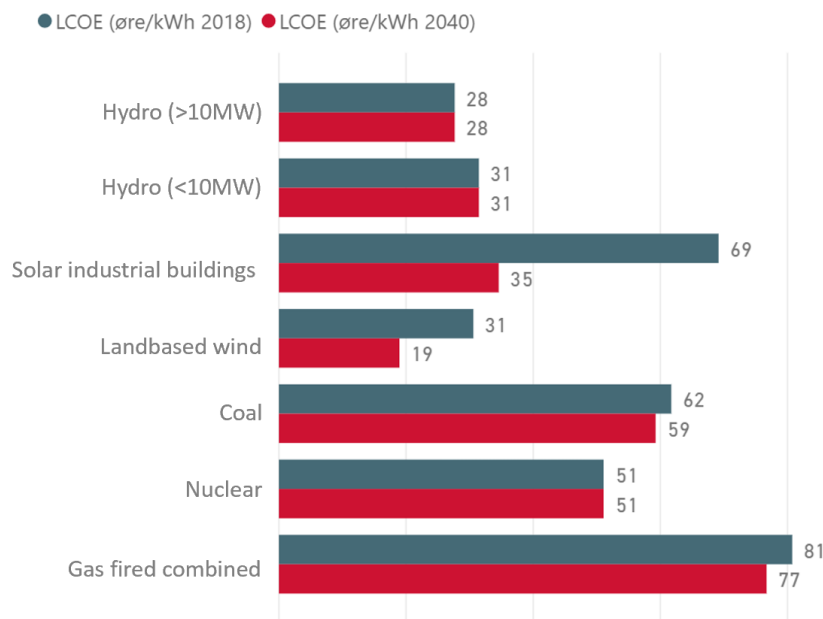


Figure 3.13: NVEs prediction for LCOE development from 2018-2040 in øre/kWh. [62] Note that the figure is translated from the original source.

The numbers are based on a technology improvement factor based on assumptions from NVE. The discount rate used is 4%. The figure illustrates that the LCOE for solar power will be reduced below the costs for coal, nuclear and gas with a LCOE of 0.35 NOK/kWh, and land based wind will be the most competitive energy source with a LCOE of 0.19 NOK/kWh. [62]

Chapter 4

Energy Storage Technologies

One of the main obstacles concerning renewable energy is the unpredictability. It is impossible to know if the wind will blow in half a year or if there will be enough sun irradiance to produce the required energy for the next month. This is an even bigger issue in Norway, considering the low production from the PV systems during the winter months. One way to solve this problem is by storing the produced energy in an ESD.

This chapter will present two such ESDs, the Li-ion battery and the HESS consisting of an electrolysis cell, storage tank and fuel cell combination. The principle of configuration of the two technologies are explained, as well as the status in the market as of 2019.

4.1 Lithium-ion Battery

The principle of the Li-ion battery is converting chemical energy to usable electrical energy. This is accomplished by utilizing the cell potential between a positive oxide cathode and a negative carbon anode, separated by a porous polymer membrane. The cathode can be e.g. manganese- or sulfur oxide. The separator allows solely positive ions through, and prevents short circuit between the sides. [69, 70]

The battery is based on a red-ox reaction, which as the name indicates consist of a reduction and an oxidation reaction. Reduction is when an atom, molecule or ion receives electrons and the reaction takes place on the cathode. Oxidation is when an atom, molecule or ion gives off electrons, and the reaction takes place at the anode. Lithium is commonly used because it is the lightest metal and Li^+ -ions have a high standard reduction potential (SEP). SEP is an atom, molecule or ions ability to receive electrons. [71] Therefore Li-ion batteries have a high power to weight ratio, and consequently the energy density is high. This makes the Li-ion battery applicable for energy storage, both in mobile- and stationary applications. [70]

During recharge, electrons are forced from the cathode to the anode, when the external circuit is connected to a energy source (e.g. a wind turbine generator). The energy source is represented by a charger in figure 4.1a. Consequently the positive Li^+ ions follow the electrons to the anode, through the membrane. One complete discharge and recharge is considered a cycle. [69]

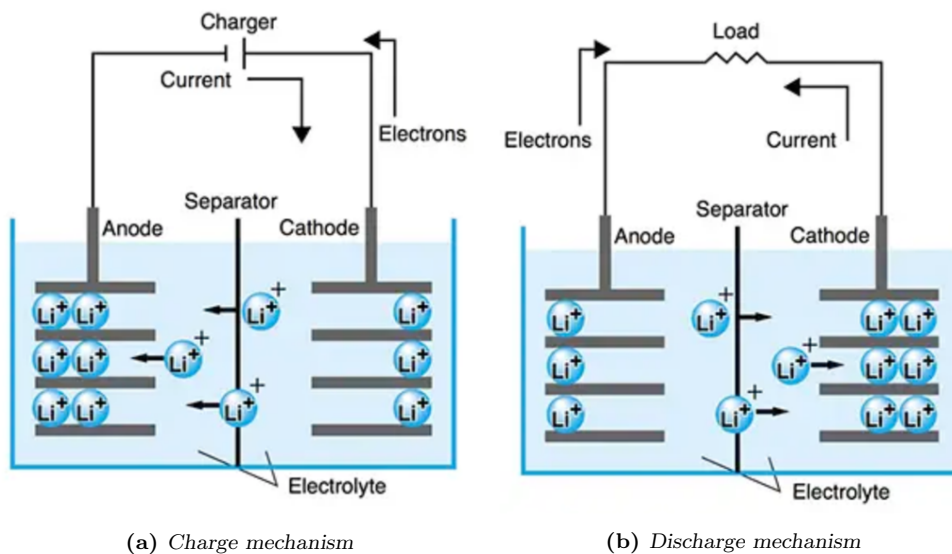


Figure 4.1: Description of charge- and discharge mechanism of Li-ion batteries. [72]

During discharge, Li^+ ions move from the anode, through the electrolyte, via the membrane and to the cathode because of the potential difference. The electrons consequently flow through the external circuit as presented in figure 4.1b. The external circuit is connected to a load.

The capacity of a Li-ion battery is the amount of electrical energy which can be retrieved from discharging the battery, and is stated in kWh. Li-ion batteries are generally recommended to be charged between a State of Charge (SoC) of 20%-90%. [73] SoC is the percentage of the total capacity the battery is charged. The Depth of Discharge (DoD) is the percentage of the capacity to which the battery discharges, where a DoD of 100% means total discharge. A total discharge will shorten the life span of the battery. The smaller the DoD, the longer the battery is expected to last. The concept for SoC is the same as for DoD, where the battery life span is decreased when the battery operates at a SoC of 100%. [74]

If it is assumed that the battery is charged between 20% and 90% SoC, which is the general recommendation for SoC, the usable energy in the battery is reduced to 70% of the total capacity. The battery efficiency is the ratio between the input power during the charging of the battery, and the output power during discharge. The battery efficiency is usually high, because there are minimal losses due to internal resistance. [75]

C-rates describe how fast a battery can maximally charge or discharge. The C-rate is stated as e.g. 1C, which implies that a battery of 1 kWh can deliver 1 kW for one hour. Another example is a battery with a capacity of 550 kWh and a C-rate of 2C can deliver 550 kW for half an hour. [76]

4.1.1 Battery Market

With an increasing implementation of unpredictable RESs, it is increasingly important to have ways to store the produced energy. The Li-ion battery has proved to be the leading technology in battery storage for mobile- and industrial applications. As the Li-ion technology has matured with increasing usage over the last few years there have been a significant decrease in prices. Figure 4.2 presents the actually prices and the predicted decrease in prices until 2030. [77]

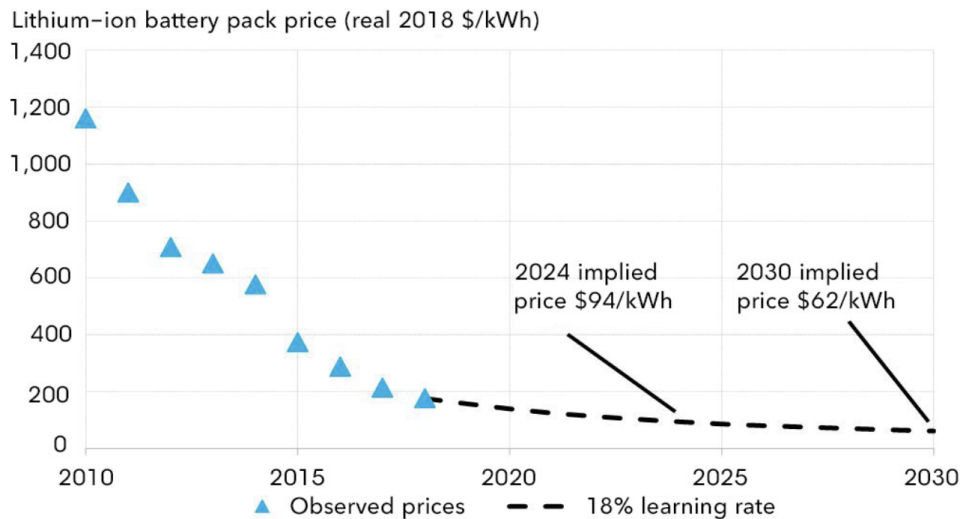


Figure 4.2: Battery prices until 2018 and prediction of prices until 2030 for Li-ion battery packs. [77]

4.2 Hydrogen Energy Storage System

Hydrogen being the most simple element is also the most abundant element in the world. Due to hydrogen only having one electron, it is highly reactive. This means that most of the hydrogen is in some sort of compound. The challenge with hydrogen gas as a storage medium, is that in order to use hydrogen gas in a fuel cell, the hydrogen gas has to be close to 100% purity. This is to avoid a rapid decrease in performance of the fuel cell. To achieve this level of purity, the hydrogen gas has to be separated from its normal state within compounds consisting of other elements. [78]

This can be done in several ways, but in order for it to be renewable the hydrogen is extracted from water in a process called electrolysis with the use of electricity from a RES. After the hydrogen is extracted, it can be stored in a pressurized tank and further utilized for power production with the use of a fuel cell. [78]

Hydrogen gas has a much higher energy density than gasoline and other common fuel sources. On a mass basis hydrogen has nearly three times the energy content of gasoline. Hence it is not needed to store as large amounts of hydrogen in mass as other fuels in order to store large quantities of energy. Gasoline has an energy density of approximately 44 MJ/kg, in comparison hydrogen has approximately 120 MJ/kg or 33.33 kWh/kg. The energy capacity in the tank is the product of the tanks mass capacity and energy density. However, since the natural state of hydrogen is in gas form it will take up significantly more volume or need to be compressed in order to be stored efficiently. [78]

The carbon footprint of hydrogen varies greatly depending on how the hydrogen gas is produced. If the production is from sources with relatively low carbon intensity, the carbon footprint will primarily be from gathering and the decommissioning of the unit. The result will thus be a low carbon footprint overall from hydrogen technologies. However, this can change a lot if the hydrogen is produced from fossil fuels. This is also how most of the hydrogen is produced as of 2019. [79]

4.2.1 PEM Fuel Cell and Electrolysis Cell

There are several different electrolysis- and fuel cell technologies available, all with their own strengths and weaknesses. One of the most commonly used is based on the Proton Exchange Membrane (PEM) technology, which is used both for fuel- and electrolysis cells. The concept behind electrolysis is illustrated in figure 4.3a. In a PEM electrolysis cell (PEMEC) power is applied in a circuit, forcing an oxidation reaction on the anode side. This causes electrons to flow from the anode to the cathode.

Further, this produces oxygen which is left on the anode side while the hydrogen ions pass through a polymer membrane over to the cathode side. On this side a reduction reaction takes place where the electrons and protons fuse and thus the desired product hydrogen, H_2 is formed. There will be substantial energy losses during this process as heat is produced alongside the H_2 during the reaction which causes the efficiency to decrease. [78]

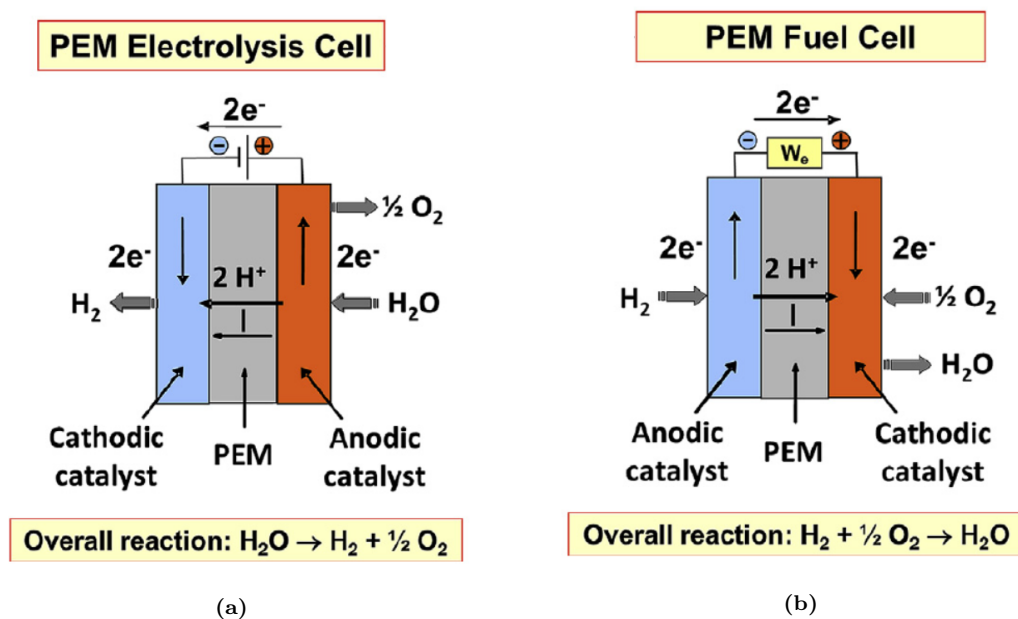


Figure 4.3: Illustration of a PEMEC and PEMFC showing how they produce hydrogen gas and generate electricity. [80]

A PEM fuel cell (PEMFC) works similarly to the PEMEC, except in reverse. As illustrated in figure 4.3b the hydrogen gas is fed into the anode where an oxidation reaction occurs. This results in an electron flow that can be used by connecting an external circuit that eventually will end at the cathode. On the cathode oxygen is fed in from air and then the reduction reaction takes place yielding the final product, H_2O . [80]

4.2.2 Hydrogen Market

The hydrogen market is in a testing stage with lacking infrastructure and few consumers, however, it is developing. As of March 2019, companies are primarily testing out prototypes such as hydrogen driven trucks, cars and ferries. There are few commercially available options, however, it is expected that hydrogen driven vehicles will be more prevalent in the future. Therefore, increasing the demand for hydrogen gas supply in the industry. [81–83]

As of March 2019, most of the hydrogen is produced in non renewable ways, mainly by steam reformation. This could change as the cost of hydrogen gas production by electrolysis is expected to decrease, and RESs are increasing worldwide. Further, there is a lot of research being done on H_2 technologies in universities, including the Norwegian University of Science and Technology (NTNU) and the independent research organization SINTEF located in Trondheim. [81–83]

In order to supply hydrogen gas, the infrastructure has to be expanded. According to the Norwegian hydrogen forum there exist five refueling stations in Norway as of February 2019, where one is in Trondheim. [84] These station usually deliver hydrogen at a pressure of 700 bar which is the standard for hydrogen vehicles. The refuelling station owned by ASKO in Trondheim delivers approximately 350 kg H_2 per day at 700 bar at full capacity. Further, the cost of hydrogen gas is 89.9 NOK/kg H_2 by UnoX, who owns two stations in Oslo. The driving range on hydrogen gas, with this price, is comparable with the driving range for fossil fuel cars. This is based on the prices of early 2019. [84–86]

Chapter 5

Components and Case Descriptions

This chapter presents the components of Rye Microgrid. The completed Rye Microgrid consists of energy production from a wind turbine and a PV system, and energy storage in a battery and a HESS. The components specifications such as lifetime and operational limitations are presented. The PV system includes several components and these are explained. In addition, the data sheets and additional information about the components are presented in appendices.

Further, the chapter presents the cases used to approach the problem statement. The components, background, and evaluation elements for each case is explained. A schematic sketch is also presented for each case to illustrate the component set up of the various cases. Any assumptions related to the cases are also presented.

5.1 The Components of Rye Microgrid

This section presents the components used in Rye Microgrid and their specifications. This includes the wind turbine, the PV system, the battery and the HESS.

Wind Turbine

The wind turbine is a Vestas V27 225 kW with a life expectancy of 20 years. It is a 3 bladed horizontal axis turbine with a cut-in speed of 3.0 m/s and a cut-out speed of 25.0 m/s. Optimal production is between wind speeds of 14 - 25 m/s and the full power curve is presented in figure 5.1. In the beginning of October 2018 the turbine was fitted with a new pitch control system. The wind turbine also shares the same technical specifications as a Vestas V29 turbine, meaning that it is possible to increase the diameter from 27 - 29 m by adding extensions to the turbine blades. This is expected to increase the yearly production by approximately 50 MWh. [5, 87]

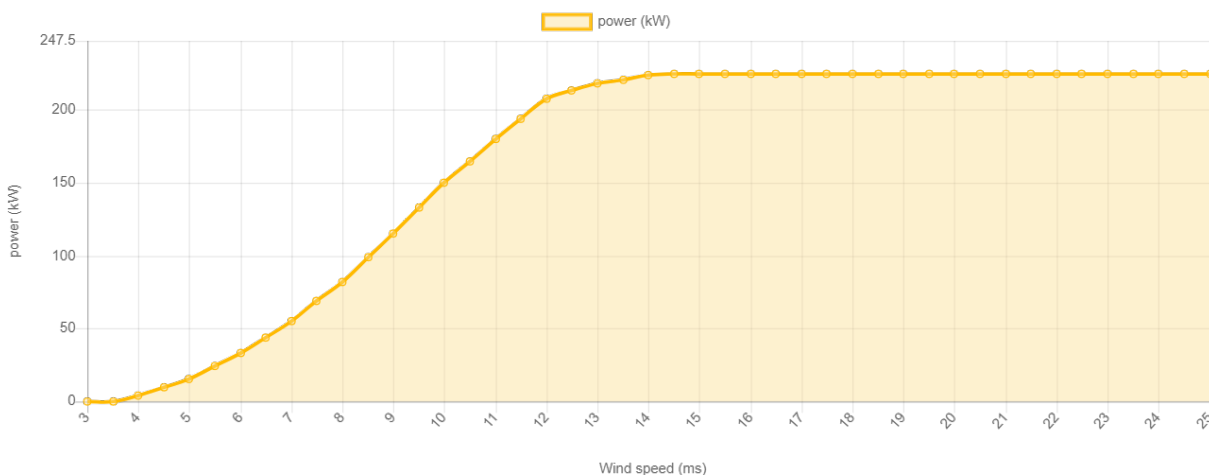


Figure 5.1: The power curve for a Vestas V27 wind turbine showing the cut-in and the cut-out speed at respectively 3.0 m/s and 25 m/s and the optimal energy production between 14-25 m/s. [87]

PV System

The PV system consists of several components and the most important components are the PV modules, the inverters and the power optimizers.

PV Modules: The PV system consists of two different PV modules, REC Twinpeak 2 Mono Series 310 Wp and REC Twinpeak 2 Series 295 Wp. REC Twinpeak 2 Mono Series is a monocrystalline module with a conversion efficiency of 18.6%, while REC Twinpeak 2 Series is a multicrystalline module with a conversion efficiency of 17.7%. The expected lifetime of the PV modules are 30 years, more detailed parameters are presented in their respective data sheets. The data sheet for the REC Mono Series module is presented in appendix A and the REC Series module data sheet is presented in appendix B. [88, 89]

Power Optimizers: There are used two different power optimizers in the PV system. The SolarEdge P650 is paired with the REC Twinpeak 2 Mono Series modules and the SolarEdge P600 is paired with the REC Twinpeak 2 Series modules. In addition, the power optimizers are equipped with a "SafeDC" feature developed by SolarEdge. This feature is designed to automatically reduce the connected modules DC voltage to a safe level if the inverter or grid is shut down. Thus providing an additional level of security. [49] Further, detailed information about the power optimizers are presented in the data sheet in appendix C.

Inverters: The PV system also includes three Solar Edge SE27.6k inverters. The inverters have a 20 year manufactures warranty and an efficiency of 98%. [90] Further details are presented in the data sheet in appendix D.

Installed System: The total installation consists of 288 PV modules at Rye. 104 modules of REC Twinpeak 2 Mono Series 310 Wp and 184 modules of REC Twinpeak 2 Series 295 Wp. The PV modules are mounted on stands secured to concrete blocks. The stands have an inclination giving the modules a tilt angle of 35% and an azimuth angle of 0%. Further, each module pair is equipped with a power optimizer in order to track the maximum power point and increase the efficiency. [49] There are three arrays consisting of 96 modules, distributed on three strings consisting of 32 modules. Array 3 is split into two sections due to an elevation at the site. Each array is connected to one inverter. Figure 5.2 presents an illustration of the PV system installed. The illustration presents the placement of PV modules in arrays and the connection to a inverter.

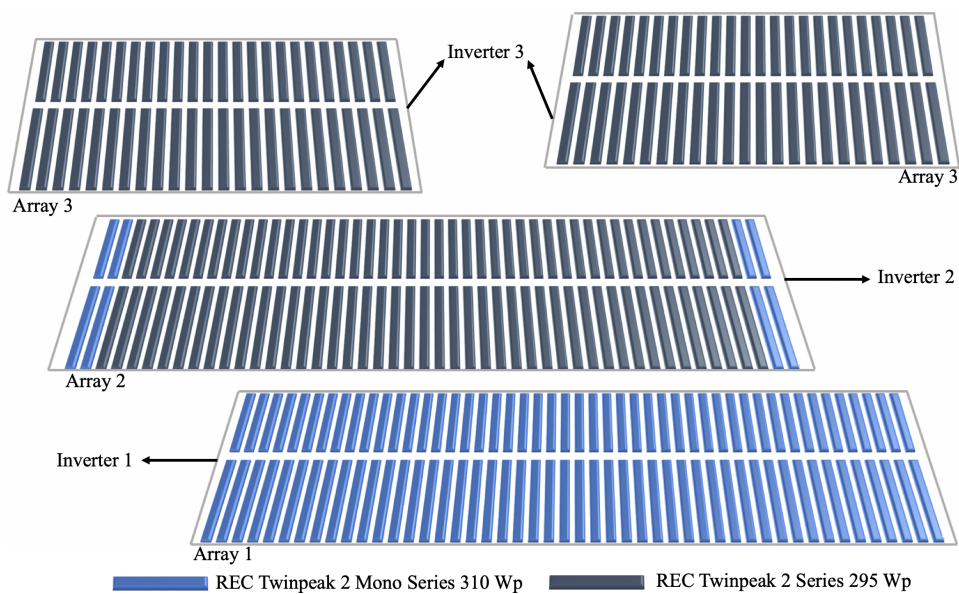


Figure 5.2: An illustration of the installed PV system based on information from Solbes AS. The illustration is an overview of the PV system, is not in exact proportions and does not include all electrical components.

Battery

The battery at Rye Microgrid consists of five racks of 110 kWh Li-ion batteries. The battery is charged between 20% and 80% SoC, leading to an effective capacity of 330 kWh. The batteries are designed to operate in the temperature conditions between -25°C and 30°C. The racks are described in further detail in appendix E. The battery has an expected lifetime of 10 years considering 400 complete cycles per year. It has a rate of charge and discharge limit at 1 100 kW. The battery has an efficiency of 93%. [2, 91]

Hydrogen Energy Storage System

The HESS at Rye Microgrid consist of a PEMEC, a storage tank and a PEMFC. The PEMEC is in use when the battery is above 80% SoC and is rated at 55 kW with an efficiency of 63%. The produced hydrogen gas is stored in a 30 bar tank with a total mass capacity of 100 kgH₂ and energy capacity is 3.33 MWh. The PEMFC is only in use when the battery is at 20% SoC and is rated at 100 kW with an efficiency of 49%. The expected lifetime of the complete hydrogen unit is 20 years, however, every 10 years the electrolysis cell require replacing. [2]

Transformers

There are three transformers on the site, of which there are two Siemens 415 V/22 kV transformers and one Norsk Transformator AS 240 V/22 kV transformer. The specifications for the transformers are presented in table 5.1.

Table 5.1: Transformer specifications for the two transformer types on the site.

	Transformer 1&3 (T1&T3)	Transformer 2 (T2)
Voltage	415 V/22 kV	240 V/22 kV
Nominal power	315 kVA	100 kVA
No-load loss	360 W	202 W
Load loss	2 900 W	1 264 W

5.2 Case Descriptions

The five cases of Rye Microgrid make it possible to highlight the different attributes of the components. The case structures allows insight in the interaction between separate components and how they complement each other. The case description clarifies the motive of each case, explains the various structures of the microgrid and how the cases are used in the evaluation of Rye Microgrid.

Base case

The base case is a scenario where the consumer is supplied entirely with power from the grid. It provides a foundation for evaluating the integration of Rye Microgrid. The base case is used as a reference both when evaluating the economic aspect and the environmental impact of Rye Microgrid.

Case Wi

In case Wi, the wind turbine's supply to the consumer is of interest. The wind turbine is the first component that was installed at Rye Microgrid. It is the only component that will remain on the site after the completed project. The wind turbine is connected to the consumer and TEN by T1 and T2. A schematic sketch of the case structure is presented in figure 5.3.

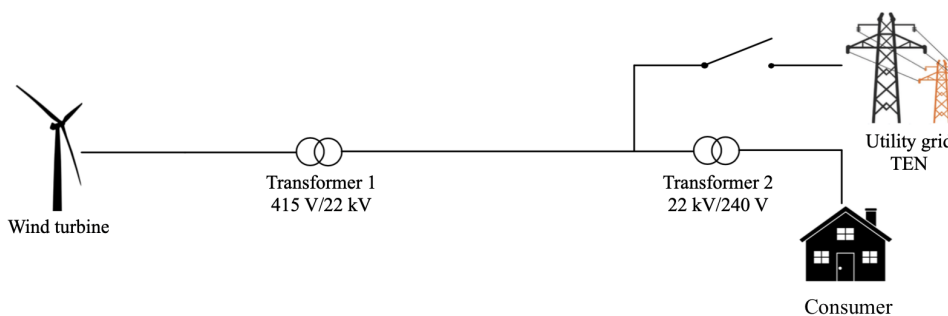


Figure 5.3: Schematic sketch of case Wi, presenting the connection between the wind turbine, the consumer and TEN.

The focus of this case is to examine how the energy produced from the wind turbine meets the consumption, and use this for further reference. The consumer is connected to the grid for security of supply. The case study consists of an evaluation of the percentage self supply from the wind turbine alone, and the income and expense from exchange with TEN.

The case is used as a reference for cases WiSo and WiBa, as further investments in the components is possible after the completed project. It is therefore of interest to evaluate the security of supply, economic aspect and environmental impact for further comparison.

Case WiSo

In case WiSo, the PV system is of interest in addition to the wind turbine. The PV system assumed to be connected to the same transformer as the wind turbine. Hence, case WiSo consists of a wind turbine, PV system, T1, T2, the consumer and connection to TEN. The schematic sketch of the system in case WiSo is presented in figure 5.4.

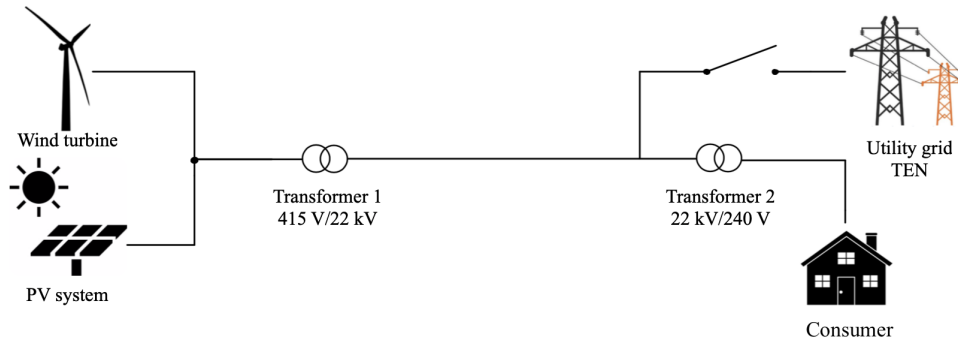


Figure 5.4: Schematic sketch of case WiSo, presenting the connection between the wind turbine, the PV system, the consumer and TEN.

As an investment in the PV system is a possibility for the consumer after the completed project, there is value in evaluating this case. Like case Wi, the focus is to analyse the self supply. In case WiSo, the energy production is increased, and the impact of the PV system on the self supply share is assessed. In addition, the profitability is an essential factor to the investment. The profitability of the case is evaluated by considering the income and expense from net exchange with TEN.

Case WiBa

Another possibility for the consumer is to invest in the battery rather than the PV-system. Hence, case WiBa focus on the wind turbine in combination with battery storage. The motive is to evaluate how the self supply percentage changes when there is storage capacity available. The schematic sketch of the microgrid in case WiBa is presented in figure 5.5.

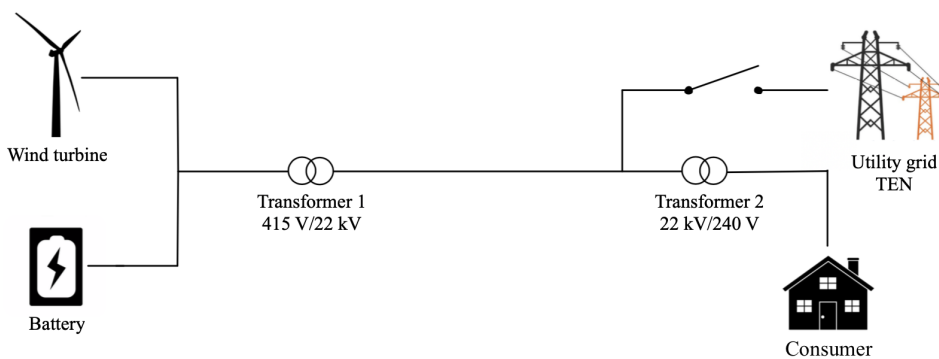


Figure 5.5: Schematic sketch of case WiBa, presenting the connection between the wind turbine, the battery, the consumer and TEN.

As in case Wi and case WiSo, the consumer needs to be connected to the utility grid to ensure security of supply. In contrast with the previous cases, the excess energy produced is used to charge the battery before the surplus is sold to TEN. Therefore, the energy stored in the battery is used when there is a production deficit. However, if the battery is fully discharged the consumer needs to purchase energy from TEN.

An important consideration when evaluating an investment in the battery energy storage is the economic outcome. There is a significant investment cost related to the battery. The costs that are evaluated in the economic analysis is the exchange with TEN, and the money saved from using stored energy instead of purchasing from TEN. The evaluation of this case is of value when comparing to case WiSo, as these are the two options available to the consumer.

Assumption: To simplify the microgrid in case WiBa, the battery is connected to the same transformer as the wind turbine. The master controller from PowiDian is not a part of this case. It is therefore assumed that there is a master controller in the battery that controls which load, battery or consumer, is used.

Case WiSoBa

Case WiSoBa differs from the other cases by having two energy producing components, the wind turbine and the PV system, as well as energy storage in the battery. As in the previous cases the components are connected to the same transformer. Figure 5.6 presents a schematic sketch of the microgrid.

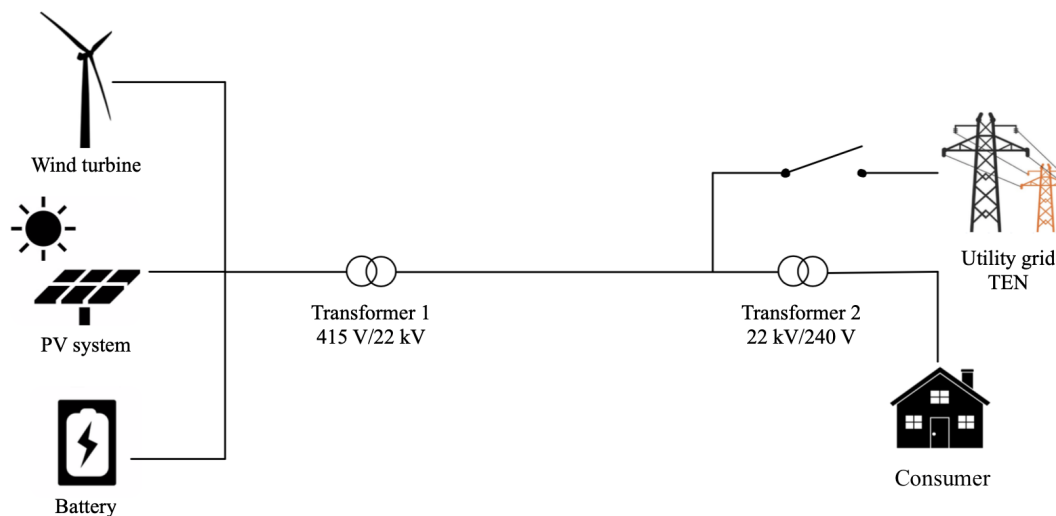


Figure 5.6: Schematic sketch of case WiSoBa, presenting the connection between the wind turbine, the PV system, the battery, the consumer and TEN.

This case evaluates the battery usage and the self supply share, as a result of an increase in the energy production. The combination of higher energy production and an ESD makes this microgrid an alternative for the off grid solution at Froan. Therefore, the off grid potential is evaluated. As this case is not initially dimensioned for an off grid scenario the battery capacity is tested and scaled to meet TrønderEnergi's requirements for Rye Microgrid.

Assumption: The microgrid is simplified by having the wind turbine, the PV system and the battery connected to the same transformer. As in case WiBa there is no master controller from PowiDian, it is therefore assumed that there is a master controller in the battery.

Case WiSoBaHy

Case WiSoBaHy consist of all the components in the completed Rye Microgrid. This includes the installation of a HESS and the master controller from PowiDian. In contrast to the other cases, there are three transformers. T1 is located by the wind turbine, T3 is located by the PV system and ESS, and T2 remains by the consumer. This is illustrated in the schematic sketch of the microgrid in figure 5.7.

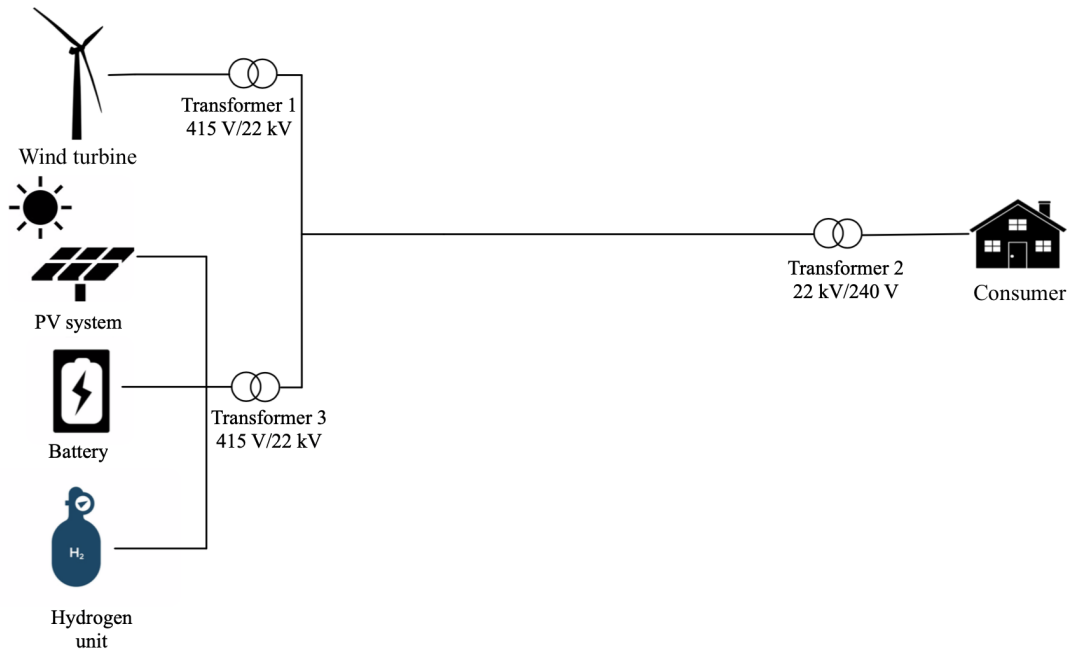


Figure 5.7: Schematic sketch of case WiSoBaHy, presenting the connection between the wind turbine, the PV system, the battery, the hydrogen unit and the consumer.

Case WiSoBaHy is evaluated off grid as it equals the completed Rye Microgrid. Firstly, it is evaluated if the microgrid meets the requirements from TrønderEnergi. Then the ESS usage is evaluated to see if it can cover the energy production deficit. The RES-share and self supply share are evaluated to see if they are sufficient. If the self supply share is below 95%, the battery and the hydrogen unit are tested and scaled to reach the required self supply share.

As an off grid scenario results in not being allowed to sell excess energy to TEN, thus alternate usage of the surplus energy is evaluated. Case WiSoBaHy is also considered operating on grid, to be able to evaluate the economic perspective compared to a microgrid operating off grid. When the case is evaluated in an off grid scenario in remote areas, for example at Froan, the deficit energy is supplied by a diesel generator. Otherwise, the energy is supplied from TEN.

Chapter 6

Methods

This chapter begins with a description of the data acquisition. In order to fully simulate the microgrid data, measurements for energy consumption and production were required, as well as transformer- and transmission line losses.

The wind energy production- and energy consumption data had to be compiled from various sources due to incomplete measurements. Further, the simulation of the solar energy production in PVsyst is explained. This includes the system parameters and the losses accounted for in the simulation. The next section presents the calculated losses of the transformer and transmission lines.

Additionally, the chapter presents the model of Rye Microgrid made in Simulink. The structure of the model is presented as well as an explanation of important subsystem. The chapter ends by presenting the calculations and approaches used to compile the results. This section is divided into security of supply, economic analysis and environmental impact.

6.1 Data Acquisition

In order to analyze Rye Microgrid, measurements have been acquired for the wind energy production and energy consumption. The solar energy production data simulations is explained as well as the calculated losses. The origin and configuration of these data are explained.

6.1.1 Measured Data

It was intended to have a full year of energy production from the wind turbine and energy consumption data, as a base year. Therefore, TrønderEnergi provided measurements of the energy production and consumption. The measurements were accessed from a spreadsheet titled "Measurements Rye", which includes data from January 2016 to August 2018, and in addition, access was given to Safemon. Safemon is a monitoring website developed by SafeBase, which allows advanced monitoring of substations. The website gives an overview of the performance- and operating status from the measurement stations at Rye. TrønderEnergi have installed two advanced meters from SafeBase, one by the wind turbine and one by the consumer, as explained in section 1.2. These provide hourly measurement data of the energy production from the wind turbine and the energy consumption from the consumer, and were installed at the end of May 2018.

The measurement data provided from "Measurements Rye" and Safemon did not include a full year of data, and there were several inaccuracies when comparing the data. Therefore, it was decided in cooperation with Anniken Auke Borgen from TEK to mainly use the data from Safemon, and insert data from "Measurements Rye" in the periods with lack of measurements. This presents some uncertainties as the data is from different years. However, the data illustrate the hourly variation in energy production and consumption.

The calculations are mainly based on 2018, there is expected yearly variations when looking at a longer time perspective. It can therefore be argued that uncertainty due to different data sources are not of a significant matter. Another solution would have been to extrapolate the data from 2018, but there would still be problems regarding the validation as the hourly variation is lost.

Table 6.1 presents the composition of data to compile the base year of the energy consumption. Most of the data is from 2018, however, neither Safemon or "Measurements Rye" had measurements in the period from 24.09.18 until 02.10.18 due to downtime. Therefore, data from 2017 had to be inserted during this period.

Table 6.1: *The composition of energy consumption data, showing the data source and period used to compile the base year.*

Source	Start Date	Start Time	End Date	End Time
Measurements Rye 18	01.01.18	01:00	31.05.2018	14:00
Safemon	31.05.18	15:00	24.09.2018	17:00
Measurements Rye 17	24.09.18	18:00	02.10.2018	10:00
Safemon	02.10.18	11:00	31.12.2018	00:00

Figure 6.1 presents the energy consumption during the base year, while highlighting the transition between the various data sources. It can be observed that even though the data source changes, the data still follows approximately the same pattern at the transition points.

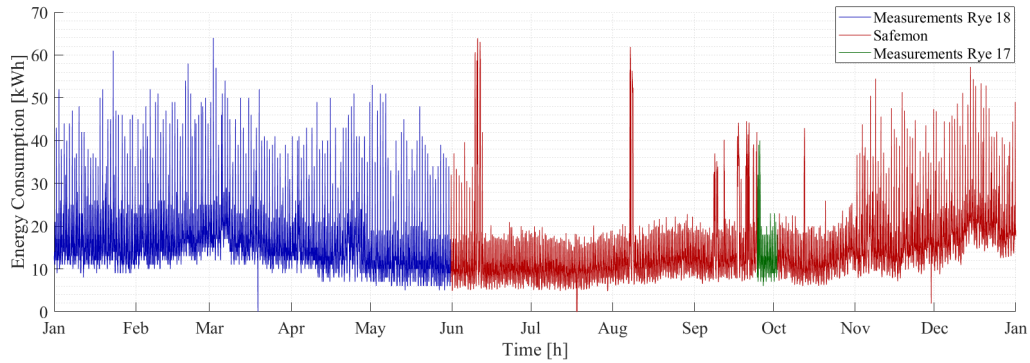


Figure 6.1: The composition of the energy consumption presenting the sources and the transition between the various sources during the base year.

From figure 6.1 it can also be observed that there are significant peaks in June, August and September. The peaks in June and August are caused by the use of the silo and the peaks in September are caused by the use of the grain dryer. The smaller peaks throughout the winter and spring months from November to June are caused by usage of the silo for short periods of time, generally about 30 minutes. The silo is not used consistently from June to November, and this leads to the uneven consumption pattern.

Table 6.2 presents the composition of the wind energy production data during the base year. As Safemon had downtime from 20.07.18 until 13.09.2018 data had to be retrieved from "Measurements Rye", both from 2016 and 2018, as the data from 2018 was not sufficient to cover the whole period.

Table 6.2: Wind energy production composition, showing the data source and period used.

Source	Start date	Start time	End date	End time
Measurements Rye 18	01.01.18	01:00	31.05.2018	14:00
Safemon	31.05.18	15:00	20.07.2018	15:00
Measurements Rye 18	20.07.18	16:00	01.09.2018	00:00
Measurements Rye 16	01.09.18	01:00	13.09.2018	12:00
Safemon	13.09.18	13:00	31.12.2018	00:00

Figure 6.2 presents the energy production composition. The production data from "Measurements Rye" 2016 seems to be slightly lower than the other data. However, the production still follows a similar pattern and presents a realistic hour by hour variation.

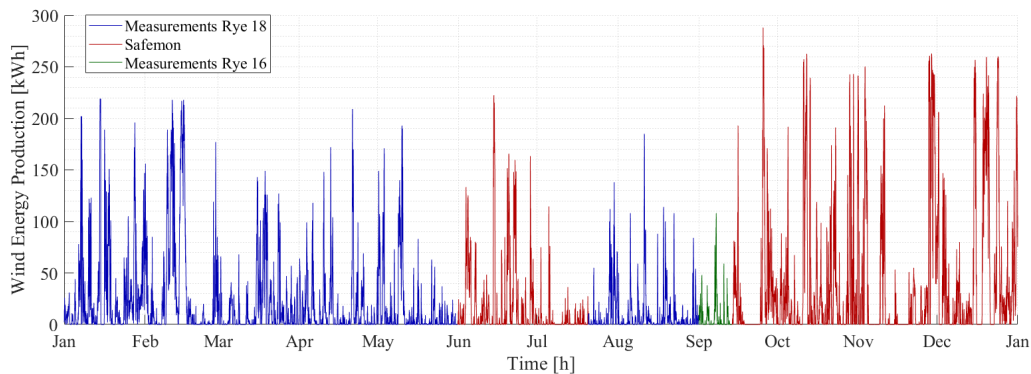


Figure 6.2: Wind energy production at Rye presenting the sources and the transition between the various sources during the base year.

It can be observed from figure 6.2 that the energy production increases from October to January. The increased production in the last months of the year might be a result of data collected from various sources, seasonal variation or due to the installation of a new pitch control in the wind turbine.

6.1.2 Simulated Solar Energy Production

PVsyst was used to simulate the PV system, as there is no measured energy production from the PV system. PVsyst is a program which allows simulation of PV systems and offer system studies roughly correspondent to the different development stages one would have in a real project. This section presents roughly how the results were obtained and a more detailed guide for the simulation is presented in appendix F.

Starting the Project: A project design for a grid connected system was chosen, which means that the important value was the energy delivered to the grid. In this project, this value equals the energy that is delivered to the microgrid from the PV system.

Generating Solar Irradiance Data: To be able to simulate the PV system, solar irradiance data had to be generated for the Rye site. In cooperation with Eirik Lockersen, Solbes AS, it was decided that the best option for solar irradiance data was Metenorm, due to a safer estimate and ease of use in PVsyst.

Metenorm software provides access to meteorological data across the world and the database includes a total of 8325 weather stations. Metenorm software use ground based stations as a reference if they are closer than 10 km to the site in Europe. If the distance to the site varies between 10-50 km, a combination of ground based- and satellite measurements are used, and if the distance exceed 50 km, only satellite measurements are used as a reference. For Rye, the data is mainly generated by satellite measurements as the closest ground based station, Værnes, is approximately 50 km away from the site. [42]

Input Parameters: PVsyst provides the user with several input options to define a PV system. The first relevant parameters for Rye Microgrid was the orientation of the modules. This was done by setting the tilt angle to 35° and the azimuth angle to 0° .

Further, the PV system was divided into three sub-arrays each consisting of 96 PV modules. This presents an issue because eight 310 Wp modules were not accounted for in the simulation, resulting in less installed capacity. The installed system at Rye is explained in section 5.1.

PVsyst provides a database including PV modules, power optimizers and inverters. The database included all components presented in section 5.1, except the P650 power optimizer. Instead the P700 power optimizer was used in the simulation, however, this does not significantly impact the results, as agreed with Solbes AS. The simulated components in their respective sub-arrays are presented in table 6.3.

Table 6.3: PVsyst system parameters for the simulated PV system.

	PV Module	Optimizer	Inverter
Sub-array #1	REC 310 Wp	P700forSE16k	50/60Hz SE27.6K
Sub-array #2	REC 295 Wp	P600forSE15k	50/60Hz SE27.6K
Sub-array #3	REC 295 Wp	P600forSE15k	50/60Hz SE27.6K

Defining the Losses: An important input in the simulation are the losses and therefore several adjustments were made in PVsyst in order to match the Rye site. Table 6.4 presents the estimated soiling losses for the PV system at Rye. The average soiling losses are estimated to be 19.6%, however, the losses are more prevalent during low energy production periods.

Table 6.4: Array soiling losses for each month from the PVsyst report for the PV system at Rye.

Jan	Feb	Mar	Apr	May	June	July	Aug	Sep	Oct	Nov	Dec
80.0%	50.0%	20.0%	5.0%	0.0%	0.0%	0.0%	0.0%	0.0%	0.0%	0.0%	80.0%

Further, the IAM losses had to taken into account. These are created by PVsyst for each specific module used from the database. The IAM losses are presented in table 6.5 were the first row illustrate the incidence angle and the second illustrate the corresponding loss factor.

Table 6.5: The IAM losses estimated for the PV system at Rye from the PVsyst report.

0°	30°	50°	60°	70°	75°	80°	85°	90°
1.000	0.999	0.987	0.926	0.892	0.816	0.681	0.440	0.000

Lastly, the shading losses are also of importance. The shading losses used in the simulation were determined by the use of a shading profile created by Solbes, specifically for Rye. The accuracy of the profile is unknown, and therefore include uncertainties. The losses are compared to the useful energy in figure 6.3.

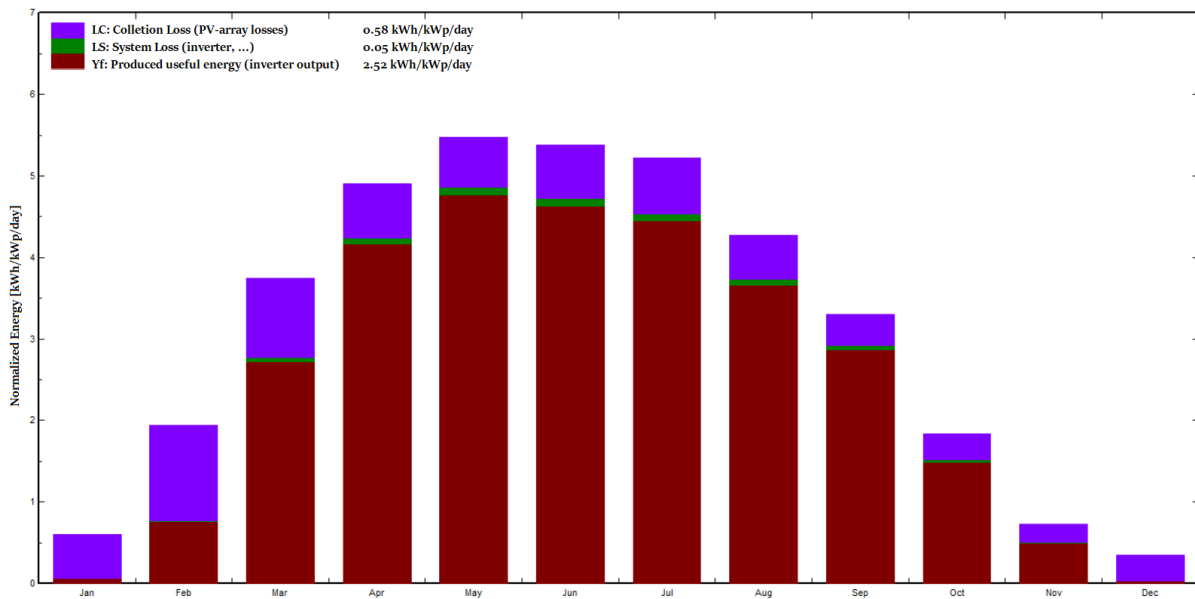


Figure 6.3: The simulated energy produced by the PV system including the losses.

The purple bars represent the collection losses, which include among other, the soiling-, IAM- and shading losses. The green bars represent the system losses due to efficiency in the inverter and power optimizer. The useful energy produced is represented by the red bars and includes the production from the PV system. The unit used is kWh/kWp/day and relate to the produced energy per installed kWp. This means that the produced useful energy is on average 2.52 kWh per installed kWp each day. The full PVsyst report is located in appendix G.

6.1.3 Calculated Losses

In order to realistically simulate Rye Microgrid, losses from the transmission grid at Rye had to be calculated. These include the losses in the transformers and the 1 km of three phased transmission lines.

Transformer Efficiency

The losses from the transformer are dependent on the transformers no-load and load losses. The losses per hour were calculated in MATLAB, and further a transformer efficiency was assumed. The mean transformer efficiency was calculated for the time period with available data. Table 6.6 presents the transformer specifications used as a foundation for the calculations.

Table 6.6: Specifications for the transformers with the calculated losses and efficiency.

	T1 & T3	T2
Voltage	415V/22kV	240V/22kV
Nominal power	315 kVA	100 kVA
No-load loss	360 W	202 W
Load loss	2900 W	1264 W
Calculated efficiency	94.94 %	98.23 %
Assumed efficiency	95 %	98 %

The efficiency for T1 was calculated from the wind energy production load, and the efficiency for T2 was calculated from the energy demand load. The energy consumption- and production data was acquired from SafeBase. During this time period, there was some downtime for a couple of weeks. These measurements were not taken into the calculation of the mean efficiency.

Calculating the Power Factor: As the transformer ratings are stated in apparent power and the losses are stated in active power, the power factor was required. For T1, the wind production data was imported in both active- and apparent power. From this data, the power factor was calculated for each hour by equation 2.2. For T2, there were measurements available for the power factor, so the hourly power factor values were imported directly into MATLAB.

Calculating the Load Losses: The load loss is dependent on the ratio between the load and the nominal power. For T1, the hourly ratio was found directly from the imported apparent power. For T2, the active power had to be converted to apparent power using the power factor.

Finding the Total Loss and Efficiency: The total losses in both transformer types were found from equation 2.1. The efficiency was further found by using equation 2.3.

An important difference between T1 and T2 is the measurement point. The energy is measured on the LV side, which for T1 equals the "in"-side, and for T2 equals the "out"-side. Effectively, this means that the measurement from T2 has already taken the losses into account. For T1, the measurements were also on the LV side, and there is required more production to account for the losses.

Transmission Line Losses

Rye Microgrid also includes 1 km of three-phased TLs. The TLs go from the wind turbine and PV system (from the energy production) to the consumer. These lines includes the losses described in section 2.4.

To be able to calculate the losses, the resistivity in the cable was found from the Nexans cable-book in table "PEX PEX-isolert 24 kV en leder med aluminiumsleder". A cable with a 1x50 cross section has a resistivity of 0.641 Ω/km [92, p.53]. The resistance in the TLs was found using equation 2.5 and equalled 0.641 Ω. The current measured at the LV side of T2 was used to calculate the current on the HV side, and find the maximum current flowing in the TLs.

By using the maximum current in equation 6.1 the maximum loss in the TLs were calculated. This was multiplied by 3 to account for all the phases in the TLs.

$$P_{\text{maxloss}} = R_{\text{TL}} \cdot I_{\text{max}}^2 \cdot 3 = 0.641 \, \Omega \cdot (2.09 \, \text{A})^2 \cdot 3 = 8.40 \, \text{W} \quad (6.1)$$

The maximum loss was 8.40 W and the energy consumption at this time was 31 230 W. These results were then used in equation 6.2 to calculate the efficiency in the TLs.

$$\eta_{\text{TL}} = \frac{31230 \, \text{W}}{31230 \, \text{W} + 8.40 \, \text{W}} \cdot 100\% = 99.97\% \quad (6.2)$$

The corona losses are not accounted for as there is not sufficient data to estimate the losses. Hence, these losses are omitted in the analysis. The resulting efficiency is approximately 100% and this leads to the assumption of no losses in the TLs.

6.2 Simulation of Rye Microgrid in Simulink

To simulate Rye Microgrid, a model was made in Simulink. Simulink is a block based simulation program, which can be used to model and simulate systems. The blocks represent actions or components, where the characteristics can be adjusted manually. The blocks are connected through lines which represent signals. The overall system is presented as a process flow chart. The Simulink model of Rye Microgrid is presented in figure 6.4.

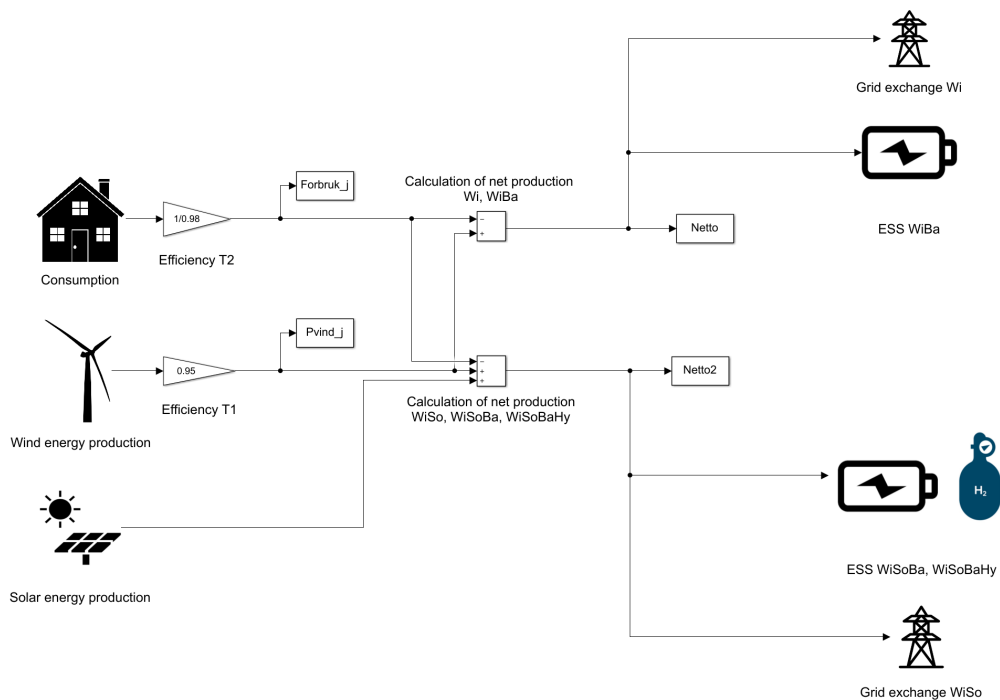


Figure 6.4: Screenshot from Simulink illustrating the model used to simulate Rye Microgrid.

Initially, a MATLAB script was used to convert the energy production- and consumption data to the same units (kWh). The MATLAB workspace was further imported to Simulink, where the net values for exchange with TEN was calculated. The net signal was connected to an energy storage subsystem. The subsystem consisted of a battery system and a hydrogen system, where the charge and discharge of the battery and hydrogen unit was simulated by using logic blocks. Using the To Workspace block, the relevant results were imported back to MATLAB. MATLAB was used for plotting the graphic representation of the results. The subsystems and blocks are further described in appendix H.

Battery storage: The energy storage system was simulated based on logic blocks. The net production, which equals the production minus the consumption, was accumulated in an integrator block that represents the battery. The block has an upper- and a lower saturation limit, where the upper saturation limit is 440 kWh, and the lower saturation limit is 110 kWh, respectively 80% and 20% SoC. During the simulation, the battery's initial condition was 440 kWh. The integrator block will accordingly represent the status of the battery during every hour. The efficiency of the battery and the transformer is taken into account in this model, as well as the rate limiter. The rate limiter limits the input of the battery, with 1 100 kW. The simulated battery is presented in figure 6.5.

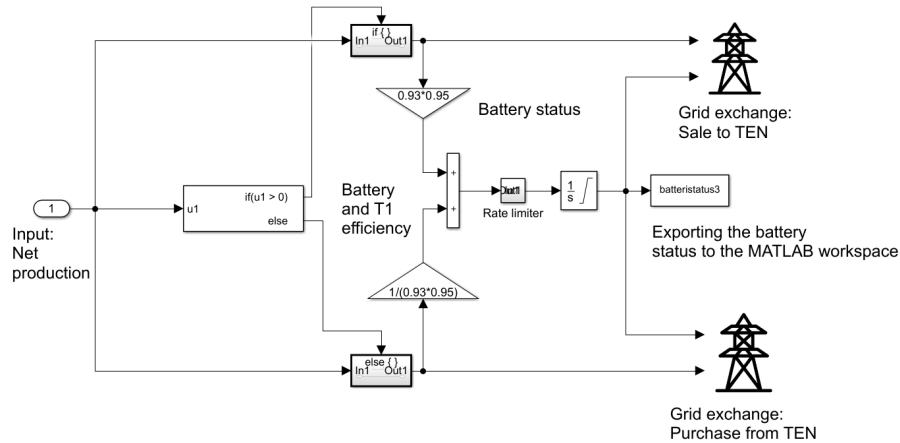


Figure 6.5: The subsystem in the model of Rye Microgrid, presenting the battery storage.

Hydrogen storage: For case WiSoBaHy, the hydrogen unit is charged when the battery is at 80% SoC and there is excess energy generation. This is like the battery represented by an integrator block. During the simulation, the hydrogen capacity's initial condition was 3 300 kWh. The charge of the hydrogen equals the net production that is sold to TEN, however, it is adjusted with the efficiency of the electrolysis cell, fuel cell and transformer. The rate limiter is also taken into account, with a rising slew rate of 55 kW and a falling slew rate of -100 kW.

Exchange with TEN: For the cases including battery storage, WiBa, WiSoBa and WiSoBaHy, the net signal is further connected to an if-block when the battery is saturated. This block evaluates whether the net production is positive or negative. A positive net value will result in exchange with TEN by selling the surplus production. If it is negative, the battery will discharge to meet the consumption. If the battery reaches a SoC of 20%, the net production value is evaluated in an if-block. If it is negative, it results in exchange with TEN by purchasing the remaining demand. For the case with hydrogen storage there is exchange with TEN only when the hydrogen gas tank is full or empty. For the cases without energy storage, Wi and WiSo, the net production goes directly to this point, evaluating whether the net is positive or negative with an if-block, to find the net exchange with the TEN.

Transformer Losses: The transformer losses were taken into account by simplifying the transformer position. As shown in figure 6.6, the losses from T3 were compensated for as a part of the battery efficiency and the fuel cell efficiency. T1 was compensated for as wind turbine efficiency, and T2 was compensated for as a loss by the consumer, leading to a bit higher energy demand. This was the same for all cases.

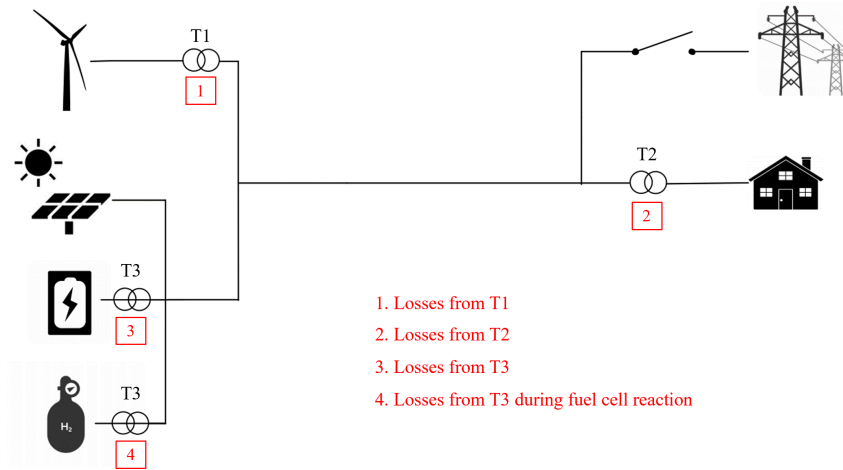


Figure 6.6: The simplification of the losses taken into account in the Simulink model of Rye Microgrid.

The purpose was to simplify the model. Hence, the transformer losses were primarily from wind production through T1, battery charge and discharge through T3, and fuel cell reaction through T3. The power that goes to supply the consumer must be stepped down through T2 and this is also taken into account.

There are some weaknesses to this simplification. First of all, the solar power voltage is not representative of the actual grid setup. The simplified model implies that the solar power is HV which does not correspond with reality. However, the energy is the same through the transformer, and because the model uses energy as input, this is not of significant matter. The simplified model does not step the voltage down through T3 when wind production is stored via electrolysis. Another weakness is that the voltage of the solar production stored in the battery is stepped down when it is used to charge the battery. In addition, there are losses due to solar energy production stored in the battery when the transformer efficiency is a part of the battery efficiency. These are weaknesses that reduce the accuracy of the output and they are important to acknowledge. However, they do not affect the output significantly because the transformer efficiency is high.

6.3 Calculations and Approaches

After running the Simulink model the data was imported to MATLAB for further calculations. This section explains how these calculations were conducted, in order to produce the results to determine security and supply, economic analysis and environmental impact of Rye Microgrid.

6.3.1 Security of Supply

The goal of Rye Microgrid is to be 95% self supplied during a year. To evaluate the security of supply, the energy consumption data, energy production data and amount of energy storage were calculated in the Simulink model. The simulation generates results on when there was excess- and deficit of energy on an hourly basis.

Battery Cycles: The amount of cycles for the battery was calculated by summarizing the charge- and discharge energy in the battery for the base year. The resulting energy usage was divided by the 550 kWh capacity of the battery.

Self Supply Percentage: The self supply percentage was calculated for all five cases. This was done by dividing the energy production covering the consumption, by the total energy consumed. The data used in the calculation of self supply percentage for each case is presented in table 6.7. The energy demand is greater than the total consumption as the losses in T2 has to be accounted for.

Table 6.7: *The self produced energy used to cover the energy demand in the five cases.*

Case	Energy Consumed from Self Production	Energy Demand
Case Wi	55 604 kWh	133 670 kWh
Case WiSo	79 010 kWh	133 670 kWh
Case WiBa	80 030 kWh	133 670 kWh
Case WiSoBa	111 480 kWh	133 670 kWh
Case WiSoBaHy	126 100 kWh	133 670 kWh

Increasing Energy Production: There were also conducted tests on the impact by increased energy production. This was done by separately increasing the energy produced by the wind turbine and PV system. As explained in section 5.1 the wind turbine blades can be extended from 27 m to 29 m and this would add 50 MWh to the energy production. This increased each hourly input with a factor of 1.23. The same increase of 50 MWh in production was added to the PV system by increasing each hourly production with a factor of 1.63. These factors were implemented in the Simulink model by adding a gain to the wind- and solar energy production, resulting in a new self supply percentage.

Increasing Energy Storage Capacity: In order to increase the off grid potential, the energy storage capacity of the battery and hydrogen gas tank were increased separately. This was done to evaluate the 95% criteria and how much energy storage is required to operate 100% off grid.

When testing the influence of the battery capacity, the integrator saturation limits were increased. In addition, the model was adjusted so that the exchange with TEN and charging of the hydrogen tank was adapted to the new battery size. The HESS capacity was constant at 3 300 kWh. Table 6.8 illustrate the test values used to increase the battery capacity in order to calculate the new self supply percentage. The same was done when testing the influence of the hydrogen tank capacity. The test values for the sensitivity test are presented in table 6.9.

Table 6.8: *Battery- and hydrogen capacity for the test points in the sensitivity test, when increasing the battery capacity.*

Battery Capacity	Hydrogen Capacity
550 kWh	3 300 kWh
750 kWh	3 300 kWh
850 kWh	3 300 kWh
1 100 kWh	3 300 kWh
2 200 kWh	3 300 kWh
3 300 kWh	3 300 kWh
5 500 kWh	3 300 kWh
6 500 kWh	3 300 kWh

Table 6.9: *Battery- and hydrogen capacity for the test points in the sensitivity test, when increasing the hydrogen capacity.*

Hydrogen Capacity	Battery Capacity
3 300 kWh	550 kWh
4 400 kWh	550 kWh
5 500 kWh	550 kWh
6 600 kWh	550 kWh
9 900 kWh	550 kWh
11 000 kWh	550 kWh
15 000 kWh	550 kWh
20 000 kWh	550 kWh

Off Grid Potential: To evaluate the two off grid alternatives at Froan, the storage capacity in case WiSoBa was increased, so that case WiSoBa had the same off grid percentage as case WiSoBaHy. This was done in the same way as when the energy storage capacities were tested, by increasing the battery size and calculating the new self supply percentage.

Utilizing Throttled Energy: The simulation also shows the excess- and deficit energy for the five cases. The total excess energy was calculated in MATLAB to explore possibilities of utilizing the otherwise throttled energy. A solution required calculating the potential hydrogen gas production. This required calculating the energy stored as hydrogen gas in the tank as presented in equation 6.3.

$$E_{\text{tank}} = E_{\text{exc}} \cdot \eta_{\text{PEMEC}} \cdot \eta_{\text{T3}} \quad (6.3)$$

In the equation E_{exc} stands for the total excess energy, η_{PEMEC} for the efficiency in the PEMEC and η_{T3} for the efficiency in T3. In reality the wind energy goes through two transformers and the solar energy goes straight to the PEMEC as seen from figure 6.6. In the equation only one transformer efficiency is accounted for in order to simplify the calculation. Further, the energy stored was converted to hydrogen mass in kg by using the energy density of hydrogen (ED_{H_2}) as shown by equation 6.4.

$$m_{\text{H}_2} = \frac{E_{\text{H}_{\text{tank}}}}{ED_{\text{H}_2}} \quad (6.4)$$

Finally, the potential profit is calculated assuming all the hydrogen gas produced could be sold. This was calculated using the same prices as the refuelling station explained in section 4.2.2.

6.3.2 Economic Analysis

The economic analysis is divided into three parts: annual profitability, NPV and LCOE.

Profitability

The profitability is evaluated by calculating the total profit of Rye Microgrid over a year. The income comes from selling the energy back to TEN. The savings were calculated either from using energy directly from self production, from the battery or from the hydrogen unit. For each category, the energy was calculated hourly in MATLAB. Further, the energy was multiplied by either sale- or purchasing price for the associated hour. The sale price only includes the hourly spot price for 2018, while the purchasing price includes the energy dependent price explained in section 2.1. Each case also begins the year with the fixed energy price of 5000 NOK/year.

Exchange with TEN: The exchange with TEN was found by examining the excess- or deficit energy for each hour. This was done to find the income and expense from exchange with TEN for each case. The income and expense depend on whether the microgrid is considered on- or off grid. The only difference between on- and off grid is the ability to sell excess energy to TEN. This is not possible in the off grid scenario.

Self Supply: To find the profit from using self produced energy in contrast to purchasing from TEN, there was used a for-loop for each hour in MATLAB. If the net production was positive or zero, the self supplied energy would equal the energy demand. If the net production was negative, the self supplied energy would equal the production. The calculation is presented in listing 1.

Listing 1: Finding the amount of energy directly from production to consumption in MATLAB.

```

1 for i=1:length(netproduction)
2     if netproduction(i)>0;
3         consumed_selfprod(i)=energydemand(i);
4         %Self produced energy used equals hourly consumption
5     elseif netproduction(i)<0;
6         consumed_selfprod(i)=windproduction(i)*efficiency_T1;
7         %Self produced energy used equals hourly wind production
8     else netproduction(i)==0;
9         consumed_selfprod(i)=energydemand(i);
10        %Self produced energy used equals hourly consumption
11    end
12 end

```

Battery: The profit from the battery is a result of the energy stored in the battery covering additional self supply. The energy supplied from the battery was found by using a for loop in MATLAB. First, the energy change in the battery was found by subtracting the battery status as presented in listing 2. Further, the value was checked using if-logic if the change was positive or negative. If the value was negative, the consumer was supplied from the battery, and this energy amount was used to find the profit. The profit is the energy used from the battery times the purchasing price, as the consumer does not need to purchase from TEN. The calculation is presented in listing 2.

Listing 2: Finding the charge- and discharge energy in the battery in MATLAB.

```

1 % Change in battery status
2 for i=1:8759
3     energychange(i)=batterystatus3(i+1)-batterystatus3(i);
4     energychange(8760)=0;
5 end
6
7 % Charge- and discharge energy in the battery
8 for i=1:8760
9     if energychange(i)>0
10        energy_charge(i)=energychange(i)/(eff_battery*eff_T3);
11        energy_discharge(i)=0;
12    elseif energychange(i)<0
13        energy_charge(i)=0;
14        energy_discharge(i)=-energychange(i)*(eff_battery*eff_T3);
15    else energychange(i)==0
16        energy_discharge(i)=0;
17        energy_charge(i)=0;
18    end
19 end

```

Hydrogen: The profit from using energy stored in the HESS was found similarly to the profit from using the battery. The difference between the two is that the hydrogen status is investigated, instead of the battery status.

Net Present Value

The net present value was found after 20 and 30 years for each case. The time period was based on the expected lifetime for the wind turbine and the PV system, respectively 20 and 30 years. The present value was calculated in Excel for each year. The yearly values were accumulated, and the NPV was equal to the accumulated value in year 20 and 30.

The NPV was calculated using equation 3.1. The investment is done in year 0 and the investment cost, C_0 , includes the cost of the component(s) and the installation cost. All the future cash flows are the income, expenses and savings, as specified in the section explaining the profitability calculations. From this, the net cash flow, C_t was calculated. C_t also includes any renewed investments. A renewed investment is necessary when a component, or a part of a component, reaches its lifetime. Table 6.10 presents the components and in which years investments had to be done.

Table 6.10: Required investments for all of the components in the microgrid.

Year	Wind Turbine	PV System	Battery	Hydrogen Unit
Year 0	Wind turbine	PV system	Battery	Hydrogen Unit
Year 10			New battery	Renewed electrolyzer
Year 20	New wind turbine	New inverters	New battery	New hydrogen unit
Year 30		New PV system	New battery	Renewed electrolyzer

From table 6.10 it can be observed that there are investments in year 20 and year 30. However, when evaluating a 20 year perspective, the investments in year 20 is not accounted for. This also applies for the investments in year 30, when evaluating a 30 year perspective.

Case WiSo Expansion: Case WiSo includes an expanded case analysis where additional calculations of NPV is done to represent the actual situation for the consumer at Rye. As the consumer already owns the wind turbine the question is whether it would be profitable to purchase the PV system after the completed project at Rye. Therefore, an additional NPV calculation was done for the PV system exclusively.

This expanded case is based on the wind turbine being operational from 2016 until 2036 and the PV system operation for the consumer from 2022 until 2049. The expected lifetime of the PV system is reduced by three years, because of its usage in the Rye project. The NPV is based on the 27 year operation of the PV system and will therefore exclude the wind turbine cost and income from year 2022 until 2036. The years after 2036 until decommissioning in 2049 only includes the solar energy production, and following costs and income.

The calculations for the NPV was done in Excel, in a similar way as the NPV for the other cases. However, the investment is done in 2022, and there were income and expenses in 2022 because the PV system is already installed when the investment is made. When calculating the cash flows, only the contribution from the PV system is of interest. To find this, the difference between the cash flows is case WiSo and case Wi was found. The calculated NPV is then compared against the NPV of the base case. This comparison represents the potential profit the consumer can make with the PV system investment.

Levelized Cost of Energy

The third and last part of the economic analysis was done by calculating the LCOE for wind- and solar power, using equation 3.2. Initially, all the costs over the lifetime were discounted to a present value and summarized to a net cost. To find how much this equals in annuity payment, the Excel function PMT was applied. PMT (short for payment) gives the annuity payments when the total discounted costs, discount rate and lifetime are given. Further, the LCOE was found by dividing the annuity payment by the annual production. Table 6.11 presents the values used in the LCOE calculation.

Table 6.11: *The calculated LCOE for the energy sources at Rye Microgrid.*

	Wind Power	Solar Power
Discounted costs	-2 959 032.6 NOK	-1 290 504.0 NOK
Lifetime	20 years	30 years
Annual installment	217 730.8 NOK	74 630.0 NOK
Annual production	216 910 kWh	79 343 kWh

6.4 Environmental Impact Rye Microgrid

In order to evaluate the environmental impact from Rye Microgrid, the carbon emissions and the renewable energy share in each case was calculated.

Carbon Emissions

The carbon emissions were determined using the total energy production from the various sources and the energy consumption. The total carbon emissions from the RES are calculated and compared against the emissions from the grid. This was done by multiplying the carbon intensities from table 2.2 with the energy production from the according energy source. The total carbon intensities for each case was calculated from equation 6.5.

$$CI = CI_w \cdot \frac{E_w}{E_{tot}} + CI_s \cdot \frac{E_s}{E_{tot}} + \frac{E_g}{E_{tot}} \cdot CI_g \quad (6.5)$$

CI is the carbon intensity, E is the energy generation, and the sub indices for wind, solar, total and grid are respectively w, s, tot and g. E_g is the energy demand that is not covered by self supply, and thus required from the grid. The carbon intensity for the energy demand from the grid, CI_g , is based on the GO explained in section 2.2. By using equation 6.6 the percentage of the grid intensity, with GO, was calculated for each case.

$$\% \text{ of grid} = \frac{CI}{CI_g} \cdot 100\% \quad (6.6)$$

Chapter 7

Security of Supply

This chapter presents the results related to security of supply in each case. First, the annual wind-, solar- and total energy production are presented. The energy consumption is also presented and compared with the energy production. It is then evaluated and discussed if the production can supply the energy demand. In addition, the average hourly values for the yearly quarters are presented and discussed. Further, the energy storage results are presented and evaluated. The usage of the battery and HESS throughout the base year is discussed.

The percentage of self supply for each case is presented. Further, the production from both wind and solar are increased separately to evaluate the change in self supply. This in turn leads to an evaluation of the off grid potential of the microgrid, by evaluating the battery- and hydrogen capacity. The chapter is concluded with a section exploring alternative use of throttled excess energy.

7.1 Annual Energy Consumption

The annual energy consumption is the main condition required to evaluate how well the microgrid operates. For the microgrid to be viable, it has to supply enough energy to cover the consumption at all times during the year. The total energy consumption in the base year was approximately 131 MWh. Figure 7.1 present the hourly energy consumption as well as the monthly average energy consumption in the base year.

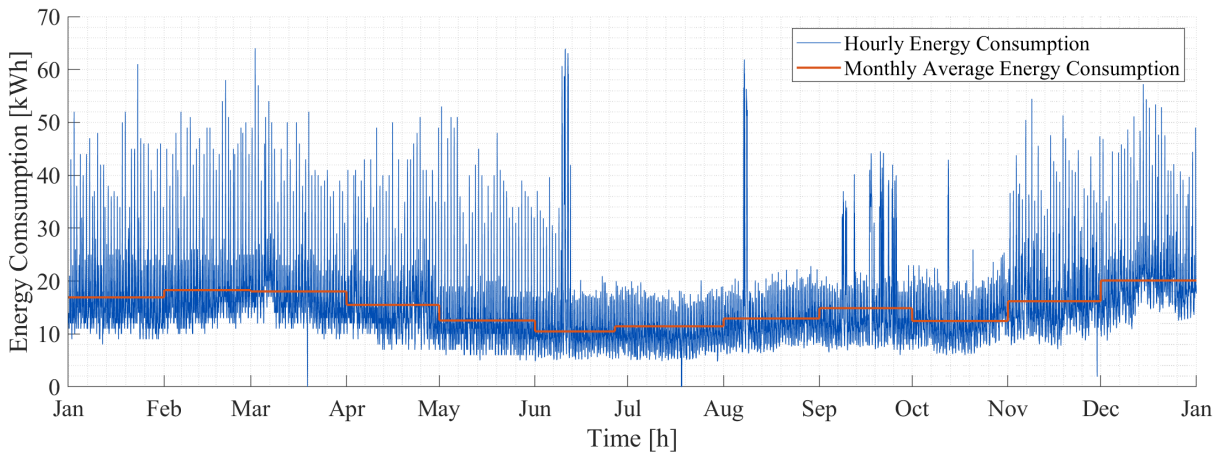


Figure 7.1: The energy consumption during the base year with monthly average energy consumption.

7.2 Annual Energy Production

The annual energy production from the wind turbine in the base year was 217 MWh, which is 86 MWh more than the demand during the base year. The distribution over the year with monthly averages are presented in figure 7.2.

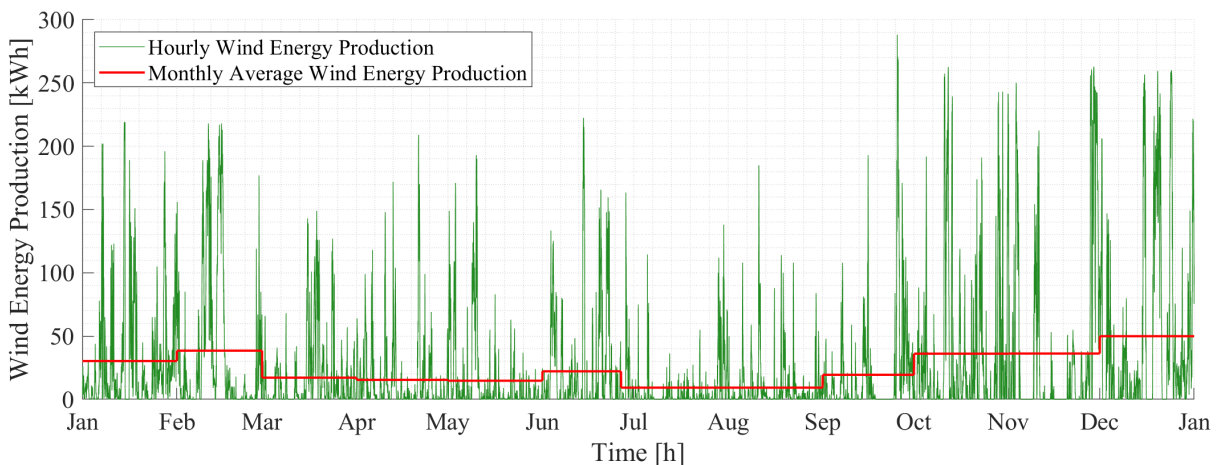


Figure 7.2: Wind energy production with hourly inputs and monthly averages for the base year.

It can be observed from the figure that the energy production has great variations throughout the year. Section 3.3 describes how the average wind speeds in Norway are generally higher in the winter months. This might explain why figure 7.2 presents an increase in energy production during the winter.

Figure 7.3 present the distribution of solar production during the base year as well as the monthly average production. The total solar energy production during a year is 79.3 MWh. It can be observed that the peak production is from May to July, and there is close to no production from December to February.

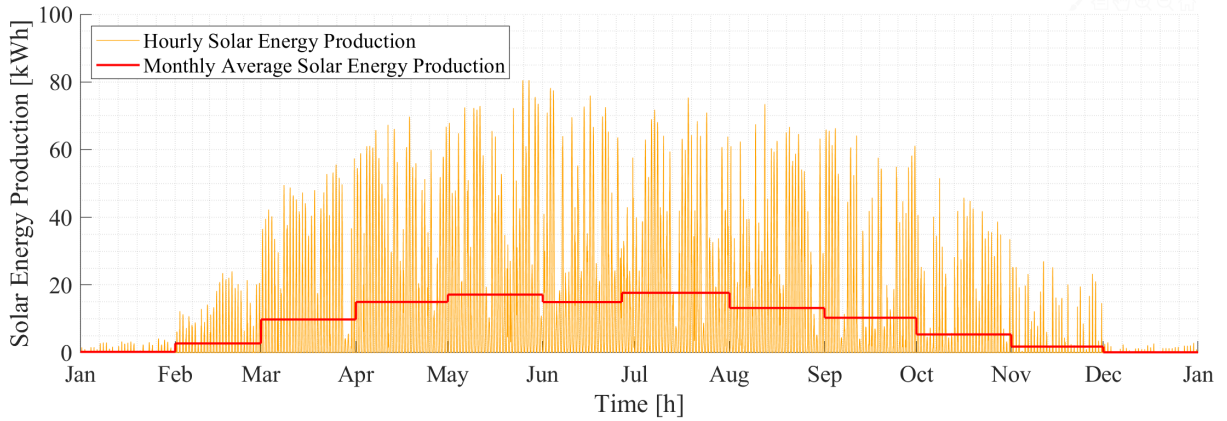


Figure 7.3: The simulated production from the PV system throughout the base year with hourly inputs and monthly averages.

A careful approach was done to the simulation in PVsyst. This leads to a conservative estimate of the energy production. The simulation also included several losses, as illustrated in figure 6.3. The loss estimations in the simulation varies depending on the implemented method. This includes the soiling losses and shading profile, which for the Rye site were estimated by Solbes AS. This could lead to the PV system actually producing more energy than in the simulation.

The wind- and solar energy production are the two energy sources at Rye Microgrid, combined they make up the total annual production for the base year. This is presented in figure 7.4, including the monthly average energy production.

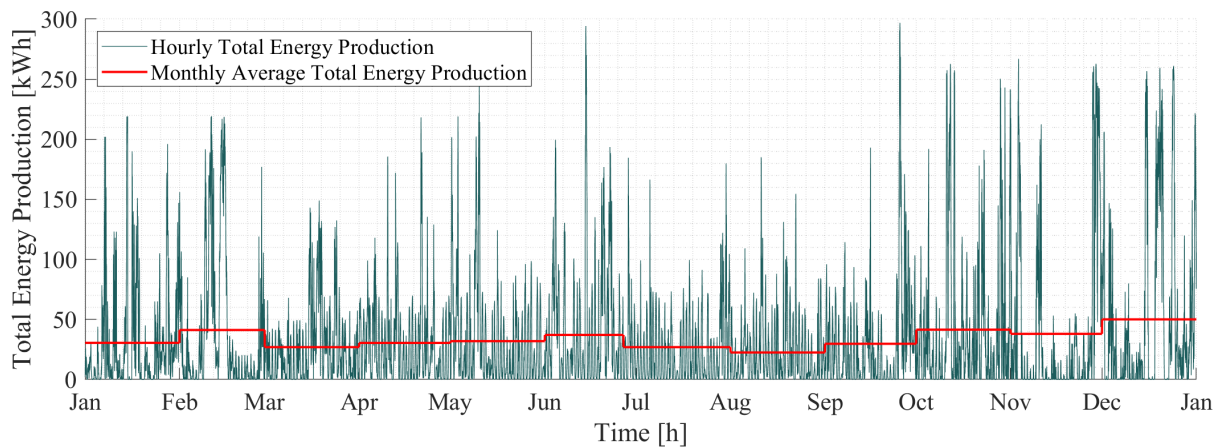


Figure 7.4: Total production from the base year, including wind-, simulated solar-, and the monthly average energy production.

It can be observed from figure 7.4 that when the wind- and solar production are summarized, the monthly average production is more stable throughout the year. The two energy production sources seem to be compatible, which is in line with the theory presented in section 3.3. To evaluate the compatibility of the energy production and consumption it is essential that the sources are compatible on an hourly- and daily basis. The daily average hour-by-hour values were found for each quarter (Q) of the base year and are presented in figure 7.5.

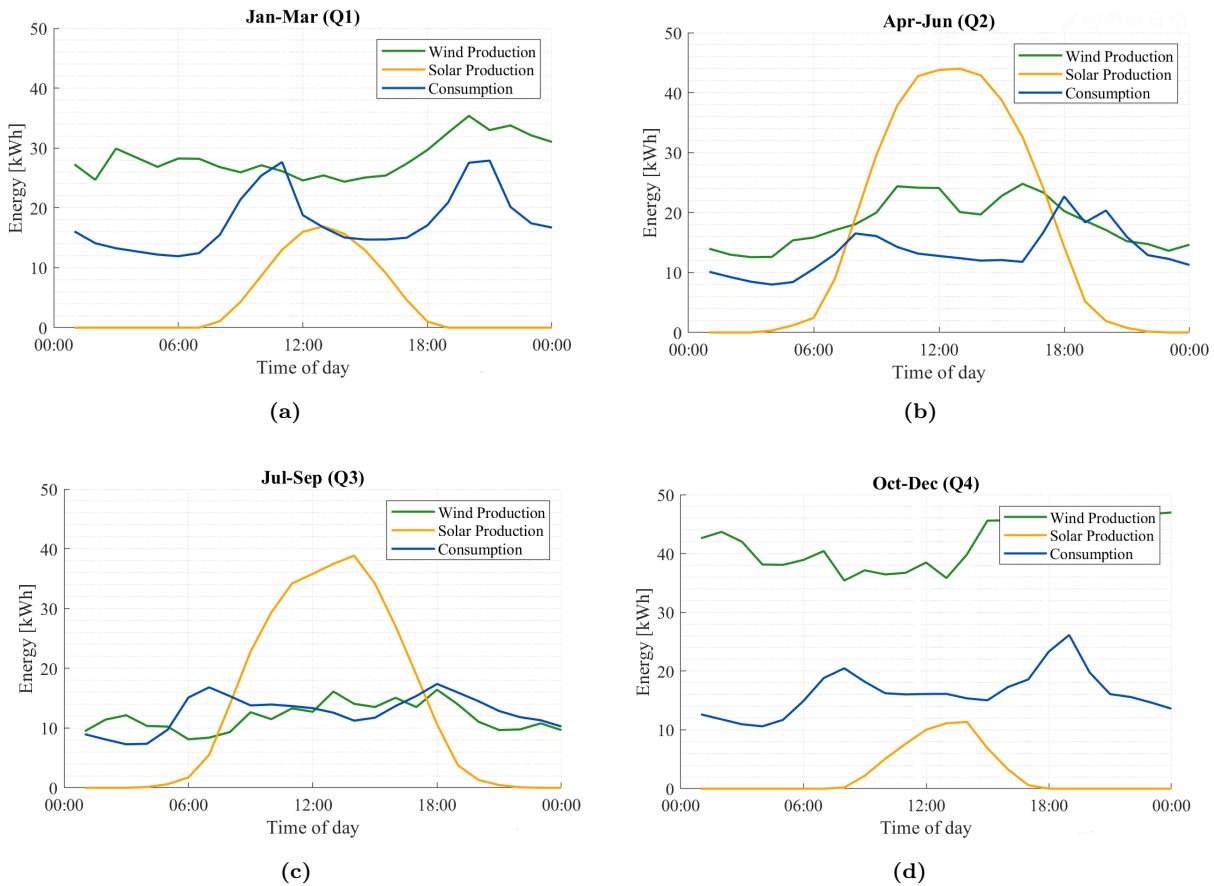


Figure 7.5: The hourly average wind- and solar energy production and energy consumption. The figure presents the quarter based average of the daily pattern.

The common trend from figure 7.5 is that the wind production curve complements the consumption curve. During all quarters the consumption peaks in the morning and afternoon. In general the wind production follows the same pattern and is mostly higher than the consumption. However, during Q3 the consumption is more even and is also higher than the production from the wind as can be seen from figure 7.5c. This matches the theory presented in section 3.3 as the mean wind speeds are lower during summer.

From figure 7.5b and figure 7.5c it can be observed solar energy production is the highest during the middle of the day. This can also be observed from figure 7.5a and figure 7.5d, however, the energy production is lower due to seasonal variations. Further, it can be observed that the solar energy production is the highest, when the consumption is declining in all quarters of the year.

The wind energy production is generally higher than the consumption throughout the day. From figure 7.5 it can be observed that when the wind production is high, the solar production is low and this also applies inversely. Wind- and solar production seem to be compatible on a daily basis, and this is the pattern in all the quarters. It can therefore be debated that wind and solar energy also complements each other on a seasonal basis.

The hourly averages seem to point towards wind production being the optimal energy source. However, daily energy production from wind or solar can never be guaranteed. When investigating especially figures 7.5b and 7.5c the wind production would have to stay consistently at the average production in order to meet the hourly consumption demand. This can never be guaranteed as the wind speed fluctuates hourly. In order to mitigate this fluctuation the addition of solar energy production allows additional flexibility. This will mean that the solar energy is able to cover the hours from approximately 8 to 17 during Q2 and Q3, even if there is no energy production from the wind turbine.

7.3 Energy Storage

In the cases WiBa, WiSoBa and WiSoBaHy, there are EDSs available, which provides added security of supply. Figure 7.6 presents the battery SoC based on the energy production and consumption from the base year in case WiBa. The total amount of cycles for the battery in case WiBa is 403 cycles.

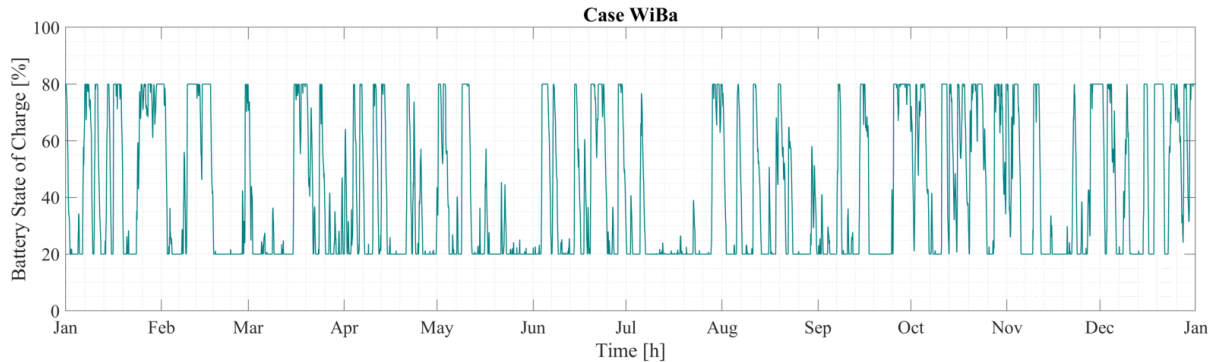


Figure 7.6: Battery status during the course of the base year with hourly inputs for case WiBa. The battery is charged and discharged between 20%-80% SoC.

Figure 7.7 presents the battery SoC when the simulated solar energy production is supplied in addition to the wind power, as in the cases WiSoBa and WiSoBaHy. The total amount of cycles increases as the energy production increases, leading to a total of 444 cycles in cases WiSoBa and WiSoBaHy.

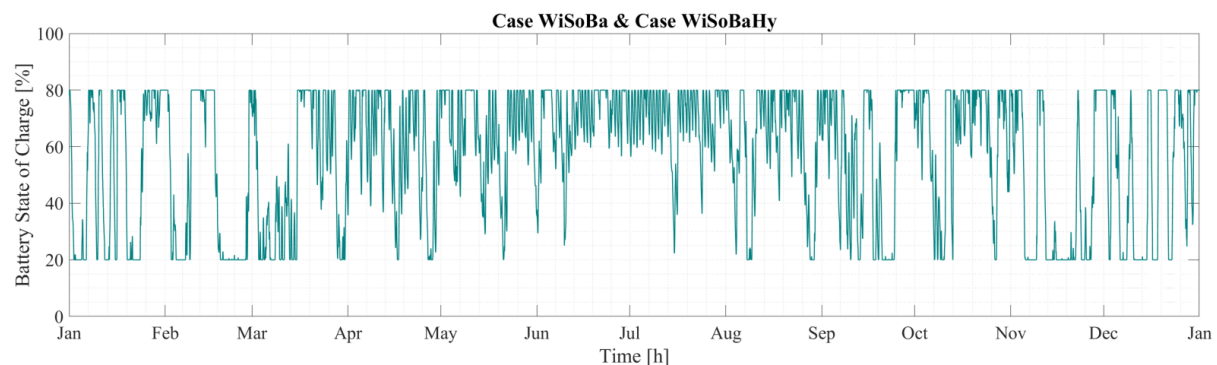


Figure 7.7: Battery status during the course of the base year with hourly inputs for case WiSoBa and WiSoBaHy. The battery is charged and discharged between 20%-80% SoC.

When comparing the battery usage in cases WiBa and WiSoBa, there is a significant difference in the usage of the battery. Figure 7.6 illustrates that the SoC is consistently at a low level during the summer months. On the other hand, in figure 7.7, the SoC during the summer months stays mostly at maximum capacity allowing for increased flexibility to the changes in energy demand. This is because of the addition of solar energy to the microgrid which has its peak production during summer. The production from the PV system does not have a significant impact during the rest of the year.

The addition of solar energy production leads to a more frequent use of the battery. The amount of cycles used increases from 403 in case WiBa to 444 in cases WiSoBa and WiSoBaHy. The more frequent usage means that more tension is put on the battery system and could lead to a decrease in the life expectancy. As described in section 5.1, the expected lifetime of the battery is 10 years based on an annual usage of 400 cycles per year.

In case WiSoBaHy, there is also energy storage in the form of hydrogen gas. The hydrogen tank has a capacity of 3.3 MWh usable energy. In combination with the battery, the hydrogen gas status is presented in figure 7.8.

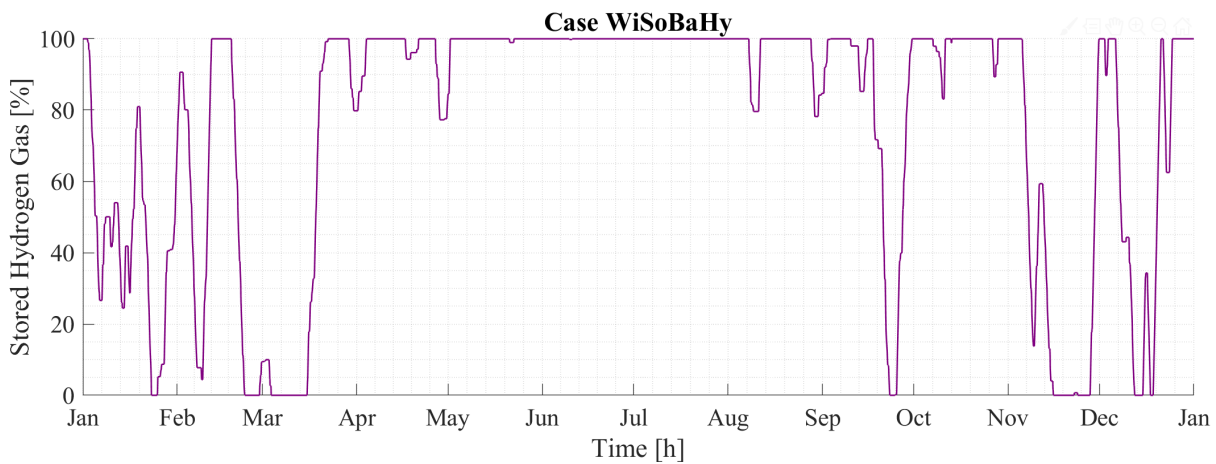


Figure 7.8: Hydrogen status during the course of the base year with hourly inputs for case WiSoBaHy.

The HESS is the secondary ESS and when the hydrogen gas tank is empty, the consumer has to purchase energy from TEN. Figure 7.8 shows that the consumer has to purchase from TEN in the period between October and April. On the other hand the period between April and September requires little usage of the HESS as a result of the battery rarely dropping below 20% SoC.

7.4 Self supply

The amount of self supply for each case in the base year is presented in table 7.1. It can be observed that the combination in case WiSo offers a self supply percentage of 59.1%, and in case WiBa the self supply percentage is 59.9%. Hence, the PV system offers approximately the same security of supply as the battery, with only a difference of 0.8%. A hybrid system has a significant impact on the security of supply.

Table 7.1: Self supply percentage in the five cases.

Case	Self Supply Percentage
Wi	41.6%
WiSo	59.1%
WiBa	59.9%
WiSoBa	83.4%
WiSoBaHy	94.3%

The cases WiSoBa and WiSoBaHy are the cases with the largest off grid potential, as they are closest to 100% percentage self supplied, with respectively 83.4% and 94.3%. As Case WiSoBaHy reflects the complete Rye Microgrid it is supposed to have a self supply of 95%. However, the deviation might be due to the use of different dimensioning tools. The deviation might also be due to the careful estimate of the solar energy production. Further, the losses during transmission and storage might differ from the original assessment of Rye Microgrid. These aspects could explain why case WiSoBaHy does not reach the required self supply of 95%.

The energy production and storage influences the self supply in different amounts. Figure 7.9 presents in what fraction of the power supply they each influence in the five cases.

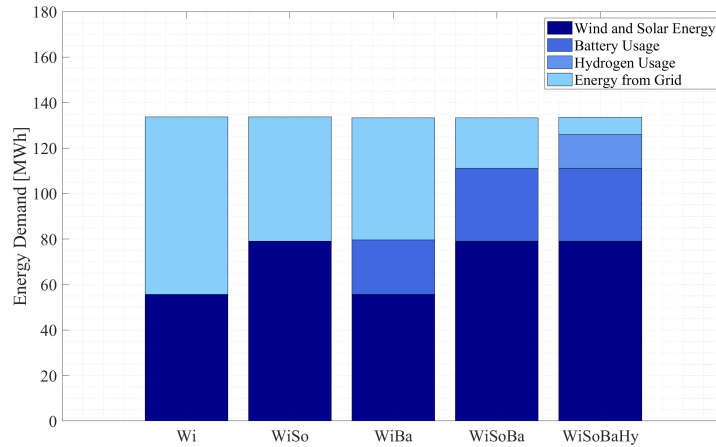


Figure 7.9: The energy supply from the different energy sources in all the cases. The sources are divided into wind- and solar energy, battery- and hydrogen usage and energy from the grid.

From figure 7.9, it can be observed that cases WiSo and WiBa impact the energy supply with the same amount when the PV system and battery are included, with respectively 17.5% and 18.3%. In addition, it can be observed that the battery supplies more energy in case WiSoBa and case WiSoBaHy than in case WiBa, respectively 24.3% and 18.3%. The increased battery usage is due to the additional energy production. Table 7.2 presents self supply percentage from all the various components in all the cases.

Table 7.2: The energy supply from the different energy sources in all the cases. The sources are divided into wind- and solar energy, battery- and hydrogen usage and energy from the grid.

Case	Wind and Solar Energy	Battery Usage	Hydrogen Usage	Energy from Grid
Wi	41.6%			58.4%
WiSo	59.1%			40.9%
WiBa	41.6%	18.3%		40.1%
WiSoBa	59.1%	24.3%		16.6%
WiSoBaHy	59.1%	24.3%	10.9%	5.7%

The battery supplies the same amount of energy in case WiSoBa and case WiSoBaHy. This is because the cases have the same energy production and consumption. Further, the battery is the primary component of the ESS. Therefore, the HESS supplies less energy as it is only in use when the battery is discharged. The HESS provides 10.9% of the total energy demand in case WiSoBaHy.

Increasing the Energy Production

As mentioned in section 5.1, extensions can be added to the wind turbine blades and thus expand the diameter from 27 m to 29 m. This addition is expected to increase the annual wind production by 50 MWh, and hence increase the the total wind capacity by 23%. The expansion increases the production evenly throughout the year. This should allow more of the energy consumption to be self supplied, thus increasing the self supply percentage.

Table 7.3 present the percentage self supply before and after the expansion of the wind turbine diameter. It can be observed that the expansion increases the difference between case WiSo and case WiBa from 0.8% to 3.0%. Further, it can also be observed that case WiSoBaHy reaches the target of being 95% self supplied.

Table 7.3: Percentage self supply in the cases with the 27 m and 29 m diameter wind turbine.

Case	Self Supply Percentage Vestas V27	Self Supply Percentage Vestas V29
Wi	41.6%	43.7%
WiSo	59.1%	60.7%
WiBa	59.9%	63.7%
WiSoBa	83.4%	84.9%
WiSoBaHy	94.3%	95.3%

By expanding the wind turbine diameter the self supply percentage was expected to increase. This was the result in all the cases, however, by examining figure 7.1 and figure 7.4 it was assumed that increasing the wind energy production would yield an even higher increase in self supply percentage. This assumption was made as the monthly average wind energy production and energy consumption seemed to be very compatible. This should have been especially prevalent in case Wi and case WiSo as wind power is the largest power component and there is no ESS to store the energy. Case Wi increases by 2.1% and case WiSo by 1.6%, which is not as significant of an increase as expected. It could therefore be argued that the hourly wind energy production does not match up consistently with the energy demand.

In addition, the self supply percentage were compared against a similar increase in the PV system. The PV system was increased to a total energy production of 129.3 MWh which is 1.63 times greater than the original system. The result are presented in table 7.4.

Table 7.4: Percentage self supply in the cases containing solar energy production, comparing original PV system and a 1.63 times larger PV system.

Case	Self Supply Percentage PV Original	Self Supply Percentage PV Times 1.63
WiSo	59.1%	61.7%
WiSoBa	83.4%	86.3%
WiSoBaHy	94.3%	96.1%

Table 7.4 presents the percentage self supply when the solar production is increased by the same amount as the wind energy production. In case WiSo, case WiSoBa and case WiSoBaHy the self supply percentage increases with respectively 1.0%, 1.4% and 0.8% compared to the self supply with blade extensions. This is in contrast with the expectation from the investigation of figure 7.5. The figure led to the expectation that an increased wind production would be the better solution to increase the self supply. This is not the case, which is likely due to the added flexibility by having two separate energy producing sources.

Before any changes were made the wind turbine produces 2.7 times more energy than the total PV system. During the year, figure 7.5 shows that the wind production will on average already produce more energy than the consumption. This is not the case with the solar energy as it is below the demand during especially Q1 and Q4. When also considering the unpredictability in the production from RESs, the addition of extra solar energy leads to increased cover of the consumption when there is little or no production from the wind turbine, while there is still production for the PV system.

The optimal solution for increasing the self supply percentage would be increasing the energy production from the PV system. However, increasing the size of the PV system will require a substantially larger area and might not be feasible at Rye. This is an issue which is non-existent as the extensions are added to the blades. This will not influence the area usage on the site.

7.5 Off Grid Potential

As mentioned case WiSoBa and case WiSoBaHy have the greatest off grid potential with a self supply percentage of respectively 83.4% and 94.3%.

Case WiSoBaHy

In order to evaluate the off grid potential, it is important to address the amount of deficit energy, and when it occurs. Figure 7.10 presents the annual deficit- and excess energy throughout the base year for case WiSoBaHy.

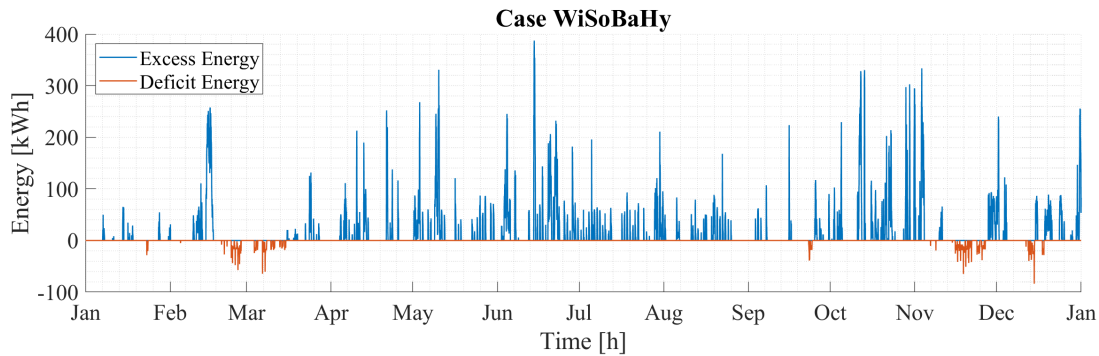


Figure 7.10: The excess and deficit energy for case WiSoBaHy. In an off grid scenario, the excess energy is throttled and the deficit energy is purchased from the grid. In an on grid scenario, the excess energy can be sold to the grid.

As seen from figure 7.10, there is a total of 113.6 MWh excess energy production throughout the year. However, there is not enough energy production to cover the consumption when the energy demand is the highest. Further examinations shows that the largest energy deficit is from 19. February to 15. March with a total of 3.1 MWh. The excess energy produced in the time period before the deficit, 8. February to 18. February, has a total of 10 MWh, which shows that the excess energy produced should be able to cover the deficit. Hence, it could be an idea to increase the storage capacity. A sensitivity test was conducted to test the influence of increased storage capacity. The results are presented in tables 7.5 and 7.6 respectively.

Table 7.5: Percentage self supply in case WiSoBaHy when expanding the capacity of the battery.

Battery capacity	Self supply	Factor
550 kWh	94.3%	1
750 kWh	95.0%	1.36
850 kWh	95.2%	1.55
1 100 kWh	95.8%	2
2 200 kWh	97.6%	4
3 300 kWh	98.5%	6
5 500 kWh	99.8%	10
6 500 kWh	100%	11.82

Table 7.6: Percentage self supply in case WiSoBaHy when expanding the capacity of the hydrogen gas tank.

Hydrogen capacity	Self supply	Factor
3 300 kWh	94.3%	1
3 700 kWh	95.0%	1.12
5 500 kWh	96.8%	1.67
6 600 kWh	97.5%	2
9 900 kWh	99.6%	3
11 000 kWh	99.9%	3.33
15 000 kWh	99.9%	4.55
20 000 kWh	99.9%	6.06

It can be observed that the hydrogen gas tank capacity is never sufficient to be 100% self supplied. This is because of the rate limiter for the fuel cell. Even if there is enough hydrogen gas in the tank, the demand is too abrupt compared to what the fuel cell can supply. The fuel cell has a rate limit of 100 kWh/h. Theoretically, the farm can never be 100% self supplied by solely increasing the hydrogen capacity because of this restriction. However, if the rate limit was increased to 125 kWh/h, the microgrid could be 100% off grid. By increasing the battery capacity to 6 500 while hydrogen remains at 3 300 case WiSoBaHy has the opportunity to be 100% off grid.

Comparing the tables, it can be observed that the hydrogen gas tank requires significantly more capacity to reach the same self supply. This is because in order to sufficiently supply the microgrid, the energy stored in the HESS has to pass through the PEMFC with a low efficiency. However, another important point is that the energy density of hydrogen is high, as explained in section 4.2. The HESS capacity is also increased by increasing the size of the tank, meaning the fuel- and electrolysis cell can remain the same. As these are most expensive components it does not impact the cost as significantly. For these reasons hydrogen is well suited when large quantities of energy storage is required.

If the battery size should be increased new racks need to be added. This is a more significant investment than increasing the HESS. Therefore an important evaluation is how much energy storage is required. The results from the evaluation will impact which ESD is the most optimal.

Case WiSoBa

Case WiSoBa originally has a self supply percentage of 83.1%, as presented in table 7.5. It was conducted a test of various battery capacities to find out what capacity was needed to have the same self supply percentage as case WiSoBaHy, 94.3%. The test results are presented in table 7.7.

Table 7.7: Percentage self supply in case WiSoBa with different storage capacities for the battery.

Battery capacity	Self supply	Factor
550 kWh	83.4%	1
1 100 kWh	87.8%	2
2 200 kWh	92.2%	4
2 900 kWh	94.3%	5.3
3 200 kWh	95.0%	5.8
4 400 kWh	96.8%	8

It can be observed that to have the same self supply percentage as case WiSoBaHy, the battery capacity is 2 900 kWh. With this battery size, the excess and deficit power during the base year would be as presented in figure 7.11.

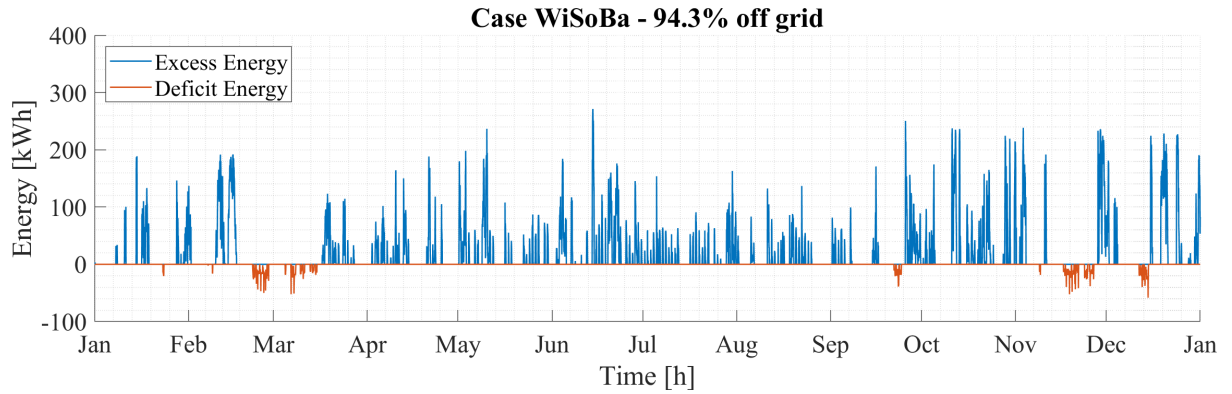


Figure 7.11: The excess and deficit energy for case WiSoBa. In an off grid scenario, the excess energy is throttled and the deficit energy is purchased from the grid. In an on grid scenario, the excess energy can be sold to the grid.

The excess energy is 113.6 MWh in case WiSoBaHy and 147.3 MWh in case WiSoBa. In an off grid scenario, the excess energy is be throttled and there is not an income from selling to TEN. That leads to a difference in profitability in the two cases. The energy produced is either distributed to the consumption, battery charge, electrolysis or throttled. The energy distribution in the two cases are presented in figure 7.12.

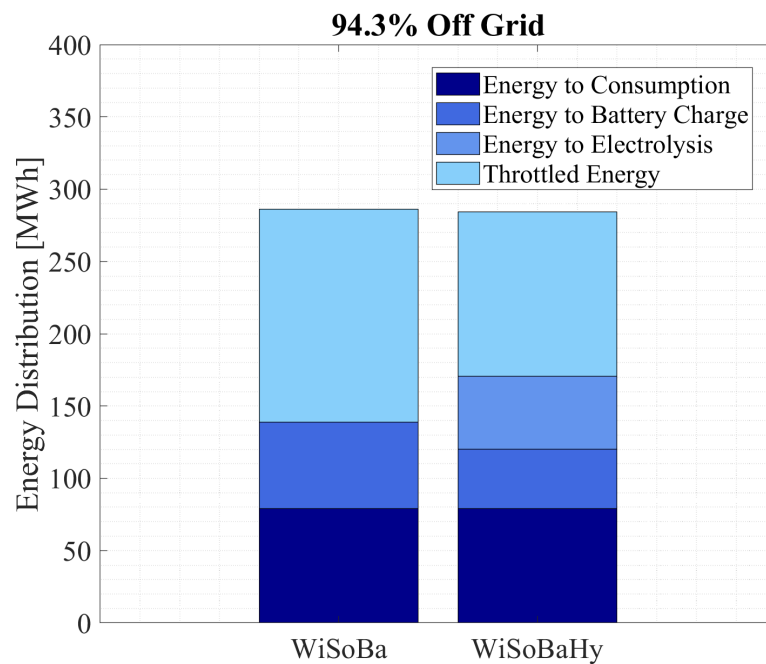


Figure 7.12: The energy distribution in an 94.3% off grid scenario for cases WiSoBa and WiSoBaHy. The energy is distributed to either energy consumption, battery charge, electrolysis or throttled.

The unused energy is 51.5% of the production in case WiSoBa, and 39.9% in case WiSoBaHy. The two cases have the same power supply from wind- and solar production, however, the energy distribution is different in the two cases. When the energy distributed is used for charging the battery or to producing hydrogen, the efficiency has to be accounted for. The efficiency in the electrolysis cell is significantly lower than the efficiency in the battery.

Utilizing Throttled Energy

In case WiSoBaHy 113.6 MWh of energy is throttled, this equals 39.9% of the total energy production. However, instead of throttling the surplus energy, it could be utilized.

The largest amount of excess energy is during the summer months as less power is generally needed. Therefore, a regular load could be added e.g. an air condition unit. Norway has a high percentage of electrical vehicles. An option could be using the excess energy to supply a makeshift charging station during the summer.

Another option could be to take advantage of the hydrogen unit as the surplus energy could be used to produce hydrogen. As explained in section 4.2.2 there is a lack of refuelling stations for hydrogen vehicles in Norway and in Trondheim there is only one station. Therefore, the consumer could provide a service for the region and turn a profit. The hydrogen unit would not be able to produce a sufficient amount of hydrogen gas to be viable. Using equation 6.3 shows that a maximum of 68.0 MWh can be stored in the hydrogen tank, as presented below.

$$113.6 \text{ MWh} \cdot 0.63 \cdot 0.95 = 68.0 \text{ MWh}$$

There are some issues with this option. First of all, the demand for hydrogen gas for vehicles is still low as it is a developing industry and suffer from a lack of infrastructure. The hydrogen unit also produces hydrogen at 30 bar, which is substantially lower than the usual 700 bar required for use in vehicles. Therefore, some of the surplus energy has to be used to compress the hydrogen. This would lead to significant energy losses and is not accounted for.

By assuming all of the 68.0 MWh of energy stored in the hydrogen tank could be used to produce hydrogen gas. Using equation 6.4 shows that at most 2 040 kgH₂ can be stored, as presented below.

$$\frac{68\,000 \text{ kWh}}{33.33 \text{ kWh/kgH}_2} = 2\,040 \text{ kgH}_2$$

Comparing this to the refuelling station at Tiller, which produces approximately 350 kgH₂ per day at full capacity, shows that this will not account for much when compared to the other refuelling station. As Trondheim is a university city with research it could be an option to deliver the hydrogen to the labs at NTNU or SINTEF. The maximum profit possible is calculated in equation 7.1. In the equation the price is based on a refuelling station in Oslo.

$$2\,040 \text{ kgH}_2 \cdot 89.9 \text{ NOK/kgH}_2 = 183.4 \text{ kNOK} \quad (7.1)$$

The result is a maximum potential profit of 183.4 kNOK. This profit is idealized and in reality the profit will be lower. It also means that the simplification done in equation 6.3 will not impact the results significantly. However, it shows that it is possible to make some kind of profit by utilizing the excess energy for hydrogen gas production.

Chapter 8

Economic Analysis

This chapter presents the results from the economic analysis of the cases, including the on grid scenario for case WiSoBaHy. The analysis is done by evaluating three various economic factors; the annual profitability, the net present value and LCOE.

To fully evaluate the annual profitability the net exchange with TEN for case Wi, case WiSo, case WiBa and case WiSoBa are presented and compared. Further, the income and expense are presented for all the cases. The income is divided into sale to TEN and savings from using self produced energy, while expense is from purchasing from TEN. Thereafter, the annual profit during a year for each case is accumulated to better illustrate the economic development over a year.

The profitability gives a clear picture of which case is the most profitable during a year, however, to evaluate the value of the investment over time the NPV over 30 years is presented. This results in a presentation of the economic development including the investment-, installation-, maintenance- and renewed investment costs. In addition, the annual profitability from each case is accounted for. The chapter also includes an evaluation of the impact of the PV system on the profitability for the consumer, and compared against the base case. The chapter is concluded with an evaluation of the LCOE of the wind turbine and PV system. The results are compared and discussed in relation to the cost trends of RESs.

8.1 Energy Exchange with TEN

During the base year there is exchange with TEN for cases Wi, WiSo, WiBa and WiSoBa. For case Wi, the exchange with TEN was continuous during the year. This can be observed from figure 8.1, which presents the sold- and purchased energy from TEN.

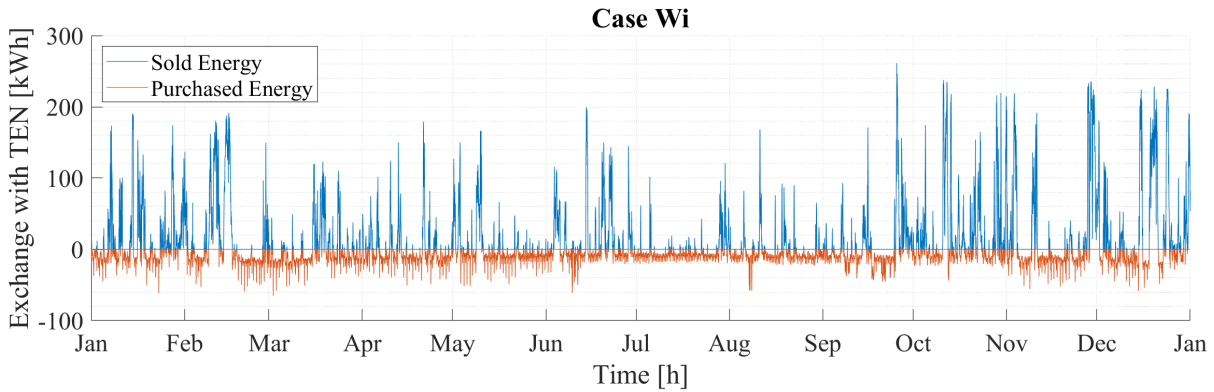


Figure 8.1: Hourly net exchange with TEN for case Wi during the base year.

From the figure 8.1 it can also be observed that the energy deficit is lower from June to September than for the rest of the year. This is due to the decreased energy demand, which can be observed from figure 7.1. In addition, the excess power is greater from October to February. This is in line with the wind energy production presented in figure 7.2. A total of 150.4 MWh was sold and 78.1 MWh purchased for case Wi.

In case WiSo the energy sold increases to 206.4 MWh, while the need to purchase energy decreases to 54.7 MWh. The decrease in energy demand from TEN during the summer is due to the added PV system. Figure 8.2 presents the energy sold and purchased from TEN.

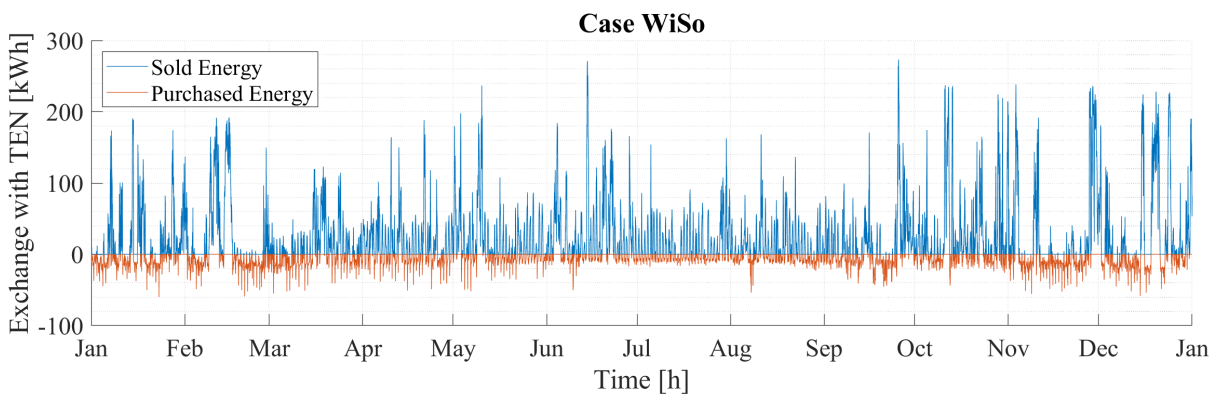


Figure 8.2: Hourly net exchange with TEN for case WiSo during the base year.

For case WiBa, the energy sold to TEN decreases to 120.0 MWh, compared with case Wi and case WiSo. The need to purchase energy decreases from case Wi, however, it is approximately the same as in case WiSo at 53.6 MWh. The energy sold and the energy purchased from TEN during in case WiBa is presented in figure 8.3.

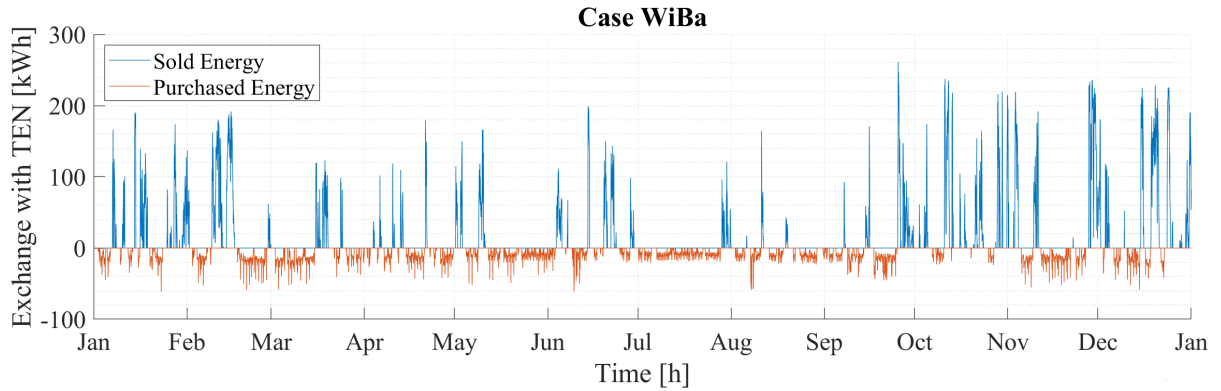


Figure 8.3: Hourly net exchange with TEN for case WiBa during the base year.

Case WiBa has a lower total energy production than case WiSo, however, the need to purchase energy is approximately the same. This is due to the fact that excess wind energy in case WiBa is stored in the battery rather than being sold to TEN. By comparing figure 8.1 and figure 8.3 it can be observed that excess energy curve in case WiBa is more uneven than in case Wi. The abrupt decrease in excess energy curve in case WiBa is because the battery is empty. The abrupt increase in excess energy is due to the fact that the battery is fully charged.

For case WiSoBa a total of 165.9 MWh was sold to TEN during the base year, while 22.2 MWh was purchased from TEN. Figure 8.4 presents the energy exchange with TEN for case WiSoBa. It can be observed that the consumer is self supplied from June to August with case WiSoBa.

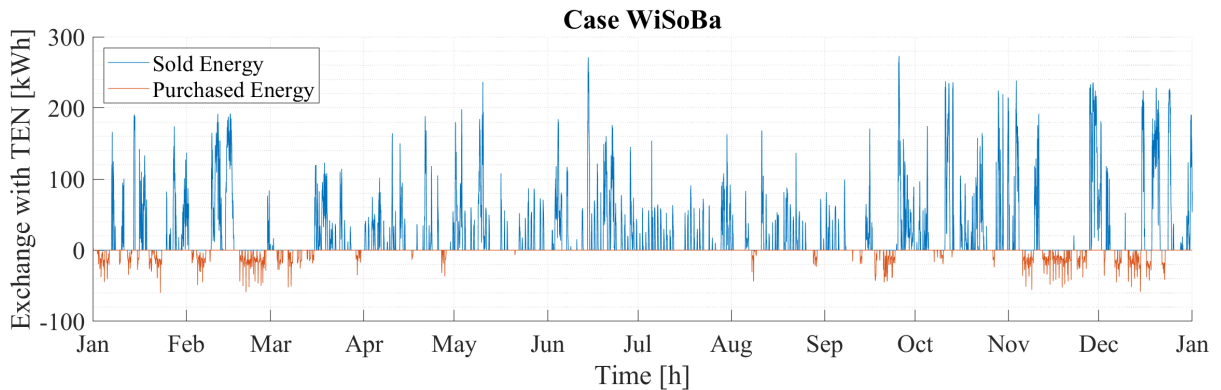


Figure 8.4: Hourly net exchange with TEN for case Wi during the base year.

By comparing figure 8.4 to figures 8.1, 8.2 and 8.3 it can be observed that case WiSoBa has the lowest need to purchase energy from TEN. There is a need to purchase- and sell energy continuously for all the cases in varying degree.

A significant observation is made from comparing figure 8.2 and figure 8.4, where the difference between the cases is the battery. By installing a battery the energy sold to TEN decreases from 206.4 MWh in case WiSo to 165.9 MWh in case WiSoBa. In addition, the need to purchase energy from TEN decreases from 54.7 MWh in case WiSo to 22.2 MWh in case WiSoBa. The installation of a battery therefore leads to a more flexible energy supply.

8.2 Profitability

To determine the profitability over a year, the income from sale to TEN and purchase from TEN had to be considered. This also includes case WiSoBaHy on- and off grid to be able to compare the difference in profitability between the two scenarios. In addition, the savings from using self produced energy, either directly from wind or solar, or from the ESS, had to be taken into account. This is presented in kNOK for each case in table 8.1, with the total profit from each case.

Table 8.1: The profit from energy exchange with the grid, self supply, battery- and hydrogen usage for all of the cases in kNOK.

	Wi	WiSo	WiBa	WiSoBa	WiSoBaHy (on grid)	WiSoBaHy (off grid)
Sale	60.8	85.3	48.0	67.6	46.3	0
Purchase	- 72.6	- 52.0	- 51.7	- 24.2	- 11.6	- 11.6
Self supply	46.8	67.5	46.8	67.5	67.5	67.5
Battery	0	0	20.6	27.5	27.5	27.5
Hydrogen	0	0	0	0	12.7	12.7
Total	35.0	100.8	63.7	138.4	142.4	96.1

From table 8.1 it can be observed that case WiSoBaHy on grid is the most profitable during a year. However, case WiSoBa is just 4.0 kNOK less profitable. Case WiSoBaHy on grid is more profitable than case WiSoBa due to savings from using the HESS. Both of the cases have the same profit from using the battery.

Further, there is a greater income from using self produced energy rather than selling to TEN. This is because the sale price is lower than the purchasing price, as it includes other expenses explained in section 6.3.2. Using self produced energy leads to the consumer saving the purchasing price.

Table 8.1 only present the profit for each case at the end of the year. Therefore, to better illustrate the yearly economic development, the hourly profit for each case was accumulated. This illustrates during which part of the year there is income and expense. The accumulated profitability for each case is presented in figure 8.5.

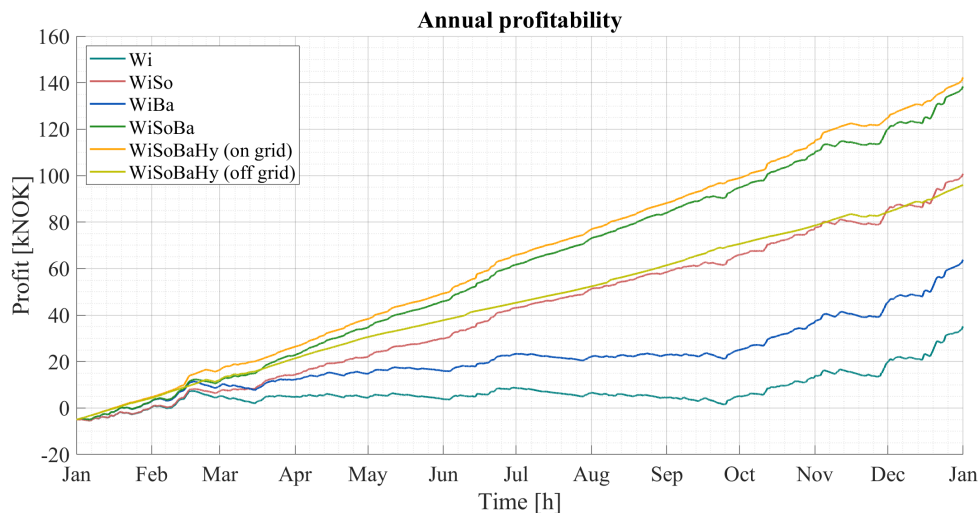


Figure 8.5: The annual profitability development for all the cases. All cases include a fixed price of 5 000 NOK/year as a part of the grid rent, hence all the cases start at -5 000 NOK.

From figure 8.5, it can be observed that case WiSoBaHy on grid has a linear increasing tendency due to almost no expense from purchasing from TEN. By comparing the curve for case WiSoBaHy on grid with the curve for case WiSoBaHy off grid it can be observed that the off grid version has a lighter increase. This is due to no income from selling to TEN.

Case WiSoBa is less profitable than both scenarios of case WiSoBaHy in the beginning of the year. However, during March it becomes more profitable than case WiSoBaHy off grid, because energy is sold to TEN rather than used for electrolysis or throttling. The difference between case WiSoBaHy on grid and case WiSoBa is mostly stable during the rest of the year, however, in November case WiSoBa experiences a more fluctuating profit. This is a result of less energy storage capacity and therefore expense from purchasing from TEN.

It can be observed that the cases including wind and solar have the same development in the beginning and end of the year, when the solar production is close to zero. During the summer months, the cases including solar power have a significantly steeper increase than Wi and WiBa.

A significant observation from 8.5 is that the profit from case WiSo rises over the profit for case WiSoBaHy off grid. This is a result of high sale to TEN for case WiSo, while case WiSoBaHy off grid has no income from sale of excess energy. The two least profitable cases are case Wi and case WiBa due to a lower energy production than the other cases. The difference between the cases is approximately stable trough the year, however, case Wi is slightly less profitable than case WiBa. By installing the battery annual profitability almost doubles from case Wi to case WiBa.

It can be observed that case WiSo results in a higher annual profitability than case WiBa. This is the result of both cases having approximately the same expense from purchasing energy from TEN and approximately the same savings from using self produced energy. However, the main difference is the income from sale to TEN as case WiSo almost has twice the income as case WiBa.

8.3 Net Present Value

The NPV, in MNOK, for each case over the course of 20 and 30 years are presented in table 8.2. It can be observed from table 8.2 that all cases will have a negative NPV throughout the project lifetime. It is important to note that the negative NPV can be compared to an alternative investment, e.g. a submarine cable. Therefore, a negative NPV does not necessarily mean that the project is not viable, as it can be more profitable than the alternative.

Table 8.2: The net present value for each case after 20 and 30 years in MNOK.

Net present value	Wi	WiSo	WiBa	WiSoBa	WiSoBaHy (on grid)	WiSoBaHy (off grid)
20 years	-2.5	-2.5	-7.6	-7.8	-18.8	-19.3
30 years	-3.4	-3.6	-9.6	-9.6	-24.7	-25.5

Further, it can be observed that the cases with an ESS are the most negative. This is because the investments cost both in the battery and the HESS are significantly higher than for the energy producing components.

Figure 8.6 presents the accumulated NPV for each case, including the base case, after 30 years. It can be observed that there are dips in NPV in year 10 and 20, and this is due to renewed investments. In a 20 year perspective, the renewed investments in year 20 is not taken into account. This leads to a deviation between year 20 in figure 8.6 and table 8.2.

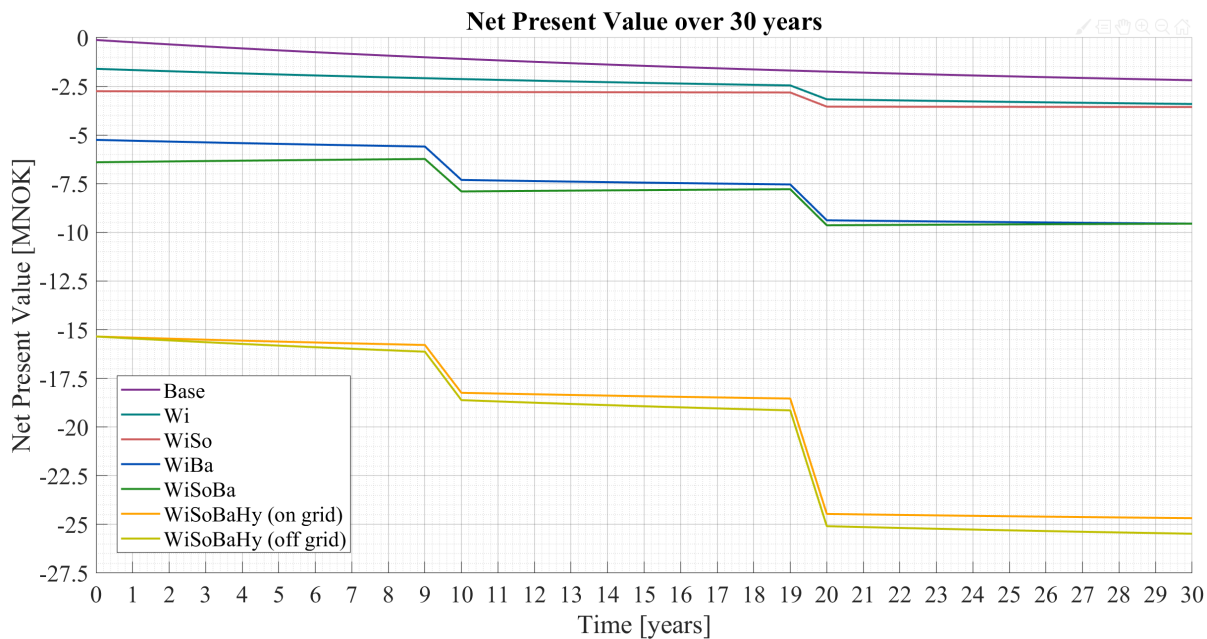


Figure 8.6: The net present value over 30 years for all cases including the base case.

Figure 8.6 shows that the base case is the most optimal as there are no investment cost related to the case. This is therefore a more inexpensive solution than investing in energy producing- and storage components. In addition to the initial investment cost, the battery and electrolysis cell needs reinvestments in year 10, and the wind turbine, inverters and HESS needs reinvestments in year 20.

It can be observed that the cases including solar power have an increasing NPV, except when there is a reinvestment in year 10 and 20. The exception is case WiSoBaHy, which has great investment costs related to the HESS. It can therefore be observed that the PV system has a positive contribution to the microgrid. This is especially noticeable when comparing case Wi against WiSo, and WiBa against WiSoBa.

Case WiSo and case WiBa are the two options relevant for the consumer after the completed project at Rye. It can be observed from table 8.2 that WiSo has a NPV that is 6 MNOK higher than case WiBa. It can therefore be assumed that it is more profitable for the consumer to invest in the PV system than the battery. It can be observed that case WiBa and case WiSoBa intersect after 30 years, making the investments equally profitable. If the consumer decides to invest in the battery, the same profit could be made by also investing in the PV system. The cases with the highest security of supply, WiSoBa and WiSoBaHy, are the cases with the lowest NPV. WiSoBa has an NPV that is 15.1 MNOK higher than for case WiSoBaHy (on grid) and 15.9 MNOK higher than WiSoBaHy (off grid).

Case WiSo Expansion

The PV system is operational from the year 2019, and will operate through year 2048. To evaluate how much the PV system contributes, the NPV of the contribution from the PV system was compared to the base case, where all the energy is purchased from TEN. The base case would include a yearly expense of 119.4 kNOK/year, and no income from selling to TEN. Hence, the NPV would decrease yearly, as presented in figure 8.7.

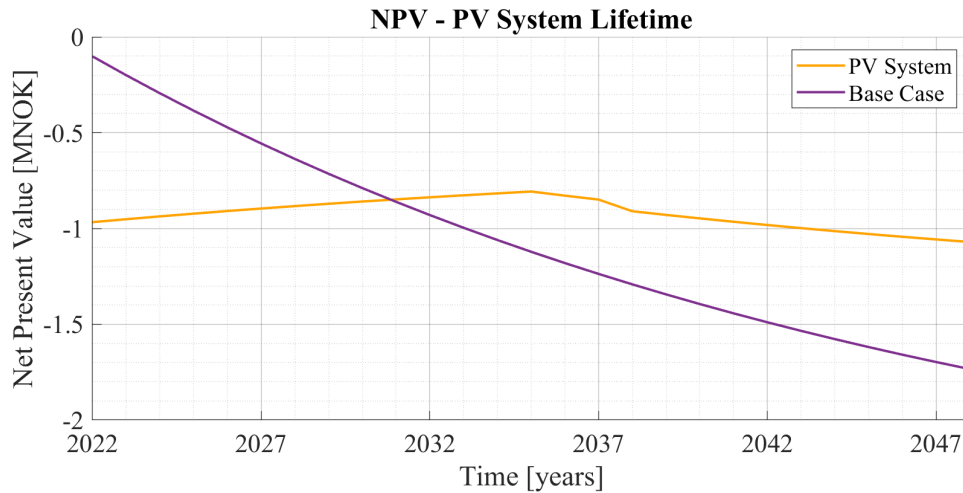


Figure 8.7: The net present value over the 27 year lifetime of the PV system. The figure compares the NPV of the PV system and the base case, where all the energy is purchased from the grid.

Considering the PV system, it can be observed that the NPV would cross the base case NPV at the end of year 2030. From this intersection, the consumer would save money by investing in the PV system in contrast to purchasing all the energy from the grid. By the end of year 2035, the wind turbine would reach its lifetime, and it would no longer be operational. From this point, the only energy source would be the PV system, and the NPV would decrease yearly. In year 2038, the inverters need replacing, and causes a dip in NPV

Even though the NPV is decreasing towards the lifetime of the PV system, the base case NPV has a steeper slope and at the of the PV system lifetime, the total profit from investing in the PV system is 663.2 kNOK. This is based on the difference between the NPV of the PV system and base case at the end of 2048. Even though the NPV is negative, the profit from the PV system investment is positive.

8.4 LCOE

The energy produced at Rye Microgrid stems from both wind and solar. In order to evaluate which energy source is most economically viable the LCOE has been calculated for both and are presented in table 8.3

Table 8.3: The calculated LCOE for the energy sources at Rye Microgrid.

	Wind power	Solar power
Discounted costs	-2 959 032.6 NOK	-1 290 504.0 NOK
Lifetime	20 years	30 years
Annual installment	217 730.8 NOK	74 630.0 NOK
Annual production	216 910 kWh	79 343 kWh
LCOE	1.00 NOK/kWh	0.94 NOK/kWh

The LCOE for the wind turbine at Rye Microgrid was calculated to be 1.00 NOK/kWh, and 0.94 NOK/kWh for the PV system. This is based on data from the base year, and thus will vary yearly. This in turn means that the LCOE is not exact. However, the numbers give an indication of the difference in price between the two sources. The PV system will have the lowest LCOE meaning that it provides the most energy for the lowest price.

If the consumer does not have any energy production, the energy demand is supplied from TEN. The mean price including the fixed price of 5000 NOK/year, was 1.42 NOK/kWh when purchasing from TEN in 2018. This shows that both energy sources are significantly cheaper than purchasing from TEN. However, there is need to purchase from TEN because of the unpredictability of wind and solar power.

As described in section 3.4.2, the LCOE for utility scale solar and wind power is expected to fall significantly until 2040. There is reason to believe that cost reductions will have a snowball effect and lead to improved technology and hence, further reduction in prices.

Chapter 9

Environmental Impact

Decreasing carbon emissions is an important goal when expanding the power- and distribution grid. This is observed in Norway and the rest of Europe with an increasing RES-share in the utility grid. Microgrids based on RES could be a solution to further decrease carbon emissions.

This chapter focuses on the environmental impact of the installation of Rye Microgrid. To evaluate this, the total carbon emissions from the energy production is calculated and compared against the emissions from using energy from the grid. The carbon intensities for the different cases at Rye is calculated and discussed, both with and without accounting for GO. The emissions related to the implementation of the microgrid at Froan is discussed, and compared to the renewable energy share in the Norwegian energy mix.

9.1 Carbon Emissions

Table 9.1 presents the calculated carbon emissions for Rye Microgrid. The calculations are done based on the energy production and energy consumption data as well as the carbon intensities stated in section 2.2. Grid with GO is used as a baseline, as this is the maximum emissions for Rye Microgrid and it is the emissions accounted for by the market. It also works as a close representation of the average European mix.

The total energy production from wind and solar is expected to cover the total energy consumption. Therefore, the emissions from the energy produced by wind and solar are compared to the consumed energy. As RESs are unpredictable, the total production will be more than the total power consumed. Table 9.1 presents the carbon emissions from the sources at Rye Microgrid.

Table 9.1: *Calculated carbon emissions from Rye Microgrid both with and without GO*

Energy Source	Total Energy Produced	Carbon Emissions
Wind	216.9 MWh	4.338 tonCO _{2,eq}
PV	79.34 MWh	1.428 tonCO _{2,eq}
Wind and PV	296.2 MWh	5.766 tonCO _{2,eq}
Grid with GO	131.0 MWh	69.56 tonCO _{2,eq}
Grid without GO	131.0 MWh	2.148 tonCO _{2,eq}

When comparing the emissions in table 9.1 from wind and PV to the emissions from the grid with GO, the total decrease in carbon emissions are 91.7%. This is in agreement with the direction both Europe and Norway are heading. Further, by comparing the emissions from wind and solar to the grid without GO, the emissions from wind and solar are slightly higher. This is because the carbon intensity from the utility grid in Norway is low due to the high share of energy production from hydro power.

Rye Microgrid has 2.68 times higher carbon emissions than if the energy consumption demand was supplied purely from the grid without GO. The large discrepancy is mostly due to the need to throttle or sell energy, and other losses from converting between storage and consumption. If Rye Microgrid was connected to TEN, the power demand would equal the power used. However, it is not possible to reach the carbon emission from the grid without GO, unless the microgrid consisted of mostly hydro power. Therefore, it is of more interest to compare towards the marked standard in the Norwegian grid in 2017, thus accounting for the GO provided by NVE, which is explained in section 2.2 when comparing the emissions.

As Rye Microgrid is based on both solar- and wind production, the actual carbon intensity for energy production at Rye Microgrid is calculated by equation 9.1.

$$20 \text{ gCO}_{2,\text{eq}}/\text{kWh} \cdot \frac{216.9 \text{ MWh}}{296.4 \text{ MWh}} + 18 \text{ gCO}_{2,\text{eq}}/\text{kWh} \cdot \frac{79.34 \text{ MWh}}{296.4 \text{ MWh}} = 19.46 \text{ gCO}_{2,\text{eq}}/\text{kWh} \quad (9.1)$$

The result is a carbon intensity of 19.46 gCO_{2,eq}/kWh. The carbon intensity of the energy production at Rye Microgrid is close to the Norwegian utility grid, as Norway's energy production has a carbon intensity of 16.4 gCO_{2,eq}/kWh without accounting for GO.

Carbon Emissions from the Cases

In order to have the carbon intensity for the cases, the power supplied from TEN also has to be accounted for. The carbon intensity for each case and the percentage of the grid carbon intensity are presented in table 9.2. Further, the table compares this with a worst case scenario where all the power supplied from the grid is from coal power.

Table 9.2: The total carbon intensity taken into account all energy production required to supply the microgrid in all five cases.

Energy Source	Carbon Intensity with GO	% of Grid with GO
Case Wi	329.6 gCO _{2,eq} /kWh	62.1%
Case WiSo	236.6 gCO _{2,eq} /kWh	44.6%
Case WiBa	232.4 gCO _{2,eq} /kWh	43.8%
Case WiSoBa	107.6 gCO _{2,eq} /kWh	20.3%
Case WiSoBaHy	49.73 gCO _{2,eq} /kWh	9.37%

The results presented in table 9.2 illustrate that there is a significant decrease when there is a connection to TEN. In case WiSoBaHy the intensity is reduced to 49.73 gCO_{2,eq}/kWh, which is 9.37% of the grid with GO. This is a significant reduction in intensity which is desired in the power market. It is important to note that even though case WiSoBaHy is 94.3% self supplied, the intensity from the grid still has a large impact.

In case Wi and case WiSo the renewable energy percentage is respectively 41.6% and 59.1% and their respective carbon intensity is 329.6 gCO_{2,eq}/kWh and 236.6 gCO_{2,eq}/kWh. The addition of solar power to wind power decreases the carbon intensity substantially. A more even energy production curve leads to a decreased need to purchase power from TEN and thus the carbon intensity decreases. The carbon intensity in case WiBa is 232.4 gCO_{2,eq}/kWh, which is slightly lower than for case WiSo. This results in approximately the same carbon intensity by expanding with solar power or a battery.

Comparing case WiSoBa with an intensity of 107.6 gCO_{2,eq}/kWh and case WiSoBaHy with an intensity of 49.73 gCO_{2,eq}/kWh, the intensity is more than halved when adding in a second ESD. An important note is that the emissions from the production of the battery and hydrogen unit is not taken into account. The increase in storage capacity from case WiSoBa to WiSoBaHy significantly reduces the carbon intensity.

The carbon intensity for a worst case scenario, where all the grid energy originates from coal, would be as in table 9.3.

Table 9.3: The total carbon intensity while accounting the energy production required to supply the microgrid in all five cases.

Energy Source	Carbon Intensity with Coal	% of Grid with GO
Case Wi	673.0 gCO _{2,eq} /kWh	126.7%
Case WiSo	477.1 gCO _{2,eq} /kWh	89.9%
Case WiBa	468.2 gCO _{2,eq} /kWh	88.2%
Case WiSoBa	205.2 gCO _{2,eq} /kWh	38.6%
Case WiSoBaHy	83.24 gCO _{2,eq} /kWh	15.7%

From table 9.3 it can be observed a significant increase in emissions in all the cases. For case Wi the emissions are above the grid with GO emission. Therefore, when constructing a microgrid solution it is important to evaluate the grid emissions as they will impact the carbon footprint of the microgrid. For case WiSoBaHy the carbon intensity is 1.67 times larger, with the additional storage capacity the influence is significantly reduced. However, the influence from a coal supplied microgrid is still noticeable.

9.2 Implementation at Froan

As discussed, TrønderEnergi is planning to use the experiences from Rye in order to implement the microgrid at Froan. The goal is to have an affordable alternative to a submarine cable. If a submarine cable would be installed, the carbon emissions would be based on the same grid solution with GO of 531 gCO_{2,eq}/kWh.

However, as experienced by Rye Microgrid, the implementation of a microgrid solution based on wind- and solar energy will yield a lower carbon intensity. If a similar solution was adapted at Froan, 94.3% of the energy consumption would have an intensity of 19.46 gCO_{2,eq}/kWh, while the remaining 5.7% will depend on what is used as a power source.

Since the goal with Froan is to avoid using a submarine cable the remaining 0-5% of the power supply has to be supplied from a different source than the grid. One solution could be to increase the storage capability, however, the impact on the emissions is unknown. Another solution is to produce more energy, preferably from a stable controllable source, e.g. a diesel generator.

The energy production from a diesel generator is simple to control, as the only thing needed is a diesel tank. It can be used whenever there is a deficit, as long as there is diesel available. The carbon intensity will be lower than the worst case, and from table 9.2, the carbon intensity was 15.7% of the grid with GO if everything came from coal. This shows that a microgrid solution could be implemented at Froan and still significantly reduce the apparent carbon emissions. However, the physical carbon emissions would not be affected by accounting for GO.

Renewable Energy Share

One of the goals for Rye Microgrid and the possible expansion to Froan is that the microgrid offers the same renewable energy share as being grid connected. The Norwegian energy mix consists of approximately 98% renewable energy generation, as described in section 3. If case WiSoBaHy would be 94.3% off grid in 2018, and the resulting 5.7% was supplied by TEN, the renewable energy share would still be sufficient. In a scenario where the microgrid is disconnected from the utility grid, as is required at Froan, the deficit of energy must be supplied from a diesel generator. As diesel is not a renewable source, this would lead to a renewable energy share of 94.3%.

Chapter 10

Evaluation of Rye Microgrid

This chapter presents an overall evaluation of the results obtained at Rye Microgrid. The focus is shifted from the case point of view to a grid consumer and a grid company perspective. The overall perspective from the consumer point of view is mostly in regard to cases Wi, WiSo and WiBa. It is unrealistic to expect a consumer to utilize the full microgrid either with WiSoBa or WiSoBaHy, because it requires a substantially larger investment cost. The evaluation of Rye Microgrid from the grid company perspective is primarily focused on the obligation of supplying the consumer. As the cases WiSoBa and WiSoBaHy are the cases with the highest fraction self supply, these are the cases of consideration.

The section presenting the consumer perspective discusses how the expansion of Rye Microgrid impacts a consumer, and illustrates which points are most relevant for a consumer. This includes the results comparing an investment in the battery or a PV system and how it impacts the energy supply and profitability. In the grid company section the factors determining if it will work for a grid company is discussed. This includes if the microgrid will provide a good enough security of supply in order to be deployed in remote areas and if it could be economically viable compared to the investments required to deliver power to these same areas. The chapter is concluded by addressing a perspective on continuation.

10.1 Consumer Perspective

The percentage self supply in case WiSo and case WiBa are respectively 59.1% and 59.9%. To increase the self supply percentage, the consumer can consider to extend the wind turbine blades. The extensions provide another 50 MWh added to the annual wind energy production. This would be an added expense, however, it would increase the self supply for case WiSo and WiBa to respectively 60.7% and 63.7%.

Another possibility is to increase the annual energy production from the PV system by 50 MWh. This would lead to a self supply percentage of 61.7% in case WiSo, which is 1.0% greater than the increase from the blade extensions. Both options result in increased profit from both self supply and sale to TEN. Increasing the PV system demands additional area usage at the site, while the blade extensions will not impact the area usage. Depending on whether or not the consumer has the necessary funds required for the investment would be the deciding factor.

The LCOE indicates that the consumer should invest in additional solar energy as that delivers the most energy per NOK invested. The LCOE for wind energy is 1.00 NOK/kWh, while solar is 0.94 NOK/kWh implying that solar energy will turn the largest profit. As presented in section 3.4.2 the LCOE is expected to fall significantly in the next 20 years. According to figure 3.13, wind power will still be the most competitive energy source. However, in this case solar energy has a lower LCOE and thus should be the better investment.

Another consideration for the consumer is what to do with the excess energy as there is excess energy in both case WiSo and case WiBa. The consumer could choose to sell all the excess energy to TEN and make a profit. The consumer could also add an extra load e.g. an air condition unit, which is a good option as there is a substantial amount of excess energy during the summer in case WiSo. However, adding a load is mainly relevant in case WiSo as the excess energy in case WiBa is erratic.

The main difference between case WiSo and case WiBa is the economic aspect. In regards to both investment cost and annual profit, WiSo is the significantly better case. The NPV after 30 years for cases WiSo and WiBa are respectively -3.6 MNOK and -9.6 MNOK. Adding PV increases the energy that goes directly to the consumption, and the amount that is sold to the grid. The increased flexibility offered by the battery, is outweighed by the income from the increased income and savings from the PV system. This indicates that case WiSo is the best case economically when considering a further investment. It can be observed from figure 8.6 that if the consumer decides to invest in the battery, he could also invest in the PV system and have the same profit after 30 years. This would also lead to a higher self supply percentage, from 59.9% in WiBa to 83.4% in WiSoBa.

The expansion of case WiSo in the NPV evaluation leads to a different NPV in case WiSo. If the consumer decides to invest in the PV system and not reinvest in the wind turbine after 20 years, the consumer could turn a profit of 663.2 kNOK after 30 years from the PV system investment. This is compared to the base case, where all the energy is purchased from TEN and excluding the cash flows related to the wind turbine.

Another observation is that adding solar power will help decrease the carbon intensity. Case WiSo and case WiBa show approximately the same carbon intensities at 236.6 gCO_{2,eq}/kWh and 232.4 gCO_{2,eq}/kWh respectively. However, the battery does not include a value for the carbon emissions so in reality it will be higher. If the consumer decides to invest in case WiSoBa, the carbon intensity would be 107.6 gCO_{2,eq}/kWh. The carbon emissions are more than halved by investing in the PV system and battery, and the NPV is the same as investing in the battery alone.

10.2 Grid Company Perspective

For Rye Microgrid, the security lies in the connection to the utility grid. For remote areas, the energy must be supplied from a different source e.g a diesel generator. There are multiple options to reach the goal of being 95% off grid and have a renewable energy share of 95%. This includes increasing the battery size, hydrogen capacity, and increasing the wind- and solar production.

By adding blade extensions to the wind turbine, case WiSoBaHy is 95.3% off grid, and by increasing the solar energy production by the same amount, the case is 96.1% off grid. Both of these adjustments allows case WiSoBaHy to meet the 95% criteria. As mentioned, the total production is sufficient to meet the consumption, but because this is not the case during all hours of the year, an option is to increase the storage capacity. Table 10.1 presents the combinations of increased energy production or storage that reach the 95% target.

Table 10.1: The energy storage capacities required to reach a self supply percentage of 95% in cases WiSoBa and WiSoBaHy. The component that is adjusted is marked with bold font.

Case	Wind Production	Solar Production	Battery Capacity	Hydrogen Capacity	Self Supply
WiSoBa	216.9 MWh/year	79.3 MWh/year	3 200 kWh	–	95.0%
WiSoBaHy	266.9 MWh/year	79.3 MWh/year	550 kWh	3 300 kWh	95.3%
	216.9 MWh/year	129.3 MWh/year	550 kWh	3 300 kWh	96.1%
	216.9 MWh/year	79.3 MWh/year	750 kWh	3 300 kWh	95.0%
	216.9 MWh/year	79.3 MWh/year	550 kWh	3 700 kWh	95.0%

From table 10.1 it can be observed that increasing the solar energy production leads to the highest self supply percentage of 96.1%. Increasing the PV system leads to a greater area usage and if this can not be implemented increasing the wind energy production is a good option. This leads to the second highest self supply percentage of 95.3% and would not demand an increase in area usage. In table 10.1, the battery- and hydrogen capacity are increased to be exactly 95% self supplied. The capacity could be increased more, however, it is important to address the economic aspect of the options.

The investment costs in the ESDs are significantly higher than for the energy production components. Therefore, increasing the battery capacity would be expensive. Increasing the capacity of the HESS only requires a larger tank, while the battery requires additional battery racks. It is therefore a better option to expand the hydrogen tank as it is less expensive.

As observed from figure 8.5, case WiSoBa is the most profitable, and the investment-, operation- and maintenance costs are significantly lower than case WiSoBaHy. When examining table 8.2, case WiSoBa is 43% more profitable than case WiSoBaHy after 30 years concerning the NPV. If the battery capacity is increased to 2 900 kWh, leading to the same self supply percentage as case WiSoBaHy, the battery size is increased with a factor of 5.3. Increasing the battery size with a factor of 5.3 lead to a significantly greater investment cost.

It can be discussed whether the added self supply from the battery and HESS is a good investment when the case is operating on grid. The investment, operation and maintenance costs for the ESD are high, and give a NPV of -19.9 MNOK in 20 years and -24.7 MNOK in 30 years for case WiSoBaHy. For remote areas, the power must be supplied either way, and the economic aspect of the microgrid must be evaluated compared to the replacement of the existing infrastructure. At Froan, this would be the replacement of the submarine cable, which is a costly process. The price development for energy storage is also expected to continue decreasing through the following years, resulting in lowered investment- and operation costs. This in turn could prove to make a microgrid solution more applicable.

In case WiSoBaHy there is a substantial amount of excess energy produced. In the off grid scenario, sale to TEN is not a possibility and therefore other solutions have to be considered than throttling the excess energy. This is especially prevalent at Froan. If there is no hydrogen unit the excess energy can be used to provide e.g. vehicle charging both at Rye and Froan. The excess energy can be used to produce hydrogen to supply e.g. a ferry to Frøya or to the mainland. This might be a good source of income and can incentivize an expansion of the energy production in order to supply the hydrogen. Producing hydrogen can also be a solution at Rye, where the hydrogen can be sold to e.g. NTNU or SINTEF for research purposes.

If case WiSoBa would applied to Froan and assuming that the microgrid will be scaled to the same self supply percentage, the remaining 16.6% of energy would be delivered by a diesel generator. As there is no data provided for the carbon intensity from the diesel generator the grid with GO emissions can be considered. The carbon intensity would then be 107.6 gCO_{2,eq}/kWh in case WiSoBa and 49.73 gCO_{2,eq}/kWh in case WiSoBaHy. The carbon intensity is more than halved by including the HESS and it can be used to argue in defence of the increased investment cost.

As described in the introduction to chapter 3 the energy demand worldwide is increasing and the energy mix consist mainly of fossil fuels. This in turn means that an increased investments in energy production is required to meet this increasing demand. If Norway is supposed to decrease their carbon emissions then these investments need to be in energy sources with low carbon intensities. As discussed in the carbon analysis, the intensity for Rye Microgrid will be 9.37% of the amount from the Norwegian grid with GO. This is a quite substantial decrease and proves that the investments in microgrids like the one at Rye is a step in the right direction.

The transmission grid in Norway is also connected to several other countries as explained in section 2.1. This means that the energy production in Norway is exchanged with the rest of Europe. This in turn also means that the emissions produced in Norway impacts the European market. Hence, it is important than Norway continues investments in low emissions energy sources.

Chapter 11

Conclusion

This thesis addresses four main questions regarding the optimization of Rye Microgrid. These questions concern the security of supply, economical value and environmental impact of Rye Microgrid. The cases are used as a method to highlight the different aspects of the components at Rye Microgrid. Evaluating the five cases made it possible to answer the questions addressed in the problem statement.

Optimal Composition for the Consumer

The consumer already owns the wind turbine, and the most optimal further investment for the consumer is the PV system, compared to an investment in the battery. This is emphasized when comparing case WiSo and case WiBa. The self supply percentage for case WiSo and case WiBa, respectively 59.1% and 59.9%, are approximately the same. Comparing cases WiSo and WiBa they have a yearly profit of 100.8 kNOK and 63.7 kNOK. The purchase from TEN and savings from using self supplied energy are approximately the same. However, the additional energy supplied by the PV system results in a income of 85.3 kNOK from selling to TEN. For case WiBa the income is significantly lower at 48.0 kNOK. In addition, the battery has significantly higher investment- and maintenance costs than the PV system.

These factors leads to case WiBa having a NPV 6.0 MNOK lower than case WiSo after 30 years. The combination of income from selling excess energy to TEN and a lower investment cost, results in the PV system being the optimal investment for the consumer. However, is it also found that if the consumer decides to invest in the battery, it is equally profitable to also invest in the PV system. This is emphasized when comparing the NPV of cases WiBa and WiSoBa, as they intersect after 30 years.

The consumer has the opportunity to purchase the PV system after the completed project. Hence, the contribution of the PV system alone was investigated. It was found that the investment in the PV system by itself yields a positive value of 663.4 kNOK compared to base case after 30 years. This results in the PV system having a profitable contribution for the consumer, and is the optimal investment.

Contribution from the HESS

The HESS supplies 10.9% of the energy demand, leading to the microgrid operating 94.3% self supplied in the base year. Compared to case WiSoBa which is 83.4% self supplied, there is a substantial increase by implementing the HESS. A positive contribution to the energy storage capacity by using a HESS is that it can be easily expanded. Increasing the hydrogen storage capacity only requires a larger hydrogen gas tank which is less economically demanding than purchasing additional battery racks.

However, the complete HESS is the most costly component of the microgrid. In a 30 year perspective, the case in including the HESS has a NPV of -25.5 MNOK, which is the lowest of all the cases. It must therefore be evaluated if the microgrid with the HESS has a higher NPV than the alternative. However, it can be concluded that the HESS is a good option for a larger ESS as it can store large quantities of energy due to a high energy density.

Off Grid Potential

For the battery in case WiSoBa to contribute with the same amount of self supply, the battery would be required to have 5.3 times the capacity. By increasing the wind- or solar energy production with 50 MWh in case WiSoBaHy the 95% off grid target is reached, with respectively 95.3% or 96.1%. Considering only the self supply percentage it can be concluded that increasing the PV system results in Rye Microgrid operating with a higher off grid percentage. It can further be concluded that the combination of wind- and solar energy are highly compatible, and hence suitable for a remote microgrid solution. In combination with ESS is it possible to be off grid.

Environmental Impact

The environmental impact from the implementation Rye Microgrid is significantly lower than the energy mix in Norway and Europe. By installing a microgrid solution the carbon intensity is approximately 9.23% of the amount of the grid when accounting for GO. Rye Microgrid also provides a renewable energy share that is comparable to the Norwegian grid when connected with TEN. In case WiSoBaHy the self supply is 94.3%, thus the remaining 5.7% will be provided by TEN and the renewable energy share is viable.

Further Work

An important consideration when evaluating microgrid establishments, is to learn from former projects. Before the establishment of the microgrid at Froan, a feasibility analysis like the one in this thesis should be conducted. This includes analyzing the NPV, and comparing it to the actual cost for the submarine cable. To ensure the security of supply and renewable energy share at Froan other options than the diesel generator should be considered. Further, more effective utilization of excess energy should be found to reduce the need to throttle energy.

It is recommended to consider further exploring the impact of energy storage. This thesis illustrated that a hydrogen unit is able to store significantly larger quantities of energy and that the battery would have to be increased by 5.3 times to match the contribution by the HESS. Therefore a more complex analysis should be conducted on these components in order to evaluate which combination is the optimal energy storage solution.

To further optimize the security of supply an analysis in the master controller from PowiDian could be conducted. Adjustments to the master controller could potentially move the energy supply more efficiently. Another potential optimization is load control and movement of the electric loads at Rye. The loads have been observed to not match up sufficiently with the energy production, if they were moved then potentially more of the security of supply would be covered.

To better evaluate the environmental impact of a microgrid solution there are several aspects that should be evaluated. There should be done a further analysis of the carbon footprint for the microgrid solution. This could include specified carbon emission data from the battery and the HESS. Another consideration would be what the local impact of placing the microgrid at a remote location could be.

References

- [1] TrønderEnergi AS. *Fakta om TrønderEnergi*. tronderenergi.no. URL: <http://tronderenergi.no/om-tronderenergi/fakta-om-tronderenergi> (visited on 03/25/2019).
- [2] Anniken Auke Borgen (Supervisor at Tronderenergi). Personal communication. 2019.
- [3] Remote EU-project. *REMOTE project*. URL: <https://www.remote-euproject.eu/remote-project/> (visited on 01/14/2019).
- [4] Anniken Auke Borgen and Andrea Dahl Viggen. *Nye TrønderEnergi*. URL: <https://www.ntnu.no/documents/1280820952/1282234318/5.+Andrea+Dahl+Viggen++Anniken+Auke+Borgen.pdf/72593dee-2f2a-44b6-84cd-ad1148868767> (visited on 01/14/2019).
- [5] Maylis Duru and Trond Rikard Olsen. “REMOTE Site specifications”. In: *PowiDian* (May 16, 2018).
- [6] Enova. *PILOT-E*. URL: <https://www.enova.no/pilot-e/> (visited on 02/22/2019).
- [7] Enova. *Om Enova*. URL: <https://www.enova.no/om-enova/> (visited on 05/08/2019).
- [8] Statnett. *Langsiktig markedsanalyse*. URL: <https://www.statnett.no/for-aktorer-i-kraftbransjen/planer-og-analyser/langsiktig-markedsanalyse/> (visited on 04/30/2019).
- [9] NVE. *Nett*. URL: <https://www.nve.no/energiforsyning/nett/?ref=mainmenu> (visited on 03/11/2019).
- [10] Regjeringen. *Kraftmarkedet og strømpris*. Nov. 19, 2014. URL: <https://www.regjeringen.no/no/tema/energi/stromnettet/kraftmarkedet-og-strompris/id2076000/> (visited on 03/11/2019).
- [11] TrønderEnergi Nett. *Privat prislister 2018*. URL: <https://tronderenerginett.no/kunde/avtaler/2018-nettleie-privat> (visited on 04/03/2019).
- [12] NVE. *Nasjonal varedeklarasjon 2017*. URL: <https://www.nve.no/reguleringsmyndigheten-for-energi-rme-marked-og-monopol/varedeklarasjon/nasjonal-varedeklarasjon-2017/> (visited on 03/31/2019).
- [13] REC Group. *REC Lifecycle analysis*. URL: https://www.recsilicon.com/RECSilicon/media/RECSilicon/corporate/sustainability%20reports/lca_brochure_020911_w eb-1.pdf?ext=.pdf%7C (visited on 03/31/2019).
- [14] NVE. *Nasjonal varedeklarasjon 2016*. URL: <https://www.nve.no/reguleringsmyndigheten-for-energi-rme-marked-og-monopol/varedeklarasjon/nasjonal-varedeklarasjon-2016/> (visited on 03/31/2019).
- [15] EnergiNorge. *Hva koster opprinnelsesgarantier?* URL: <https://www.energinorge.no/politiskesaker/opprinnelsesgarantier--forbrukerens-mulighet-til-a-pavirke-produzentene/hva-koster-opprinnelsesgarantier/> (visited on 05/15/2019).
- [16] Richard Tokle Schytte. *MicroGrid – en viktig del av morgendagens distribusjonssystem*. Powel. 2018. URL: <https://www.powel.com/no/about/temaartikler/microgrid/> (visited on 04/15/2019).
- [17] Daniel C. Esty. “Microgrids in the Evolving Power System”. In: ().
- [18] Nnamdi I. Nwulu and Xiaohua Xia. “Optimal dispatch for a microgrid incorporating renewables and demand response”. In: *Renewable Energy* 101 (Feb. 1, 2017), pp. 16–28. URL: <http://www.sciencedirect.com/science/article/pii/S0960148116307273> (visited on 01/22/2019).
- [19] Utsira kommune. *Energi*. URL: <https://www.utsira.kommune.no/tema/natur-og-miljo/energi> (visited on 03/19/2019).
- [20] IPHE. *Utsira Wind Power and Hydrogen Plant*. URL: http://www.newenergysystems.no/files/H2_Utsira.pdf (visited on 05/23/2019).

- [21] T. Nakken et al. *The Utsira wind-hydrogen system - operational experience*. Oslo, Norway: Norsk Hydro ASA. (Visited on 04/04/2019).
- [22] Electronics Tutorials. *Transformer Basics and Transformer Principles of Operation*. Aug. 31, 2013. URL: <https://www.electronics-tutorials.ws/transformer/transformer-basics.html> (visited on 04/24/2019).
- [23] Circuit Globe. *Types of Losses in a Transformer*. Sept. 23, 2015. URL: <https://circuitglobe.com/types-of-losses-in-transformer.html> (visited on 04/16/2019).
- [24] Norsk Transformator. *Vurdering av transformator tap*. URL: <https://www.nortrafo.no/?Mode=Meny&HovedMenyId=81&ThisMenyId=81&InnholdId=469&fbclid=IwAR0btVqjzznRUnZAvPRRzPi0kvBysaSJHyygENDVDQkTJza79Hibtyf04Vw> (visited on 04/27/2019).
- [25] Curt Harting. *AC Transmission Line Losses*. 2010. URL: <http://large.stanford.edu/courses/2010/ph240/harting1/> (visited on 04/24/2019).
- [26] NHO. *Energi og klima*. URL: <https://www.nho.no/publikasjoner/p/naringslivets-perspektivmelding/energi-og-klima/> (visited on 04/24/2019).
- [27] McGowan Jon G. Roger Anthony L. Manwell James F. “Wind Characteristics and Resources”. In: *Wind Energy Explained, Theory, Design and Application*. John Wiley and Sons, 2009. Chap. 2.
- [28] Knut A. Rosvold and Knut Hofstad. *vindkraftverk*. In: *Store norske leksikon*. Mar. 6, 2018. URL: <http://snl.no/vindkraftverk> (visited on 01/22/2019).
- [29] Wind Turbine Program. *Wind turbine power curves*. URL: http://www.wind-power-program.com/turbine_characteristics.htm (visited on 01/17/2019).
- [30] Danish Wind Industry Association. *Power Control of Wind Turbines*. URL: <http://xn--drnmstrre-64ad.dk/wp-content/wind/miller/windpower%20web/en/tour/wtrb/powerreg.htm> (visited on 01/18/2019).
- [31] Norsk Solenergiforening. *Norske solforhold*. URL: <https://www.solenergi.no/norske-solforhold/> (visited on 01/19/2019).
- [32] Encyclopedia Britannica. *Photovoltaic effect*. URL: <https://www.britannica.com/science/photovoltaic-effect> (visited on 01/20/2019).
- [33] Bansal Ramesh Zobaa Ahmed F. “Solar Energy Calculations”. In: *Handbook Of Renewable Energy*. World Scientific Publishing, 2011. Chap. 2.
- [34] Ion Bostan et al. “Solar Energy”. In: *Resilient Energy Systems, Renewables: Wind, Solar, Hydro*. Springer, 2013. Chap. 3.
- [35] Daryl R. Myers. *Chapter 1 Fundamentals of Solar Radiation - Solar Radiation*. URL: https://learning.oreilly.com/library/view/solar-radiation/9781466503274/xhtml/01_Cover.xhtml (visited on 05/08/2019).
- [36] Alexander P. Kirk. “From Nuclear Fusion to Sunlight”. In: *Solar Photovoltaic Cells: Photons to Electricity*. Academic Press, 2015. Chap. 2. ISBN: 978-0-12-802329-7.
- [37] Paul Breeze. “The Solar Resource”. In: *Solar Power Generation*. Academic Press, 2016. Chap. 2.
- [38] The German Society for Solar Energy. *Planning and Installing Photovoltaic Systems: A Guide for Installers, Architects and Engineers*. Google-Books-ID: fMo3jJZDkpUC. Earthscan, 2008. 397 pp. ISBN: 978-1-84407-442-6.
- [39] Johannes Skaar. *albedo*. In: *Store norske leksikon*. Feb. 20, 2018. URL: <http://snl.no/albedo> (visited on 04/30/2019).
- [40] Jay Jeong. *PHOTOVOLTAICS: Measuring the 'Sun'*. URL: <https://www.laserfocusworld.com/articles/2009/05/photovoltaics-measuring-the-sun.html> (visited on 04/30/2019).
- [41] Solargis. *Solar resource maps of World*. URL: <https://solargis.com/maps-and-gis-data/download/world> (visited on 05/08/2019).
- [42] PVsyst help. *Meteo Database > Import meteo data > Meteonorm data and program*. URL: http://files.pvsyst.com/help/meteo_source_meteonorm.htm (visited on 04/10/2019).

- [43] Frederick K Lutgens. *Chegg.com*. URL: <https://www.chegg.com/homework-help/sketch-hypothetical-orbit-polar-orbiting-geostationary-satel-chapter-12-problem-4gst-solution-9780134015965-exc> (visited on 05/08/2019).
- [44] Lynn Paul A. Fthenakis Vasilis M. “PV Modules and Arrays”. In: *Electricity from Sunlight: Photovoltaic-Systems Integration and Sustainability*. John Wiley and Sons Ltd, 2018. Chap. 3.
- [45] Lynn Paul A. Fthenakis Vasilis M. “Solar cells”. In: *Electricity from Sunlight: Photovoltaic-Systems Integration and Sustainability*. John Wiley and Sons Ltd, 2018. Chap. 2.
- [46] EnergySage. *Monocrystalline Solar Panels vs. Polycrystalline Solar Panels*. URL: <https://www.energysage.com/solar/101/monocrystalline-vs-polycrystalline-solar-panels/> (visited on 04/30/2019).
- [47] Elcics. *ABOUT US*. URL: <http://elcics.com/about-us.html> (visited on 04/08/2019).
- [48] Lynn Paul A. Fthenakis Vasilis M. “Grid-Connected PV Systems”. In: *Electricity from Sunlight: Photovoltaic-Systems Integration and Sustainability*. John Wiley and Sons Ltd, 2018. Chap. 4.
- [49] SolarEdge. *Power Optimizer | SolarEdge | A World Leader in Smart Energy*. URL: <https://www.solaredge.com/us/products/power-optimizer#/> (visited on 02/19/2019).
- [50] Phillip Newman. *Sun-Earth relationships Array Orientation Solar Radiation Data Sheets - ppt video online download*. URL: <https://slideplayer.com/slide/5297009/> (visited on 05/08/2019).
- [51] PVsyst help. *Project design > Shadings*. URL: http://files.pvsyst.com/help/shadings_general.htm?fbclid=IwAR2QcH5NGEXcj5isL1LhGrOD1FzypR0HkpF5VSW18FpjcS6zfaCv1c7YU8E (visited on 04/09/2019).
- [52] PVsyst help. *Project design > Array and system losses > Array incidence loss (IAM)*. URL: http://files.pvsyst.com/help/iam_loss.htm (visited on 04/30/2019).
- [53] PVsyst help. *Project design > Array and system losses > Soiling loss*. URL: http://files.pvsyst.com/help/soiling_loss.htm (visited on 04/10/2019).
- [54] David Edward Weir and Nikolai Aksnes. *Vindkraft - produksjon i 2017*. 2018. URL: http://publikasjoner.nve.no/rapport/2018/rapport2018_10.pdf (visited on 03/11/2019).
- [55] SSB. *Electricity balance*. URL: <https://www.ssb.no/en/statbank/table/08583> (visited on 03/19/2019).
- [56] Vindportalen. *Vindkraft i Norge*. URL: <https://www.vindportalen.no/Vindportalen-informasjonsiden-om-vindkraft/Vindkraft/Vindkraft-i-Norge> (visited on 04/30/2019).
- [57] Meteoblue. *Climate Norway*. URL: https://www.meteoblue.com/en/weather/forecast/modelclimate/norway_united-states-of-america_5004016 (visited on 02/01/2019).
- [58] Renewable Energy Website UK. *Wind Speed Distribution Weibull | REUK.co.uk*. URL: <http://www.reuk.co.uk/wordpress/wind/wind-speed-distribution-weibull/> (visited on 02/01/2019).
- [59] Erik Martiniussen. *Ekspløsv vekst i norsk solenergi*. Teknisk Ukeblad. Mar. 6, 2019. URL: <https://www.tu.no/artikler/ekspløsv-vekst-i-norsk-solenergi/459703> (visited on 04/30/2019).
- [60] NVE. *Solenergi*. URL: <https://www.nve.no/energiforsyning-og-konsesjon/solenergi/> (visited on 01/19/2019).
- [61] Kent Rammen. *Netto nåverdi (nåverdimetoden)*. URL: <https://finanssans.no/netto-n-verdi> (visited on 03/04/2019).
- [62] NVE. *Kostnader i energisektoren*. Feb. 2019. URL: <https://www.nve.no/energiforsyning-og-konsesjon/energiforsyningsdata/kostnader-i-energisektoren/> (visited on 04/15/2019).
- [63] Espen Sirnes. *prosjektanalyse*. In: *Store norske leksikon*. Jan. 2, 2018. URL: <http://snl.no/prosjektanalyse> (visited on 02/21/2019).

- [64] Dr. Kendrick T. Aung. “Economic and Life Cycle Analysis of Renewable Energy Systems”. In: (2013). (Visited on 02/25/2019).
- [65] Maria Sidelnikova et al. *Kostnader i energisektoren - Kraft varme og effektivisering*. NVE, 2015, p. 238. (Visited on 02/25/2019).
- [66] Bethel Afework et al. *Levelized cost of energy*. 2018. URL: https://energyeducation.ca/encyclopedia/Levelized_cost_of_energy (visited on 02/25/2019).
- [67] IRENA. *Renewable Power Generation Costs in 2017*. International Renewable Energy Agency, 2018. URL: https://www.irena.org/-/media/Files/IRENA/Agency/Publication/2018/Jan/IRENA_2017_Power_Costs_2018.pdf.
- [68] Norske Bank. *Valutakurser*. URL: <https://www.norges-bank.no/tema/Statistikk/valutakurser/?id=USD> (visited on 04/25/2019).
- [69] Odd Richard Valmøt. *Slik fungerer batteriet som endret verden*. Teknisk Ukeblad. Nov. 17, 2013. URL: <https://www.tu.no/artikler/slik-fungerer-batteriet-som-endret-verden/233862> (visited on 02/01/2019).
- [70] Chaofeng Liu, Zachary G. Neale, and Guozhong Cao. “Understanding electrochemical potentials of cathode materials in rechargeable batteries”. In: *Materials Today* 19.2 (Mar. 1, 2016), pp. 109–123. ISSN: 1369-7021. DOI: 10.1016/j.mattod.2015.10.009. URL: <http://www.sciencedirect.com/science/article/pii/S1369702115003181> (visited on 02/01/2019).
- [71] Per Andersen. *standard elektrodepotensial*. In: Oct. 3, 2017. URL: http://snl.no/standard_elektrodepotensial (visited on 02/01/2019).
- [72] Stephen Evanczuk. *ICs Simplify Backup Power in Energy Harvesting Designs*. DigiKey. URL: <https://www.digikey.com/en/articles/techzone/2015/mar/ics-simplify-backup-power-in-energy-harvesting-designs> (visited on 04/30/2019).
- [73] Odne Stokke Burheim. *Engineering Energy Storage*. 2017.
- [74] Battery University. *How to Prolong Lithium-based Batteries - Battery University*. URL: https://batteryuniversity.com/learn/article/how_to_prolong_lithium_based_batteries (visited on 02/01/2019).
- [75] Christiana Honsberg and Stuart Bowden. *Battery Efficiency | PVEducation*. URL: <https://www.pveducation.org/pvcdrom/battery-characteristics/battery-efficiency> (visited on 02/21/2019).
- [76] Battery University. *Charles-Augustin de Coulomb’s C-Rate for Batteries*. URL: https://batteryuniversity.com/learn/article/what_is_the_c_rate (visited on 02/20/2019).
- [77] Logan Goldie-Scot. *A Behind the Scenes Take on Lithium-ion Battery Prices*. Bloomberg NEF. Mar. 5, 2019. URL: <https://about.bnef.com/blog/behind-scenes-take-lithium-ion-battery-prices/> (visited on 05/16/2019).
- [78] Claude Lamy. “From hydrogen production by water electrolysis to its utilization in a PEM fuel cell or in a SO fuel cell: Some considerations on the energy efficiencies”. In: *International Journal of Hydrogen Energy* 41.34 (Sept. 14, 2016), pp. 15415–15425. ISSN: 0360-3199. DOI: 10.1016/j.ijhydene.2016.04.173. URL: <http://www.sciencedirect.com/science/article/pii/S0360319916304232> (visited on 02/06/2019).
- [79] Jon Cartwright. *Hydrogen use doesn’t emit carbon but its production often does. That could soon change*. Horizon: the EU Research and Innovation magazine. URL: <https://horizon-magazine.eu/article/hydrogen-use-doesn-t-emit-carbon-its-production-often-does-could-soon-change.html> (visited on 03/31/2019).
- [80] Christophe Coutanceau. *Hydrogen electrochemical production*. In collab. with Steve Baranton and Thomas Audichon. *Hydrogen and Fuel Cell Primers*. London, England: Academic Press, 2018. ISBN: 978-0-12-811251-9.
- [81] Norsk Hydrogenforum. *Hyundai Nexø*. URL: <https://www.hydrogen.no/kjoretoy/hydrogenbiler/hyundai-fe-fuel-cell> (visited on 03/29/2019).

- [82] Norsk Hydrogenforum. *Europapremiere: Heftige Nikola Tre kommer til Norge i 2020*. URL: <https://www.hydrogen.no/hva-skjer/aktuelt/europapremiere-heftige-nikola-tre-kommer-til-norge-i-2020> (visited on 03/29/2019).
- [83] Sjøfartsdirektoratet. *Breaking new ground in hydrogen ferry project*. URL: <https://www.sdir.no/en/news/news-from-the-nma/breaking-new-ground-in-hydrogen-ferry-project/> (visited on 03/29/2019).
- [84] Norsk Hydrogenforum. *Her finner du hydrogenstasjonene i Norge*. URL: <https://www.hydrogen.no/stasjoner/kart-over-stasjoner> (visited on 03/29/2019).
- [85] UnoX. *Spørsmål og svar*. URL: <http://unox.no/hydrogen/sporsmal-og-svar> (visited on 04/17/2019).
- [86] Marius Valle. *Disse brenselcellene skal drive Askos hydrogenlastebiler*. Teknisk Ukeblad. June 10, 2017. URL: <https://www.tu.no/artikler/disse-brenselcellene-skal-drive-askos-hydrogenlastebiler/395262> (visited on 04/17/2019).
- [87] Wind Turbine Models. *Vestas V27 - 225,00 kW - Wind turbine*. URL: <https://en.wind-turbine-models.com/turbines/9-vestas-v27#datasheet> (visited on 01/14/2019).
- [88] REC Group. *REC TwinPeak 2 Mono - EN*. Dec. 17, 2018. URL: <https://www.recgroup.com/en/products/rec-twinpeak-2-mono-en> (visited on 02/10/2019).
- [89] REC Group. *REC TwinPeak 2 - EN*. July 23, 2015. URL: <https://www.recgroup.com/en/products/rec-twinpeak-2-en> (visited on 02/10/2019).
- [90] SolarEdge. *se-three-phase-inverter-extended-power-datasheet*. Nov. 2018. (Visited on 11/02/2019).
- [91] PowiDian. *610-57 Technical Proposal ESS V1- V1 TECHNICAL OFFER Energy Storage Solution Tronder Energi Norway Project*. Oct. 22, 2018. (Visited on 04/30/2019).
- [92] Nexans. *Kabelboka final 2009*. 67 pp. URL: http://www.nexans.no/Norway/2009/Kabelboka_final_2009.pdf?fbclid=IwAR2quI6ad0QMHcihtiUSChtejdpqIWr9k9EM03IvXDvgrQ5pfGq90YEA9KA (visited on 04/14/2019).

Appendix A REC Twinpeak 2 Mono Series Datasheet



SOLAR'S MOST TRUSTED 

REC TWINPEAK 2 MONO SERIES

PREMIUM SOLAR PANELS WITH SUPERIOR PERFORMANCE

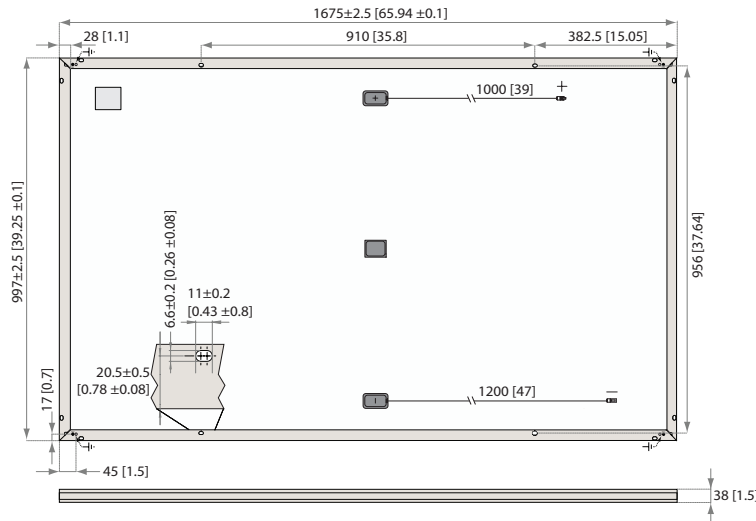
REC TwinPeak 2 Mono Series solar panels feature an innovative design with high panel efficiency and power output, enabling customers to get the most out of the space used for the installation.

Combined with industry-leading product quality and the reliability of a strong and established European brand, REC TwinPeak 2 Mono panels are ideal for residential and commercial rooftops worldwide.

NOW WITH NEW WARRANTY!

-  MORE POWER OUTPUT PER M²
-  IMPROVED PERFORMANCE IN SHADED CONDITIONS
-  100% PID FREE
-  REDUCES BALANCE OF SYSTEM COSTS

REC TWINPEAK 2 MONO SERIES



Measurements in mm [in]

ELECTRICAL DATA @ STC	Product code*: RECxxxTP2M				
Nominal Power - P_{MPP} (Wp)	300	305	310	315	320
Watt Class Sorting - (W)	-0/+5	-0/+5	-0/+5	-0/+5	-0/+5
Nominal Power Voltage - V_{MPP} (V)	33.0	33.3	33.5	33.7	33.9
Nominal Power Current - I_{MPP} (A)	9.10	9.17	9.26	9.36	9.45
Open Circuit Voltage - V_{OC} (V)	39.5	39.7	39.8	39.9	40.0
Short Circuit Current - I_{SC} (A)	9.70	9.80	9.90	10.05	10.17
Panel Efficiency (%)	18.0	18.3	18.6	18.9	19.2

Values at standard test conditions (STC: air mass AM 1.5, irradiance 1000 W/m², temperature 25°C), based on a production spread with a tolerance of V_{OC} & I_{SC} ±3% within one watt class. At a low irradiance of 200 W/m² at least 95% of the STC module efficiency will be achieved. *Where xxx indicates the nominal power class (P_{MPP}) at STC indicated above.

ELECTRICAL DATA @ NMOT	Product code*: RECxxxTP2M				
Nominal Power - P_{MPP} (Wp)	224	228	232	236	240
Nominal Power Voltage - V_{MPP} (V)	30.5	30.8	31.0	31.2	31.4
Nominal Power Current - I_{MPP} (A)	7.35	7.41	7.48	7.56	7.64
Open Circuit Voltage - V_{OC} (V)	36.5	36.7	36.8	36.9	37.0
Short Circuit Current - I_{SC} (A)	7.84	7.92	8.00	8.12	8.22

Nominal module operating temperature (NMOT: air mass AM 1.5, irradiance 800 W/m², temperature 20°C, windspeed 1 m/s). *Where xxx indicates the nominal power class (P_{MPP}) at STC indicated above.

CERTIFICATIONS

IEC 61215, IEC 61730 & UL 1703; IEC 62804 (PID)
IEC 62716 (Ammonia Resistance), IEC 61701 (Salt Mist Level 6)
ISO 9001: 2015, ISO 14001: 2004, OHSAS 18001: 2007

WARRANTY

20 year product warranty
25 year linear power output warranty
Max. performance degradation of 0.7% p.a. from 97.5% in year 1
See warranty conditions for further details.

takeaway take-e-way WEEE-compliant recycling scheme

19.2% EFFICIENCY

20 YEAR PRODUCT WARRANTY

25 YEAR LINEAR POWER OUTPUT WARRANTY

GENERAL DATA

Cell type: 120 half-cut mono-Si-p-type PERC cells
6 strings of 20 cells in series

Glass: 3.2 mm solar glass with anti-reflection surface treatment

Backsheet: Highly resistant polyester polyolefin construction

Frame: Anodized aluminum

Junction box: 3-part, 3 bypass diodes, IP67 rated in accordance with IEC 62790

Cable: 4 mm² solar cable, 1.0 m + 1.2 m in accordance with EN 50618

Connectors: Stäubli MC4 PV-KBT4/PV-KST4 (4 mm²) in accordance with IEC 62852, IP68 only when connected

Origin: Made in Singapore

MAXIMUM RATINGS

Operational temperature: -40 ... +85°C

Maximum system voltage: 1000 V

Design load (+): snow 3600 Pa (367 kg/m²)*
Maximum test load (+): 5400 Pa (550 kg/m²)*

Design load (-): wind 163 kg/m² (1600 Pa)*
Maximum test load (-): 244 kg/m² (2400 Pa)*

Max series fuse rating: 25 A

Max reverse current: 25 A

* Calculated using a safety factor of 1.5
* See installation manual for mounting instructions

TEMPERATURE RATINGS*

Nominal Module Operating Temperature: 44.9°C (+2°C)

Temperature coefficient of P_{MPP} : -0.37 %/°C

Temperature coefficient of V_{OC} : -0.28 %/°C

Temperature coefficient of I_{SC} : 0.04 %/°C

*The temperature coefficients stated are linear values

MECHANICAL DATA

Dimensions: 1675 x 997 x 38 mm

Area: 1.67 m²

Weight: 18.5 kg

Specifications subject to change without notice.
Ref: NE-05-07-16 Rev. C.2 12.18

Founded in Norway in 1996, REC is a leading vertically integrated solar energy company. Through integrated manufacturing from silicon to wafers, cells, high-quality panels and extending to solar solutions, REC provides the world with a reliable source of clean energy. REC's renowned product quality is supported by the lowest warranty claims rate in the industry. REC is a Bluestar Elkem company with headquarters in Norway and operational headquarters in Singapore. REC employs more than 2,000 people worldwide, producing 1.5 GW of solar panels annually.



Appendix B REC Twinpeak 2 Series Datasheet

SOLAR'S MOST TRUSTED 

REC TWINPEAK 2 SERIES

PREMIUM SOLAR PANELS WITH SUPERIOR PERFORMANCE

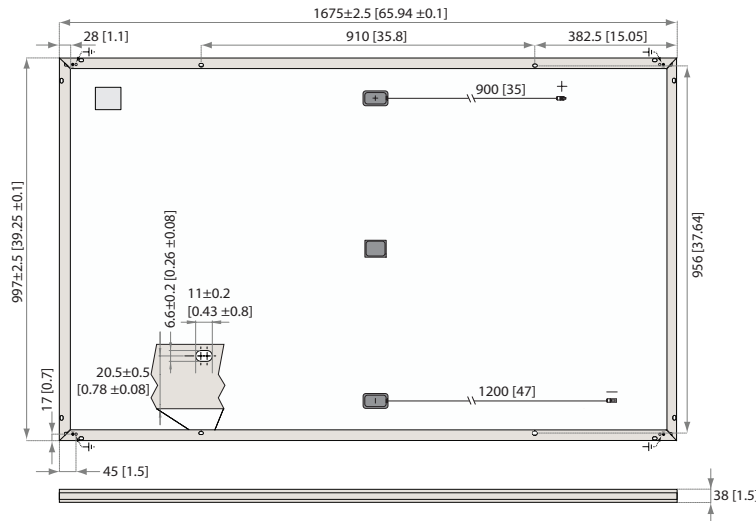
REC TwinPeak 2 Series solar panels feature an innovative design with high panel efficiency and power output, enabling customers to get the most out of the space used for the installation.

Combined with industry-leading product quality and the reliability of a strong and established European brand, REC TwinPeak 2 panels are ideal for residential and commercial rooftops worldwide.

NOW WITH NEW WARRANTY!

-  **MORE POWER OUTPUT PER M²**
-  **IMPROVED PERFORMANCE IN SHADED CONDITIONS**
-  **100% PID FREE**
-  **REDUCES BALANCE OF SYSTEM COSTS**

REC TWINPEAK 2 SERIES



Measurements in mm [in]

ELECTRICAL DATA @ STC	Product code*: RECxxxTP2					
Nominal Power - P _{MPP} (Wp)	275	280	285	290	295	300
Watt Class Sorting - (W)	-0/+5	-0/+5	-0/+5	-0/+5	-0/+5	-0/+5
Nominal Power Voltage - V _{MPP} (V)	31.5	31.7	31.9	32.1	32.3	32.5
Nominal Power Current - I _{MPP} (A)	8.74	8.84	8.95	9.05	9.14	9.24
Open Circuit Voltage - V _{OC} (V)	38.2	38.4	38.6	38.8	39.0	39.2
Short Circuit Current - I _{SC} (A)	9.52	9.61	9.66	9.71	9.76	9.82
Panel Efficiency (%)	16.5	16.8	17.1	17.4	17.7	18.0

Values at standard test conditions (STC: air mass AM1.5, irradiance 1000 W/m², temperature 25°C), based on a production spread with a tolerance of V_{OC} & I_{SC} ±3% within one watt class. At a low irradiance of 200 W/m² at least 95% of the STC module efficiency will be achieved. *Where xxx indicates the nominal power class (P_{MPP}) at STC indicated above, and can be followed by the suffix BLK for black framed modules.

ELECTRICAL DATA @ NMOT	Product code*: RECxxxTP2					
Nominal Power - P _{MPP} (Wp)	206	210	214	218	223	226
Nominal Power Voltage - V _{MPP} (V)	29.2	29.4	29.6	29.8	30.0	30.1
Nominal Power Current - I _{MPP} (A)	7.07	7.15	7.24	7.32	7.43	7.51
Open Circuit Voltage - V _{OC} (V)	35.4	35.6	35.8	36.0	36.2	36.3
Short Circuit Current - I _{SC} (A)	7.52	7.59	7.68	7.75	7.85	7.91

Nominal module operating temperature (NMOT: air mass AM1.5, irradiance 800 W/m², temperature 20°C, windspeed 1 m/s). *Where xxx indicates the nominal power class (P_{MPP}) at STC indicated above, and can be followed by the suffix BLK for black framed modules.

CERTIFICATIONS

IEC 61215, IEC 61730 & UL 1703; MCS 005, IEC 62804 (PID)
 IEC 62716 (Ammonia Resistance), IEC 60068-2-68 (Blowing Sand)
 IEC 61701 (Salt Mist level 6), UNI 8457/9174 (Class A), ISO 11925-2 (Class E)
 ISO 9001: 2015, ISO 14001: 2004, OHSAS 18001: 2007

WARRANTY

20 year product warranty
 25 year linear power output warranty
 (Max. performance degradation of 0.5% p.a. from 97.5% in year 1)
 See warranty conditions for further details.

18.0% EFFICIENCY

20 YEAR PRODUCT WARRANTY

25 YEAR LINEAR POWER OUTPUT WARRANTY

GENERAL DATA

Cell type: 120 half-cut multicrystalline PERC cells
 6 strings of 20 cells in series

Glass: 3.2 mm solar glass with anti-reflection surface treatment

Backsheet: Highly resistant polyester polyolefin construction

Frame: Anodized aluminum (silver / black)

Junction box: 3-part, 3 bypass diodes, IP67 rated in accordance with IEC 62790

Cable: 4 mm² solar cable, 0.9 m + 1.2 m in accordance with EN 50618

Connectors: Stäubli MC4 PV-KBT4/PV-KST4 (4 mm²)
 Tonglin TL-Cable01S-FR (4 mm²)
 in accordance with IEC 62852, IP68 only when connected

Origin: Made in Singapore

MAXIMUM RATINGS

Operational temperature: -40 ... +85°C

Maximum system voltage: 1000 V

Design load (+): snow 367 kg/m² (3600 Pa)*
 Maximum test load (+): 550 kg/m² (5400 Pa)

Design load (-): wind 163 kg/m² (1600 Pa)*
 Maximum test load (-): 244 kg/m² (2400 Pa)

Max series fuse rating: 25 A

Max reverse current: 25 A

*Safety factor 1.5

TEMPERATURE RATINGS*

Nominal Module Operating Temperature: 44.6°C (±2°C)

Temperature coefficient of P_{MPP}: -0.36%/°C

Temperature coefficient of V_{OC}: -0.30%/°C

Temperature coefficient of I_{SC}: 0.066%/°C

*The temperature coefficients stated are linear values

MECHANICAL DATA

Dimensions: 1675 x 997 x 38 mm

Area: 1.67 m²

Weight: 18.5 kg

Specifications subject to change without notice.
 Ref: NE-05-07-07 Rev: H 0119

takeaway take-e-way WEEE-compliant recycling scheme

Founded in Norway in 1996, REC is a leading vertically integrated solar energy company. Through integrated manufacturing from silicon to wafers, cells, high-quality panels and extending to solar solutions, REC provides the world with a reliable source of clean energy. REC's renowned product quality is supported by the lowest warranty claims rate in the industry. REC is a Bluestar Elkem company with headquarters in Norway and operational headquarters in Singapore. REC employs more than 2,000 people worldwide, producing 1.5 GW of solar panels annually.



Appendix C SolarEdge Power Optimizer Datasheet



Power Optimizer

P600 / P650 / P730 / P800p / P850

25
YEAR
WARRANTY

POWER OPTIMIZER

PV power optimization at the module-level

The most cost effective solution for commercial and large field installations

- / Specifically designed to work with SolarEdge inverters
- / Up to 25% more energy
- / Superior efficiency (99.5%)
- / Balance of System cost reduction; 50% less cables, fuses and combiner boxes, over 2x longer string lengths possible
- / Fast installation with a single bolt
- / Advanced maintenance with module-level monitoring
- / Module-level voltage shutdown for installer and firefighter safety
- / Use with two PV modules connected in series or in parallel

solaredge.com

solaredge

/ Power Optimizer

P600 / P650 / P730 / P800p / P850

Optimizer Model (Typical Module Compatibility)	P600 (for 2 x 60-cell PV modules)	P650 (for 2 x 60-cell PV modules)	P730 ⁽¹⁾ (for 2 x 72-cell PV modules)	P800p (for parallel connection of 2x 96-cell 5" PV modules)	P850 ⁽¹⁾ (for series connection of 2x high power or bi-facial modules)		
INPUT							
Rated Input DC Power ⁽²⁾	600	650	730	800	850	W	
Absolute Maximum Input Voltage (Voc at lowest temperature)	96		125	83	120	Vdc	
MPPT Operating Range	12.5 - 80		12.5 - 105	12.5 - 83	12.5 - 105	Vdc	
Maximum Short Circuit Current (Isc)	10.25	11	11	14	12.5	Adc	
Maximum Efficiency	99.5					%	
Weighted Efficiency	98.6					%	
Overvoltage Category	II						
OUTPUT DURING OPERATION (POWER OPTIMIZER CONNECTED TO OPERATING SOLAREEDGE INVERTER)							
Maximum Output Current	15			18		Adc	
Maximum Output Voltage	85					Vdc	
OUTPUT DURING STANDBY (POWER OPTIMIZER DISCONNECTED FROM SOLAREEDGE INVERTER OR SOLAREEDGE INVERTER OFF)							
Safety Output Voltage per Power Optimizer	1 ± 0.1					Vdc	
STANDARD COMPLIANCE							
EMC	FCC Part15 Class B, IEC61000-6-2, IEC61000-6-3						
Safety	IEC62109-1 (class II safety)						
RoHS	Yes						
Fire Safety	VDE-AR-E 2100-712:2013-05						
INSTALLATION SPECIFICATIONS							
Compatible SolarEdge Inverters	Three phase inverters SE15K & larger		Three phase inverters SE16K & larger				
Maximum Allowed System Voltage	1000					Vdc	
Dimensions (W x L x H)	128 x 152 x 43 / 5 x 5.97 x 1.69		128 x 152 x 50 / 5 x 5.97 x 1.93	128 x 168 x 59 / 5 x 6.61 x 2.32	128 x 162 x 59 / 5 x 6.38 x 2.32	mm / in	
Weight (including cables)	834 / 1.8		933 / 2.1	1019 / 2.2	1064 / 2.3	gr / lb	
Input Connector ⁽³⁾⁽⁴⁾	MC4			MC4 Dual Input ⁽⁷⁾	MC4		
Output Connector	MC4						
Output Wire Length	Portrait Orientation: 1.2 / 3.9 Landscape Orientation: 1.8 / 5.9		Portrait Orientation: 1.2 / 3.9 Landscape Orientation: 2.1 / 6.9	Portrait Orientation: 1.2 / 3.9 Landscape Orientation: 1.8 / 5.9	Portrait Orientation: 1.2 / 3.9 Landscape Orientation: 2.1 / 6.9	m / ft	
Operating Temperature Range ⁽⁵⁾	-40 - +85 / -40 - +185					°C / °F	
Protection Rating	IP68 / NEMA6P						
Relative Humidity	0 - 100					%	

⁽¹⁾ P730 replaced the P700; P850 replaced the P800s; each pair can be used interchangeably and can be connected in the same string.
⁽²⁾ Rated STC power of the module. Module of up to +5% power tolerance allowed.
⁽³⁾ For other connector types please contact SolarEdge.
⁽⁴⁾ Longer inputs wire length (90 cm) are available for use with split junction box modules (Order P730-XXXLXXX or P850-XXXLXXX).
⁽⁵⁾ For ambient temperature above +70°C / +158°F power de-rating is applied. Refer to Power Optimizers Temperature De-Rating Application Note for more details.

PV System Design Using a SolarEdge Inverter ⁽⁶⁾⁽⁷⁾	Three Phase SE15K and larger		Three Phase SE16K and larger					Three Phase for 277-480V grid				
	P600	P650	P600	P650	P730 ⁽⁸⁾	P800p	P850 ⁽⁸⁾	P600	P650	P730 ⁽⁸⁾	P800p	P850 ⁽⁸⁾
Compatible Power Optimizers	P600	P650	P600	P650	P730 ⁽⁸⁾	P800p	P850 ⁽⁸⁾	P600	P650	P730 ⁽⁸⁾	P800p	P850 ⁽⁸⁾
Minimum String Length	Power Optimizers	13										
	PV Modules	26										
Maximum String Length	Power Optimizers	30										
	PV Modules	60										
Maximum Power per String	11250 ⁽⁸⁾				13500		12750 ⁽⁹⁾		15300			W
Parallel Strings of Different Lengths or Orientations	Yes											

⁽⁶⁾ P600, P650 and P730 can be mixed in one string. It is not allowed to mix P600/P650/P730 with P800p/P850 or to mix P600/P650/P730/P800p/P850 with P300/P370/P500/P404/P405/P505 in one string.
⁽⁷⁾ In a case of odd number of PV modules in one string it is allowed to install one P600/P650/P730/P800p/P850 power optimizer connected to one PV module. When connecting a single module to the P800p seal the unused input connectors with the supplied pair of seals.
⁽⁸⁾ For SE27.6K: It is allowed to install up to 13,500W per string when 3 strings are connected to the inverter and when the maximum power difference between the strings is up to 2,000W; inverter max DC power: 37,250W.
⁽⁹⁾ For inverters for MV grid: It is allowed to install up to 15,000W per string when 3 strings are connected to the inverter and when the maximum power difference between the strings is up to 2,000W; inverter max DC power: 45,000W.

Appendix D SolarEdge Inverter Datasheet



Specifically designed to work with power optimizers

- / Superior efficiency (98%)
- / Small, lightest in its class, and easy to install
- / Built-in module-level monitoring
- / Internet connection through Ethernet or wireless
- / IP65 – outdoor and indoor installation
- / Fixed voltage inverter for longer strings
- / Smart Energy Management control
- / Optional integrated DC Safety Unit - eliminates the need for external DC isolators (SE25K and SE27.6K only)
- / Optional DC surge protection and DC fuses (SE25K and SE27.6K only)

solaredge.com

solaredge

/ Three Phase Inverter

SE12.5K - SE27.6K

	SE12.5K	SE15K	SE16K	SE17K	SE25K	SE27.6K		
OUTPUT								
Rated AC Power Output	12500	15000	16000	17000	25000 ⁽¹⁾	27600	VA	
Maximum AC Power Output	12500	15000	16000	17000	25000 ⁽¹⁾	27600	VA	
AC Output Voltage - Line to Line / Line to Neutral (Nominal)	380 / 220 ; 400 / 230						Vac	
AC Output Voltage - Line to Neutral Range	184 - 264.5						Vac	
AC Frequency	50/60 ± 5						Hz	
Maximum Continuous Output Current (per Phase)	20	23	25.5	26	38	40	A	
Grids Supported - Three Phase	3 / N / PE (WYE with Neutral)						V	
Utility Monitoring, Islanding Protection, Configurable Power Factor, Country Configurable Thresholds	Yes							
INPUT								
Maximum DC Power (Module STC)	16850	20250	21600	22950	33750	37250	W	
Transformer-less, Ungrounded	Yes							
Maximum Input Voltage	900						Vdc	
Nominal DC Input Voltage	750						Vdc	
Maximum Input Current	21	22	23	23	37	40	Adc	
Reverse-Polarity Protection	Yes							
Ground-Fault Isolation Detection	700kΩ Sensitivity				350kΩ Sensitivity ⁽²⁾			
Maximum Inverter Efficiency	98						98.3	%
European Weighted Efficiency	97.7	97.6	97.7	97.7	98	98	%	
Nighttime Power Consumption	< 2.5				< 4		W	
ADDITIONAL FEATURES								
Supported Communication Interfaces ⁽³⁾	RS485, Ethernet, Zigbee (optional), Wi-Fi (optional), Built-in GSM (optional)							
Smart Energy Management	Export Limitation, Home Energy Management							
DC SAFETY UNIT (OPTIONAL)								
2-pole Disconnection	N/A				1000V / 40A			
DC Surge Protection	N/A				Type II, field replaceable			
DC Fuses on Plus & Minus	N/A				Optional, 20A			
Compliance	N/A				UTE-C15-712-1			
STANDARD COMPLIANCE								
Safety	IEC-62103 (EN50178), IEC-62109, AS3100							
Grid Connection Standards ⁽⁴⁾	VDE-AR-N-4105, G59/3, AS-4777, EN 50438, CEI-021, VDE 0126-1-1, CEI-016 ⁽⁵⁾ , BDEW							
Emissions	IEC61000-6-2, IEC61000-6-3, IEC61000-3-11, IEC61000-3-12							
RoHS	Yes							
INSTALLATION SPECIFICATIONS								
AC Output Gland Diameter / Wire Cross Section	15-21mm / Solid wire 2.5-16 mm ² , Stranded wire 2.5-10 mm ²				18-25mm / Solid wire 2.5-16 mm ² , Stranded wire 2.5-10 mm ²			
DC Input	2 MC4 pairs				3 MC4 pairs			
DC Input with Safety Unit	N/A				Gland diameter 5 - 10		mm	
					Wire cross section 0.5 - 13.5		mm ²	
Dimensions (HxWxD)	540 x 315 x 260						mm	
Dimensions with Safety Unit (HxWxD)	N/A				775 x 315 x 260		mm	
Weight	33.2				45		kg	
Weight with Safety Unit	N/A				48		kg	
Operating Temperature Range	-20 - +60 ⁽⁶⁾ (M40 version -40 - +60)						°C	
Cooling	Fan (user replaceable)							
Noise	< 50				< 55		dBA	
Protection Rating	IP65 - Outdoor and Indoor							
Mounting	Bracket Provided							

⁽¹⁾ 24.99kVA in the UK

⁽²⁾ Where permitted by local regulations

⁽³⁾ Refer to Datasheets -> Communications category in Downloads page for specifications of optional communication options: <http://www.solaredge.com/groups/support/downloads>

⁽⁴⁾ For all standards refer to Certifications category in Downloads page: <http://www.solaredge.com/groups/support/downloads>

⁽⁵⁾ Models SE25K and SE27.6K only

⁽⁶⁾ For power de-rating information refer to: <https://www.solaredge.com/sites/default/files/se-temperature-derating-note.pdf>

Appendix E Battery Energy Storage System

This appendix presents the battery specification for the battery used at Rye Microgrid. Table E.1 presents information stated in the technical offer from PowiDian for the energy storage solution at Rye.

Table E.1: *Technical proposal for the battery energy storage system at Rye from PowiDian.*

Requirement	500 kWh
Max Power of ESS (MW)	400 kVA
System	JH3 2P
Total installed Energy @ BOL	554 kWh
Useable Energy @ BOL	500 kWh
Number of modules per Rack	17
Capacity per rack	112 kWh
Number of Total Battery rack	5
Voltage range	714-1000 V
Maximum rate of charge of discharge	2C
Recommended Operating Temperature of BESS	23 ± 5 °C
Humidity	<80% with none condensation

Table E.2 presents the main components of the battery energy storage system, including the cell, module and rack.

Table E.2: *Main components of the battery energy storage system.*

Component	Cell Model	Description	Energy
Cell	JH3	Energy-centric cell (63 Ah)	233 Wh
Module	JH3	14S2P configuration	6.52 kWh
Rack	JH3 - R1000	1000 CDV Rack with JH3 14S2P Module	110.9 kWh

Appendix F PVSyst Guide to Rye Microgrid

This appendix presents an depth description of how the PV system at Rye Microgrid was simulated in PVSyst. This includes a description of simulation parameters, the values used for the PV system and how they were implemented.

Starting the Project

Firstly, when opening PVSyst, the project design section was chosen and for Rye Microgrid the system is grid connected. The project menu opened as illustrated in figure F.1.

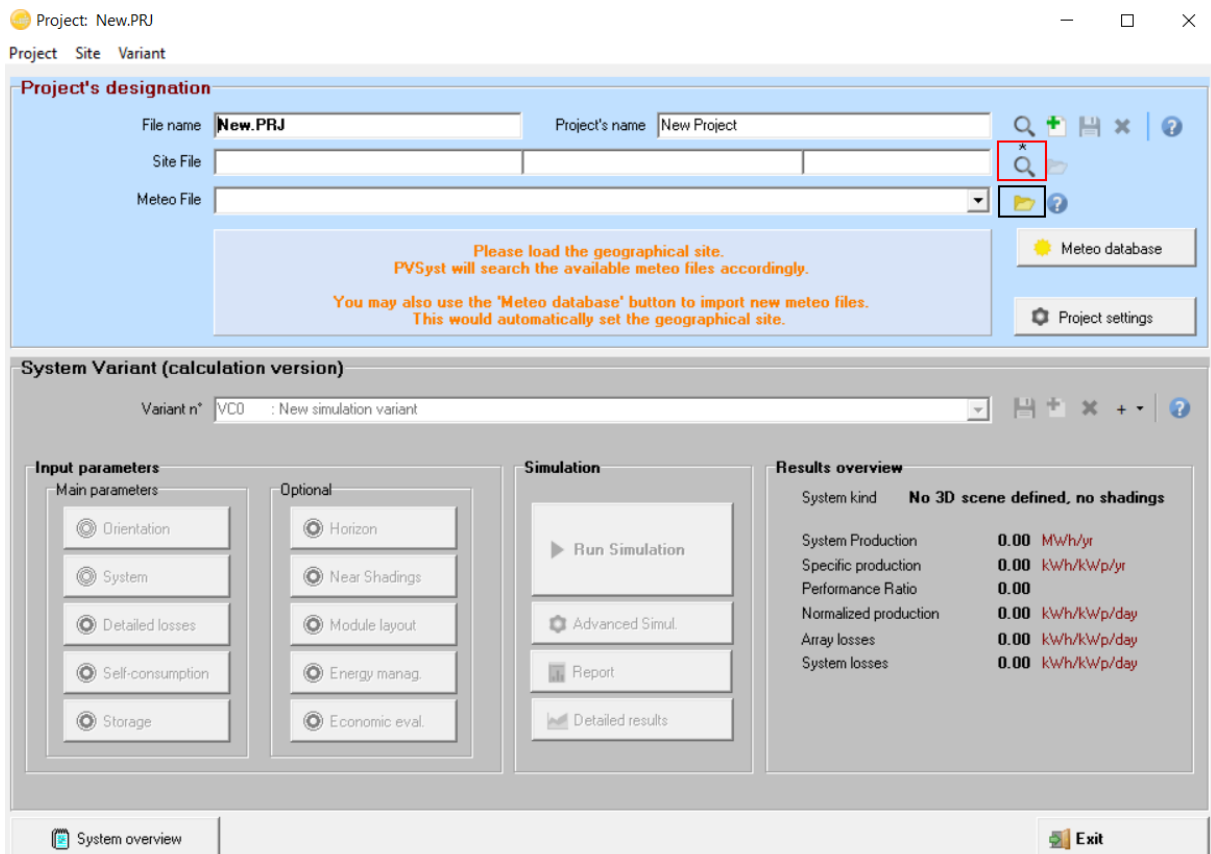


Figure F.1: Project menu in PVSyst for a grid connected system.

Further, the geographical site was chosen. This was done by clicking on the red square in figure F.1. A new menu opened up with existing locations. The correct site was selected, and further the meteo file was accessed. The meteo file can either be in the database for the site, or it has to be inputted manually. The black square in figure F.1 was selected in order to input a meteo file. For this project the meteo file was generated using Meteonorm data. This was done by clicking on "Database" → "Geographical sites" → "New". The geographical coordinates for the project were inputted, which included a latitude of 63.42 and a longitude of 10.12. To generate the data for the site, it was chosen "Meteonorm 7.2" → "Meteo data import". Before continuing to the system configurations, the project was saved.

Input Parameters

Next, the parameters were inputted. The first relevant parameter for Rye Microgrid was the orientation of the panels. This was done by clicking on "Orientation" under "Main parameters" in the system settings, as seen from figure F.1. The orientation for the project was set to 35° tilt and 0° azimuth.

Next the grid system parameters were defined by first clicking "System", and the "Grid system definition" window opened. The "Grid system definition" window is presented in figure F.2.

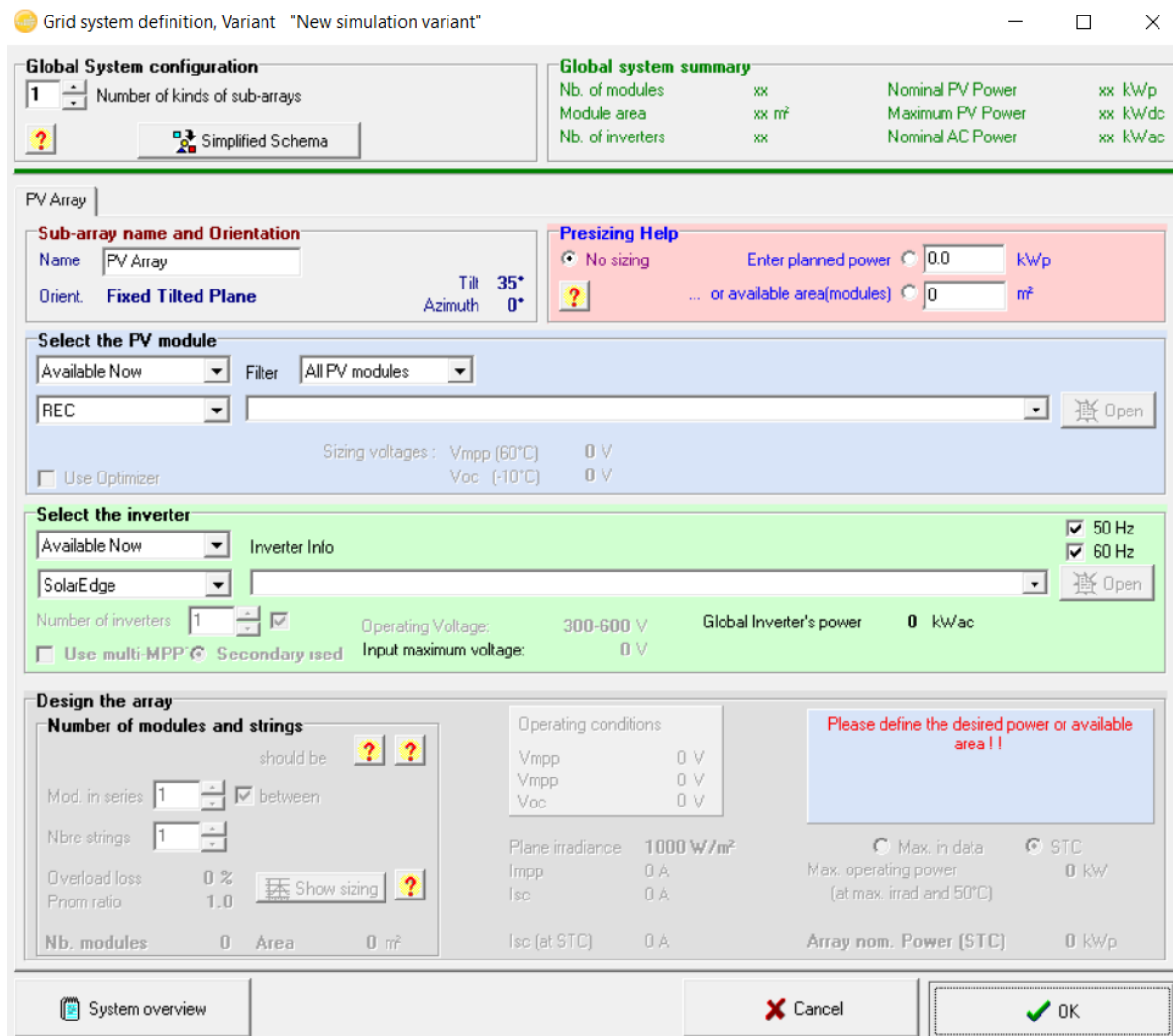


Figure F.2: The "Grid system definition" window before inputting the PV components.

Modules: The next step was to define the components. The PV modules at the site are 104 REC 310 Wp modules and 184 REC 295 Wp modules. Both modules are found in the PVsyst database. An issue with PV syst, is that PVsyst does not allow a combination of modules in one sub-array. Therefore, the number of each module differs from the real life installation to the simulation. The final simulation was done by splitting the system into three sub-arrays, which each consisted of 96 modules. This lead to a total of 96 REC 310 Wp modules and 192 REC 295 Wp modules. The difference in number of each module leads to lower installed power in the simulation than the actual installation.

The number of sub-arrays was selected under "Global System configuration". Further, the PV modules were chosen underneath "Select the PV module" by selecting "REC", and finding the correct module in the menu. In addition, the option "Use Optimizer" was checked off. For the 310 modules a "P700 for SE16k+" optimizer was chosen, and for the 295 modules a "P600 for SE15k+" optimizer was chosen.

Inverters: The inverter was added in the "Select the inverter" section where a "SolarEdge 50/60Hz SE27.6K" was used. The inverter input was 16 optimizers in series and 3 strings in parallel for all the three sub-arrays.

Power optimizer: The optimizer input was set to two modules in series. PVsyst was a bit difficult, however, by clicking on "String Configuration" which gave the strings illustrated in figure F.3, the system was further adjusted.

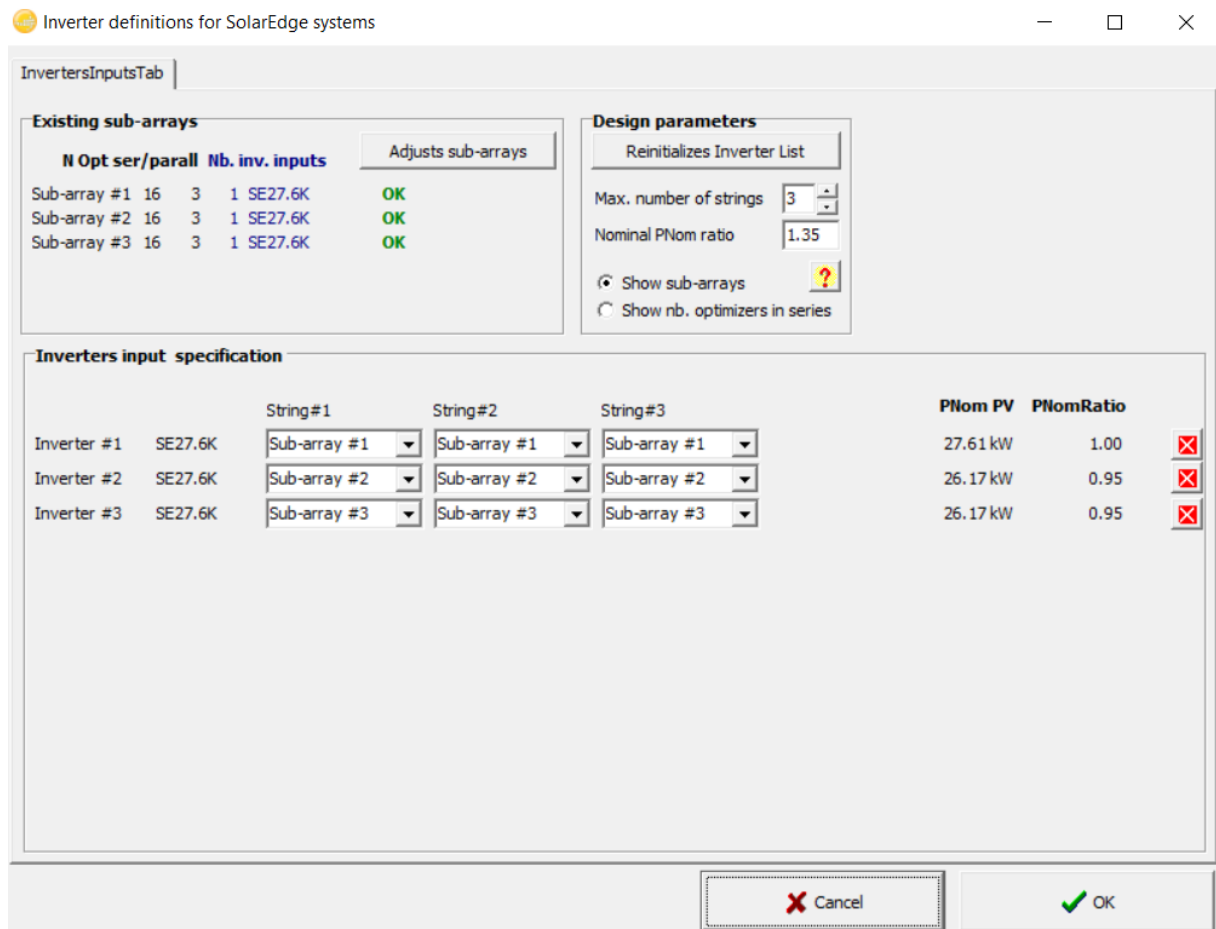


Figure F.3: SolarEdge "string configuration" illustrating the finished PV system string configuration for the PVsyst simulation.

As PVsyst sometimes reset the inverter inputs, it was necessary to select "max number of strings", add three and then make sure the strings were correct in "Inverters input specification" and then press "Reinitializes Inverter List". This changed the input specification back to the correct inverter input. By clicking "Adjust sub-arrays" the issue was solved. However, it took a couple of attempts to achieve the correct configuration.

With these inputs the system was as illustrated in figure F.4. However, the simulated system had the REC 295 Wp modules and P600 optimizers for the remaining two sub-arrays.

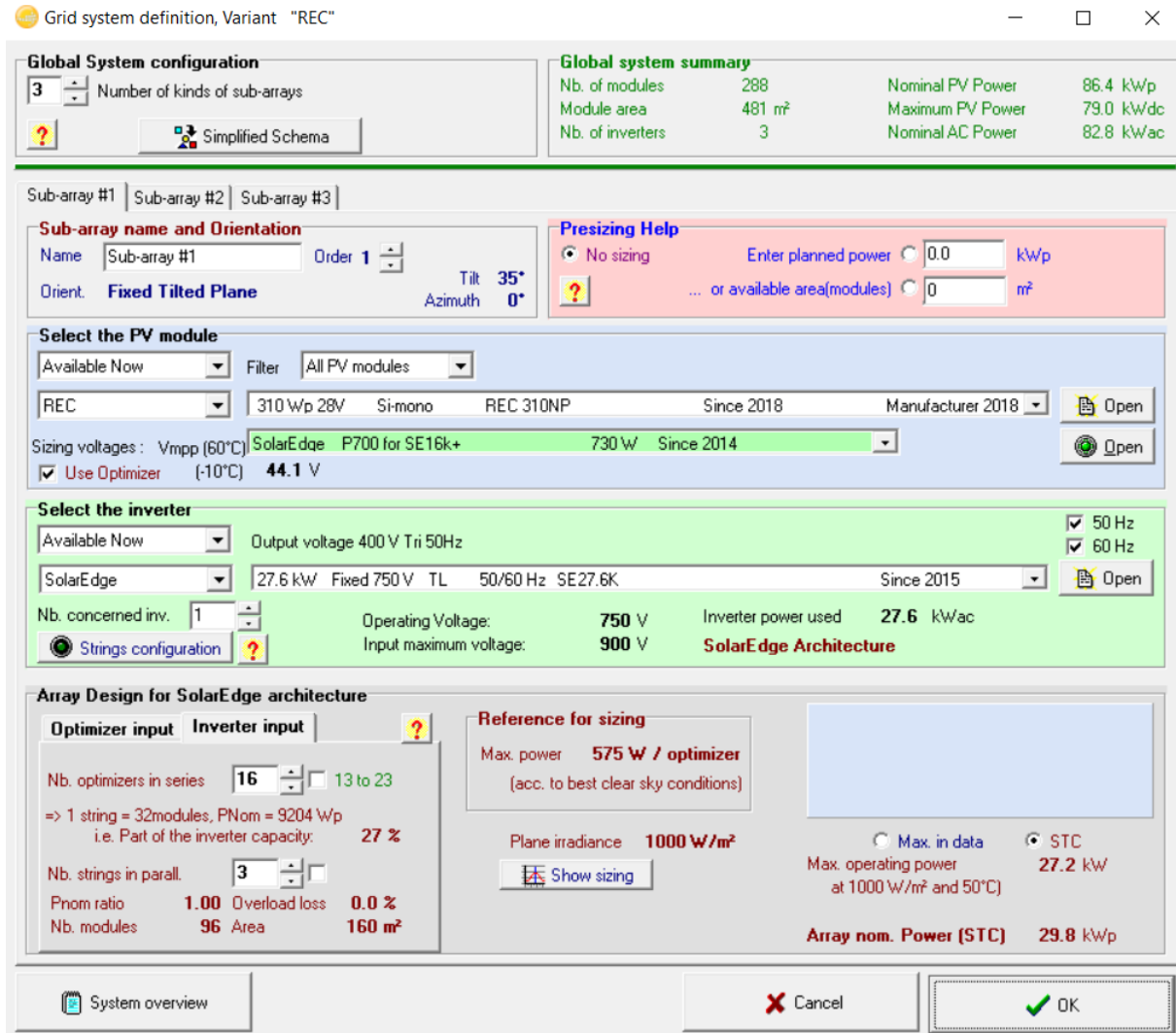


Figure F.4: Sub-array#1 after the system parameters were filled in

Defining the Losses

After all the system parameters were set, the last settings that were adjusted for Rye Microgrid were the shading- and soiling losses. In the project menu, it was clicked on "Near Shading", opening the "Near Shadings definition" window. In this project a shading profile was provided by Solbes AS. Therefore, the profile was opened in the model library, and added. The shading factor table was generated, which illustrated the shading factors for different height and solar azimuth angles.

PVsys includes a menu option to input detailed losses for the PV system. The adjustments done for Rye Microgrid was to change the monthly soiling loss factor to reflect the snowfall in Norway. The adjusted factors are presented in figure F.5.

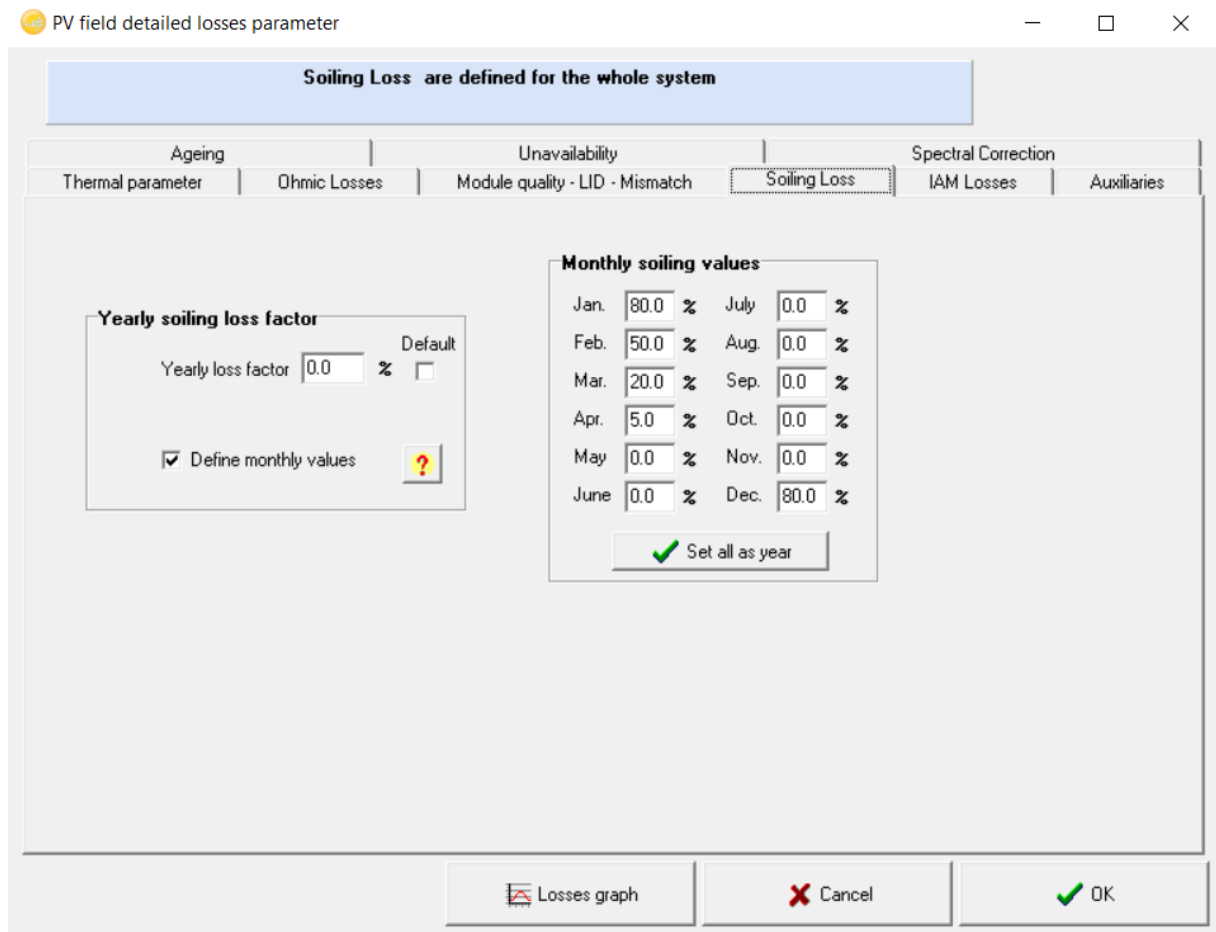


Figure F.5: The estimated monthly values for soiling losses.

Completing the Project

The simulation in PVsyst resulted in a project report detailing the simulation parameters and the output values. The report for Rye Microgrid is shown in appendix G. Some important output values from the report is the monthly energy delivered to the grid and the detailed loss diagram. The energy delivered is used as the production power from the PV system for the evaluation of Rye Microgrid. Further, the loss diagram presents how much impact the losses will have on the total power production. PVsyst can also provide additional information if needed, e.g. more detailed production graphs, an economic evaluation and hourly graphs.

Appendix G PVsyst Simulation Report

PVSYST V6.78		01/03/19	Page 1/6
Grid-Connected System: Simulation parameters			
Project :	Rye REC		
Geographical Site	Rye	Country	Norway
Situation	Latitude 63.42° N	Longitude	10.12° E
Time defined as	Legal Time Time zone UT+1	Altitude	84 m
	Albedo 0.20		
Meteo data:	Rye	Meteonorm 7.2 (1986-2005) - Synthetic	
Simulation variant :	REC		
	Simulation date	20/02/19 14h22	
Simulation parameters	System type	Sheds on ground	
Collector Plane Orientation	Tilt 35°	Azimuth	0°
Sheds configuration	Nb. of sheds 6		
	Sheds spacing 10.2 m	Collector width	3.32 m
Shading limit angle	Limit profile angle 14.4°	Ground cov. Ratio (GCR)	32.7 %
Models used	Transposition Perez	Diffuse	Perez, Meteonorm
Horizon	Free Horizon		
Near Shadings	According to strings	Electrical effect	100 %
User's needs :	Unlimited load (grid)		
PV Arrays Characteristics (3 kinds of array defined)			
Sub-array "Sub-array #1"	Si-mono	Model	REC 310NP
Original PVsyst database		Manufacturer	REC
SolarEdge Power Optimizer		Model	P700 for SE16k+
PV modules on one optimizer		in series 2	Unit Nom. Power 730 W
Nb. of optimizers		In series 16	in parallel 1
Total number of PV modules		Nb. modules 96	In parallel 3 strings
Array global power		Nominal (STC) 29.76 kWp	Unit Nom. Power 310 Wp
Output of optimizers		U oper 750 V	At operating cond. 27.22 kWp (50°C)
			I at Poper 36 A
Sub-array "Sub-array #2"	Si-poly	Model	REC 295TP2
Original PVsyst database		Manufacturer	REC
SolarEdge Power Optimizer		Model	P600 for SE15k+
PV modules on one optimizer		in series 2	Unit Nom. Power 600 W
Nb. of optimizers		In series 16	in parallel 1
Total number of PV modules		Nb. modules 96	In parallel 3 strings
Array global power		Nominal (STC) 28.32 kWp	Unit Nom. Power 295 Wp
Output of optimizers		U oper 750 V	At operating cond. 25.78 kWp (50°C)
			I at Poper 34 A
Sub-array "Sub-array #3"	Si-poly	Model	REC 295TP2
Original PVsyst database		Manufacturer	REC
SolarEdge Power Optimizer		Model	P600 for SE15k+
PV modules on one optimizer		in series 2	Unit Nom. Power 600 W
Nb. of optimizers		In series 16	in parallel 1
Total number of PV modules		Nb. modules 96	In parallel 3 strings
Array global power		Nominal (STC) 28.32 kWp	Unit Nom. Power 295 Wp
Output of optimizers		U oper 750 V	At operating cond. 25.78 kWp (50°C)
			I at Poper 34 A

PVsyst Evaluation mode

PVSYST V6.78				01/03/19	Page 2/6							
Grid-Connected System: Simulation parameters												
Total	Arrays global power	Nominal (STC)	86 kWp	Total	288 modules							
		Module area	481 m²	Cell area	424 m ²							
Inverter		Model	SE27.6K									
	Original PVsyst database	Manufacturer	SolarEdge									
	Characteristics	Operating Voltage	750 V	Unit Nom. Power	27.6 kWac							
Sub-array "Sub-array #1"		Nb. of inverters	1 units	Total Power	28 kWac							
				Pnom ratio	1.00							
Sub-array "Sub-array #2"		Nb. of inverters	1 units	Total Power	28 kWac							
				Pnom ratio	0.95							
Sub-array "Sub-array #3"		Nb. of inverters	1 units	Total Power	28 kWac							
				Pnom ratio	0.95							
Total		Nb. of inverters	3	Total Power	83 kWac							
Physical inverters												
	SE27.6K	1 units, 3 strings	3 strings of 16 optimizers P700 for SE16k+									
	SE27.6K	1 units, 3 strings	3 strings of 16 optimizers P600 for SE15k+									
	SE27.6K	1 units, 3 strings	3 strings of 16 optimizers P600 for SE15k+									
PV Array loss factors												
Array Soiling Losses					Average loss Fraction	19.6 %						
	Jan.	Feb.	Mar.	Apr.	May	June	July	Aug.	Sep.	Oct.	Nov.	Dec.
	80.0%	50.0%	20.0%	5.0%	0.0%	0.0%	0.0%	0.0%	0.0%	0.0%	0.0%	80.0%
Thermal Loss factor	Uc (const)		20.0 W/m ² K		Uv (wind)		0.0 W/m ² K / m/s					
Wiring Ohmic Loss	Array#1		283 mOhm		Loss Fraction		1.5 % at STC					
	Array#2		298 mOhm		Loss Fraction		1.5 % at STC					
	Array#3		298 mOhm		Loss Fraction		1.5 % at STC					
	Global				Loss Fraction		1.5 %					
LID - Light Induced Degradation	Array#1,				Loss Fraction		-0.4 %					
Module Quality Loss	Array#2,				Loss Fraction		-0.5 %					
	Array#3,				Loss Fraction		-0.5 %					
Module Mismatch Losses					Loss Fraction		0.0 % (fixed voltage)					
Incidence effect (IAM): Fresnel AR coating, n(glass)=1.526, n(AR)=1.290												
	0°	30°	50°	60°	70°	75°	80°	85°	90°			
	1.000	0.999	0.987	0.962	0.892	0.816	0.681	0.440	0.000			

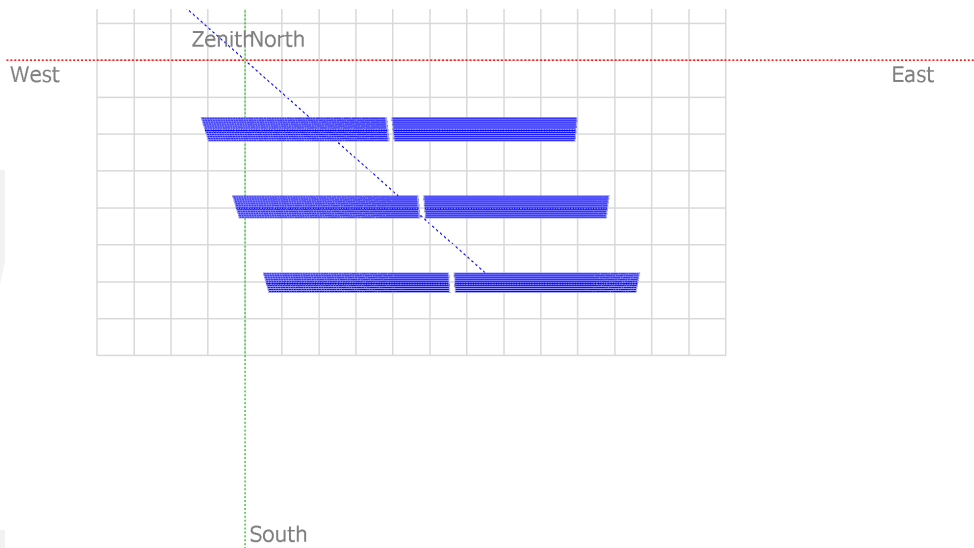
PVsyst Evaluation mode

Grid-Connected System: Near shading definition

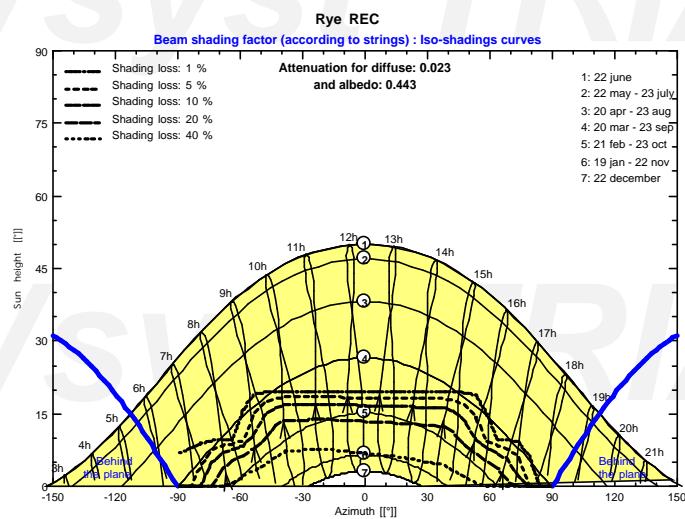
Project : Rye REC
Simulation variant : REC

Main system parameters	System type	Sheds on ground
Near Shadings	According to strings	Electrical effect 100 %
PV Field Orientation	tilt 35°	azimuth 0°
PV modules	Model REC 310NP	Pnom 310 Wp
PV modules	Model REC 295TP2	Pnom 295 Wp
PV Array	Nb. of modules 288	Pnom total 86.4 kWp
Inverter	Model SE27.6K	Pnom 27.60 kW ac
Inverter pack	Nb. of units 3.0	Pnom total 82.8 kW ac
User's needs	Unlimited load (grid)	

Perspective of the PV-field and surrounding shading scene



Iso-shadings diagram



PVSYST V6.78	01/03/19	Page 4/6						
Grid-Connected System: Main results								
Project : Rye REC								
Simulation variant : REC								
Main system parameters								
System type	Sheds on ground							
Near Shadings	According to strings	Electrical effect 100 %						
PV Field Orientation	tilt 35°	azimuth 0°						
PV modules	Model REC 310NP	Pnom 310 Wp						
PV modules	Model REC 295TP2	Pnom 295 Wp						
PV Array	Nb. of modules 288	Pnom total 86.4 kWp						
Inverter	Model SE27.6K	Pnom 27.60 kW ac						
Inverter pack	Nb. of units 3.0	Pnom total 82.8 kW ac						
User's needs	Unlimited load (grid)							
Main simulation results								
System Production	Produced Energy 79.34 MWh/year	Specific prod. 918 kWh/kWp/year						
	Performance Ratio PR 79.83 %							
<div style="display: flex; justify-content: space-around;"> <div style="width: 45%;"> <p>Normalized productions (per installed kWp): Nominal power 86.4 kWp</p> <p> Lc : Collection Loss (PV-array losses) 0.58 kWh/kWp/day Ls : System Loss (inverter, ...) 0.05 kWh/kWp/day Yf : Produced useful energy (inverter output) 2.52 kWh/kWp/day </p> </div> <div style="width: 45%;"> <p>Performance Ratio</p> <p>PR : Performance Ratio (Yf / Yr) : 0.798</p> </div> </div>								
REC Balances and main results								
	GlobHor	DiffHor	T_Amb	GlobInc	GlobEff	EArray	E_Grid	PR
	kWh/m ²	kWh/m ²	°C	kWh/m ²	kWh/m ²	MWh	MWh	
January	5.8	4.09	0.25	18.7	2.9	0.18	0.16	0.100
February	22.6	11.64	-0.60	54.5	24.5	1.88	1.83	0.389
March	64.3	25.24	1.03	116.0	88.9	7.44	7.30	0.728
April	110.7	49.69	5.76	147.1	133.7	11.00	10.79	0.849
May	153.0	67.09	9.33	169.8	162.1	13.02	12.76	0.870
June	158.4	77.59	11.95	161.3	153.5	12.24	11.99	0.860
July	153.7	79.14	15.21	161.7	153.9	12.15	11.91	0.852
August	112.3	63.30	14.62	132.4	125.9	10.01	9.81	0.858
September	66.6	29.72	10.88	99.1	94.7	7.58	7.42	0.867
October	29.5	18.22	6.58	56.9	52.4	4.08	4.00	0.812
November	7.9	5.50	2.91	22.0	17.6	1.32	1.29	0.679
December	2.6	1.99	0.40	10.8	1.5	0.09	0.08	0.087
Year	887.5	433.21	6.57	1150.3	1011.4	80.99	79.34	0.798
Legends:		GlobHor	Horizontal global irradiation	GlobEff	Effective Global, corr. for IAM and shadings			
		DiffHor	Horizontal diffuse irradiation	EArray	Effective energy at the output of the array			
		T_Amb	Ambient Temperature	E_Grid	Energy injected into grid			
		GlobInc	Global incident in coll. plane	PR	Performance Ratio			

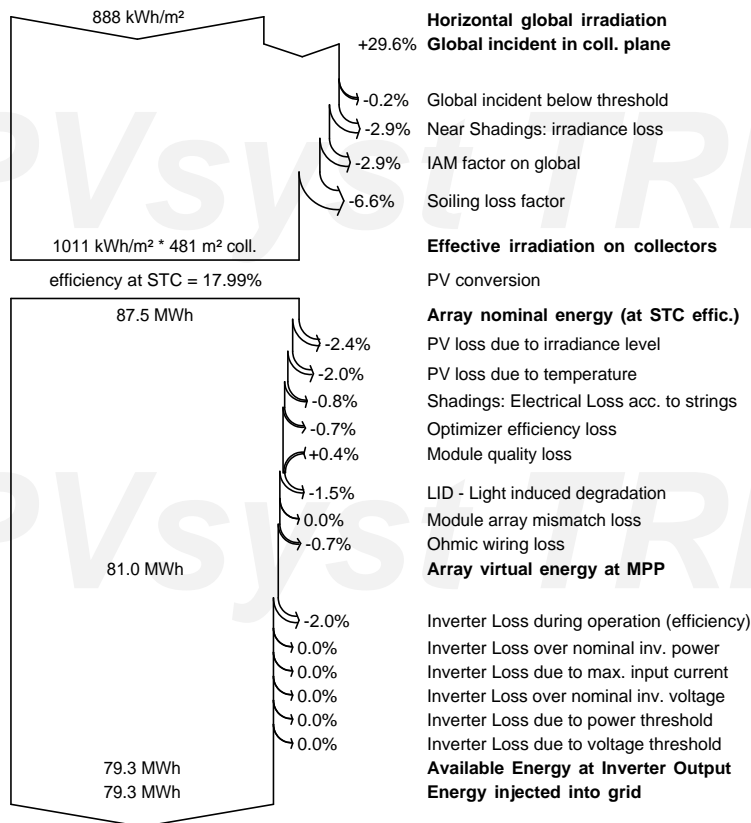
PVsyst Evaluation mode

Grid-Connected System: Loss diagram

Project : Rye REC
 Simulation variant : REC

Main system parameters	System type	Sheds on ground
Near Shadings	According to strings	Electrical effect 100 %
PV Field Orientation	tilt 35°	azimuth 0°
PV modules	Model REC 310NP	Pnom 310 Wp
PV modules	Model REC 295TP2	Pnom 295 Wp
PV Array	Nb. of modules 288	Pnom total 86.4 kWp
Inverter	Model SE27.6K	Pnom 27.60 kW ac
Inverter pack	Nb. of units 3.0	Pnom total 82.8 kW ac
User's needs	Unlimited load (grid)	

Loss diagram over the whole year



PVSYST V6.78		01/03/19	Page 6/6
Grid-Connected System: P50 - P90 evaluation			
Project : Rye REC			
Simulation variant : REC			
Main system parameters			
Near Shadings	According to strings	System type	Sheds on ground
PV Field Orientation	tilt 35°	Model REC 310NP	Electrical effect 100 %
PV modules	Model REC 295TP2	Pnom 310 Wp	azimuth 0°
PV modules	Nb. of modules 288	Pnom 295 Wp	Pnom total 86.4 kWp
PV Array	Model SE27.6K	Pnom 27.60 kW ac	Pnom total 82.8 kW ac
Inverter	Nb. of units 3.0	Pnom total	
Inverter pack	Unlimited load (grid)		
User's needs			
Evaluation of the Production probability forecast			
The probability distribution of the system production forecast for different years is mainly dependent on the meteo data used for the simulation, and depends on the following choices:			
Meteo data source	Meteonorm 7.2 (1986-2005)		
Meteo data	Kind Monthly averages	Synthetic	Multi-year average
Specified Deviation	Climate change 0.0 %		
Year-to-year variability	Variance 8.1 %		
The probability distribution variance is also depending on some system parameters uncertainties			
Specified Deviation	PV module modelling/parameters 1.0 %		
	Inverter efficiency uncertainty 0.5 %		
	Soiling and mismatch uncertainties 1.0 %		
	Degradation uncertainty 1.0 %		
Global variability (meteo + system)	Variance 8.3 %	(quadratic sum)	
Annual production probability			
	Variability 6.57 MWh		
	P50 79.34 MWh		
	P90 70.91 MWh		
	P95 68.54 MWh		
Probability distribution			

PVsyst Evaluation mode

Appendix H Simulink Model Description

Rye Microgrid is modeled in Simulink and described further in this appendix. The appendix describes the relevant blocks and the logic used to acquire the desired results. The main blocks used in the model is presented in figure H.1 and further described below. The variable that is evaluated in the model is the electrical energy flow (kWh) produced by wind and PV to cover the consumption. The time step used to evaluate is 1 hour for a total of 8760 hours.

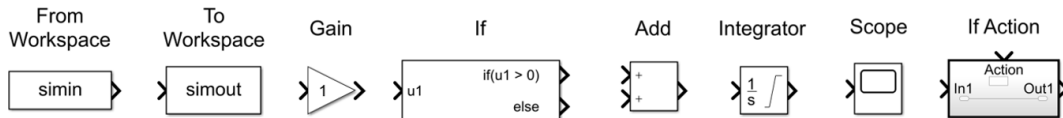


Figure H.1: The relevant blocks used in the Simulink model of Rye Microgrid.

From Workspace: The From Workspace block imports a specified vector from the MATLAB workspace into Simulink. To import from MATLAB, the vector must include a column which indicates the time. In this model, the time step was 1 value per hour for one full year. The time vector therefore included values from 1 to 8760, and the second column included the associated value, for example the wind or solar power production during that hour. To limit the amount of data points to 8760, the "Interpolate data" box was unchecked. This stops Simulink from interpolating and adding more data points to increase accuracy when there are big steps in the data. However, the model is supposed to operate with hourly values, and unchecking this box allows this. The sample time was set to 1, and the drop down menu indicating "Form output after final data value" was set to "Setting to zero".

To Workspace: The To Workspace block exports the signal to the MATLAB workspace, as the name indicates. The number of data points was limited to 8760, and the sample time was set to 1. To save the values in an expedient format, the values were saved as an array.

Subsystem: The subsystem block allows the addition of multiple levels in the model. This is used to divide the model into different sections and keep the model orderly and easier to follow as the amount of signals and blocks increases. A subsystem can contain multiple in and out ports. In the model of Rye Microgrid, there is a subsystem for the consumption, wind production, solar production, ESS in case WiBa, and ESS in cases WiSoBa and WiSoBaHy.

Gain and Add: The Gain and Add blocks are mathematical operators. The Gain block multiplies the signal with the indicated value. The block is set to multiply element-wise, which means that it multiplies each data point with the indicated value. The Add block can be used to add or subtract signals to a common signal.

If and If Action: The If block is an if-else logic based block. The input signal is considered, and the output is dependent on the conditions of the block. If the if-condition is true, the associated If Action block is executed. If the if-condition is false, the block evaluate the else-condition, and the associated If Action block is executed. This block can e.g. be used to evaluate whether a signal is positive or negative. In the model, the If block is used to evaluate whether the the battery is fully charged or empty. The If Action block can then decide what happens in the two scenarios.

Integrator: The Integrator block is used to illustrate the battery and hydrogen storage. The block accumulates the input signals, that is the net production. To make a more realistic representation coinciding with the actual battery, the block has an upper and lower saturation limit, as well as an initial condition. The upper saturation limit represents the SoC of which the ESD is considered full, and the lower saturation limit is the DoD that the ESD is considered empty.

Scope: The Scope is used to represent the signals graphically for a specific time interval.

Simulink Model of Rye Microgrid

The overall model is presented in figure H.2. The subsystems are the consumption, wind energy production, grid exchange Wi & WiSo, ESS WiBa & WiSoBa & WiSoBaHy. In the consumption subsystem, the hourly consumption data is imported from the MATLAB workspace, using a From Workspace block. The same is done for the wind and solar energy production.

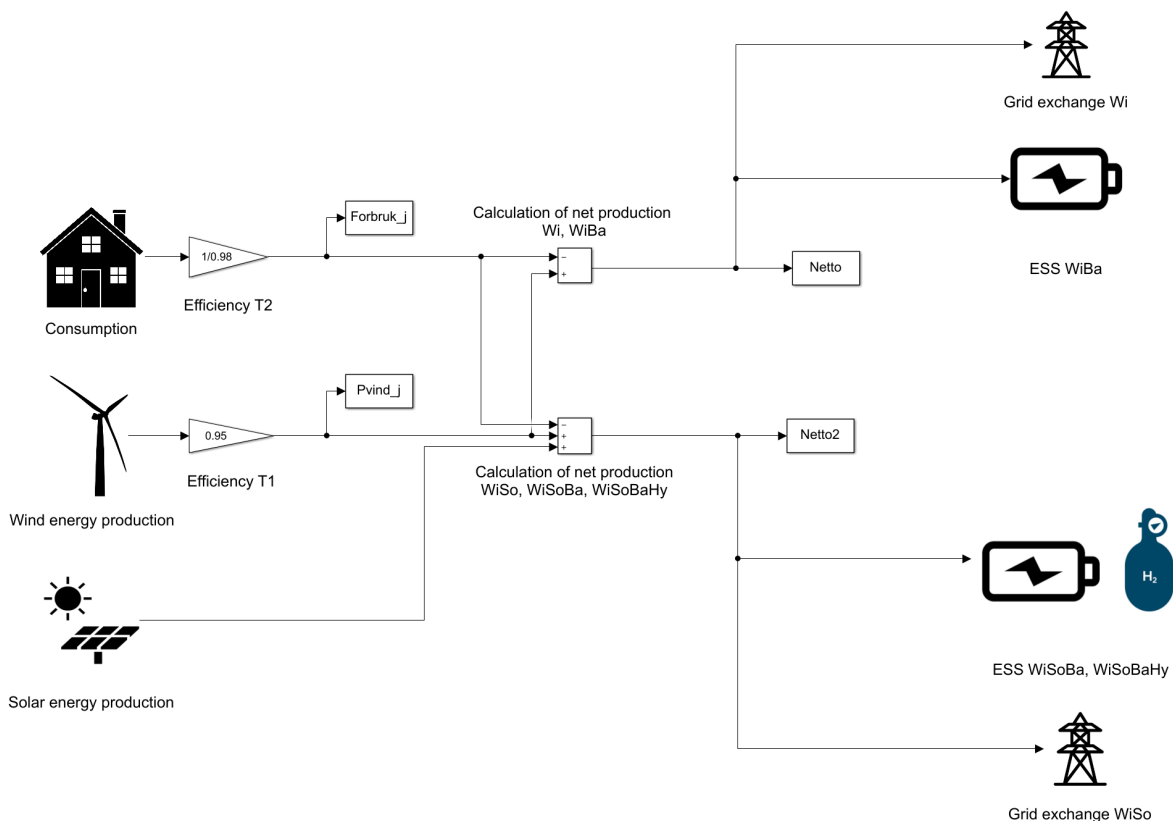


Figure H.2: Screenshot from Simulink illustrating the model used to simulate the microgrid.

There are losses due to T2 when stepping down the voltage from 22kV to 240V, hence the efficiency is taken into account by the Gain block. The energy demand is slightly more than the measured consumption, as the measurement is done on the LV side. The same is done for T1, which steps up the voltage from 400 V to 22 kV. This is taken into account by adding a Gain with the associated efficiency. The To Workspace blocks indicated "Forbruk_j" and "Pvind_j" are the wind production and consumption that is adjusted with the transformer efficiency. These are imported to the MATLAB Workspace.

Grid exchange: The net production is thereafter calculated separately for the cases concerning wind power (Wi and WiBa), and the cases concerning wind and solar (WiSo, WiSoBa, WiSoBaHy) and exported to MATLAB. The net production signal for Wi goes to the grid exchange subsystem, which separates the negative and positive net values using an If block. The purchase and sale values are exported to MATLAB. The same is done for case WiSo, where the solar power is included.

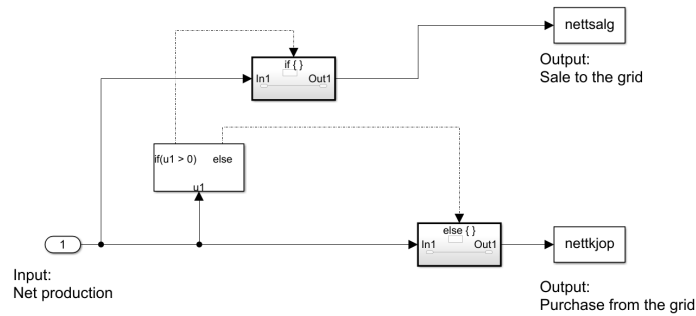


Figure H.3: The subsystem of the model showing the grid exchange in case Wi. The model is the same for the grid exchange calculation in case WiSo.

Battery energy storage system: The battery energy storage system is presented in figure H.4. If the net production is positive, the production is multiplied by the transformer and battery efficiency and accumulated in the battery. If the net production is negative, the production is divided by the transformer and battery efficiency and accumulated in the battery.

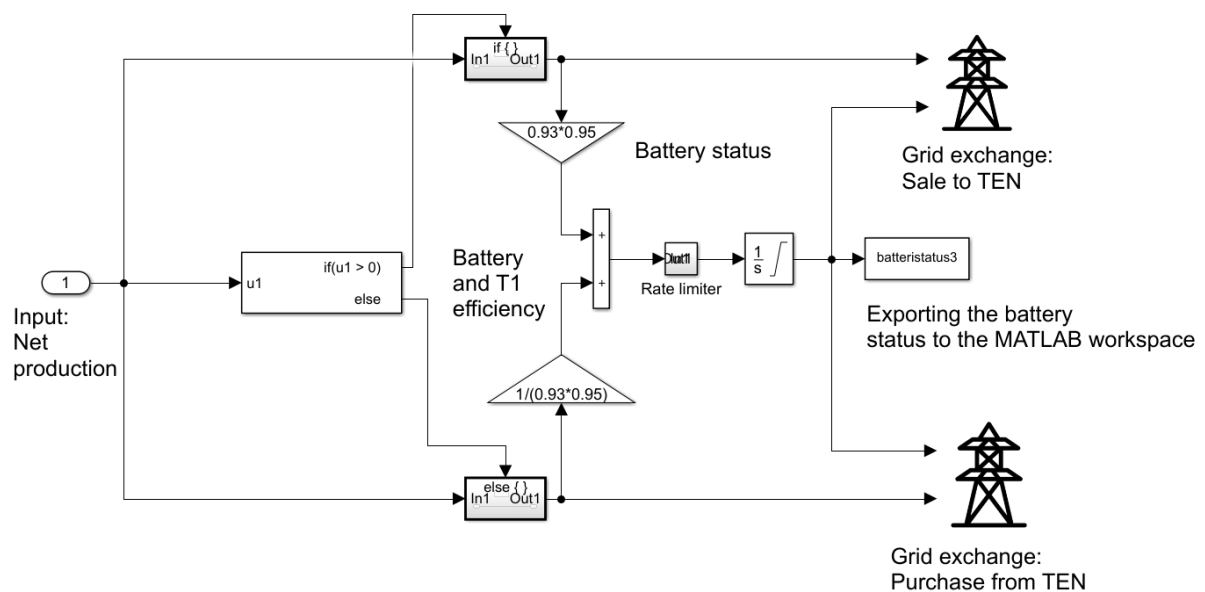


Figure H.4: The subsystem of the model showing the battery energy storage system in case WiBa. The model is the same for the battery in case WiSoBa and WiSoBaHy.

The SoC of the battery is evaluated, and if the SoC is 80% and the net production is positive, the excess production is sold to the grid. If the SoC is 20% and the net production is negative, the demand is purchased from the grid. This is calculated as in figure H.4.

Hydrogen energy storage system: For the case WiSoBaHy which includes the HESS, the hydrogen unit is charged when the battery is at 80% SoC and there is excess production. This is

like the battery represented by an integrator block. The charge of the hydrogen equals the net production that is sold to the grid, however it is adjusted with the efficiency of the electrolyzer, fuel cell and transformer. The subsystem for the HESS is presented in figure H.5.

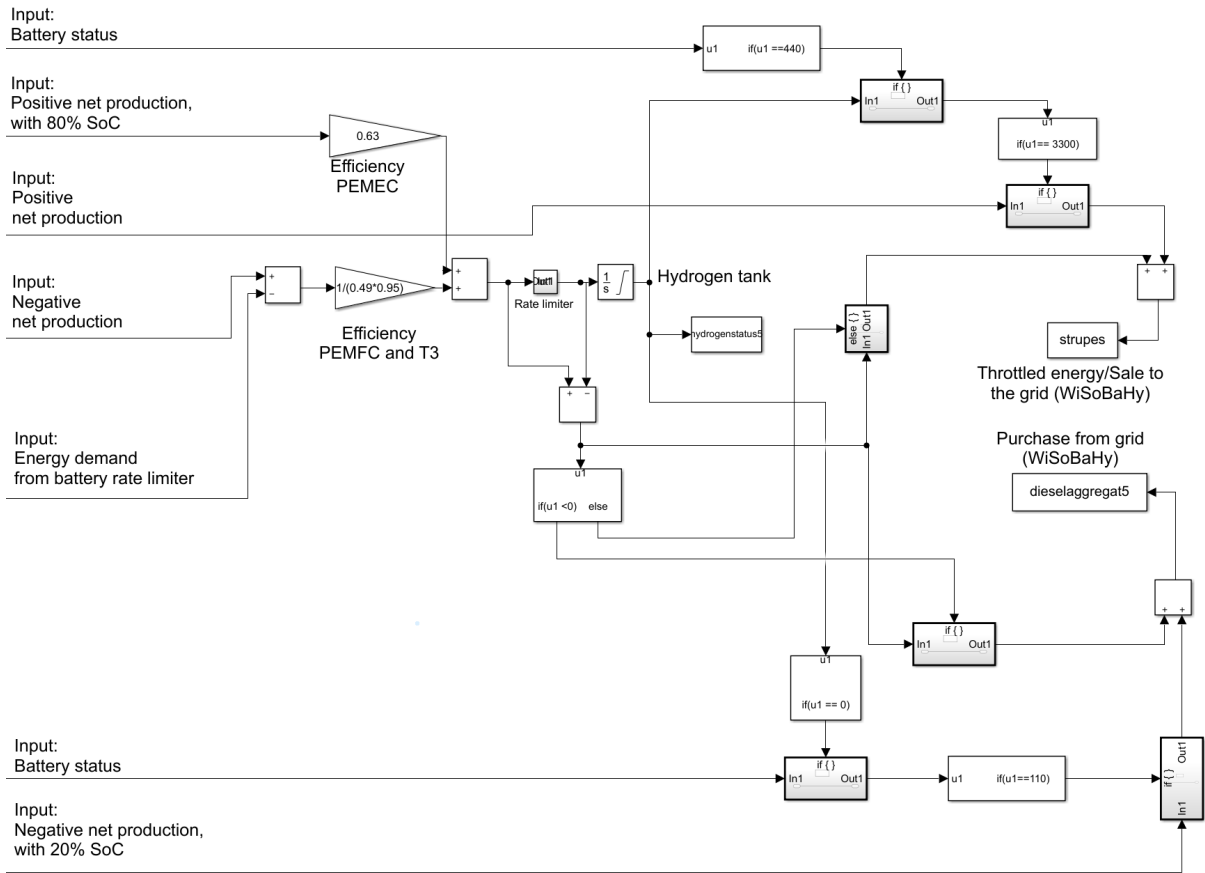


Figure H.5: The subsystem of the model showing the hydrogen energy storage system in case WiSoBaHy.

The excess energy is the throttled energy, and the deficit energy is either from the rate limiter of the fuel cell, or because the hydrogen tank and battery is empty. All the relevant values are imported to the MATLAB workspace with the To Workspace block.

The rate limiter for the hydrogen and battery charge and discharge is compiled in a subsystem, presented in figure H.6. Figure H.6 presents the rate limiter for the hydrogen ESD, whereas the rising slew rate is 55 kW and the falling slew rate is -100 kW.

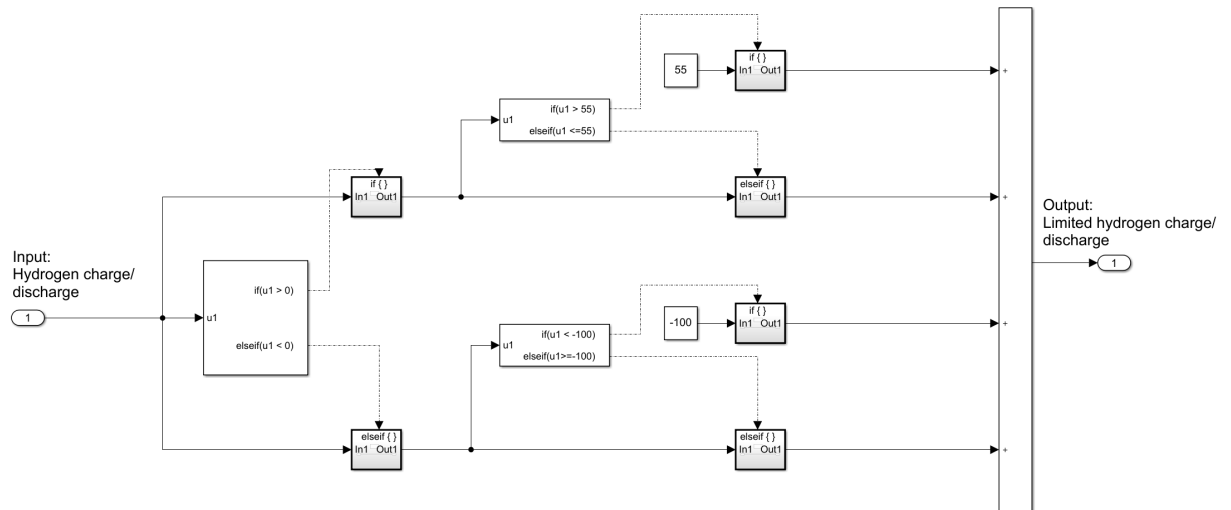


Figure H.6: The subsystem of the model that includes the rate limiter for the hydrogen charge and discharge. The rising slew rate is 55 kW and the falling slew rate is -100 kW.

The same principle is used for the rate limiter for the battery ESS. The rising and falling slew rate limits are respectively 1 100 kW and -1 100 kW.

